

PERFORMANCE ANALYSIS AND ENHANCEMENT OF UNMANNED AERIAL VEHICLE BASED FREE SPACE OPTICAL COMMUNICATION SYSTEM

Thesis

Submitted in partial fulfillment of the requirements for the degree of
DOCTOR OF PHILOSOPHY

by

NALLAGONDA VIJAYA RATNAM

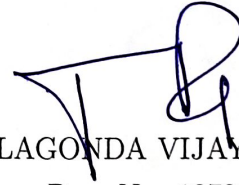


DEPARTMENT OF ELECTRONICS & COMMUNICATION ENGINEERING
NATIONAL INSTITUTE OF TECHNOLOGY KARNATAKA
SURATHKAL, MANGALORE - 575025

May 2022

DECLARATION

I hereby **declare** that the Research Thesis entitled **PERFORMANCE ANALYSIS AND ENHANCEMENT OF UNMANNED AERIAL VEHICLE BASED FREE SPACE OPTICAL COMMUNICATIONS SYSTEM** which is being submitted to the *National Institute of Technology Karnataka, Surathkal* in partial fulfillment of the requirement for the award of the Degree of *Doctor of Philosophy* in Department of Electronics and Communication Engineering is a *bonafide report of the research work carried out by me*. The material contained in this Research Thesis has not been submitted to any University or Institution for the award of any degree.



NALLAGONDA VIJAYA RATNAM

Reg. No. 187011/187EC008

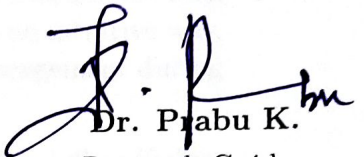
Department of Electronics and
Communication Engineering.

Place: NITK-Surathkal.

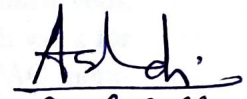
Date:30-05-2022.

CERTIFICATE

This is to certify that the Research Thesis entitled **PERFORMANCE ANALYSIS AND ENHANCEMENT OF UNMANNED AERIAL VEHICLE BASED FREE SPACE OPTICAL COMMUNICATIONS SYSTEM** submitted by **Mr. NALLAGONDA VIJAYA RATNAM** (Register Number: 187011/187EC008) as the record of the research work carried out by him, is accepted as the *Research Thesis submission* in partial fulfillment of the requirements for the award of degree of **Doctor of Philosophy**.



Dr. Prabu K.
Research Guide,
Assistant Professor,
Dept. of E&C Engg.,
NITK Surathkal - 575025.


2-6-2022
Chairman-DRPC

(Signature with Date and Seal)

प्राध्यापक एवं विभागाध्यक्ष / PROF & HEAD
ई एवं सी विभाग / E & C Department
एन आई टी के, सुरतकल/NITK, Surathkal
मंगलूर / MANGALORE - 575 025

Acknowledgements

I would like to express my sincere gratitude to my research advisor Dr. Prabu K, for guiding me throughout the research work. The valuable suggestions and guidance provided by him kept me on the right track. Discussions with him helped me to understand and analyze the concepts in an intuitive way. I am indebted to him for his support, guidance, and encouragement during my research.

I am grateful to get the right encouragement from Prof. Muralidhar Kulkarni, Dr. Krishnamoorthy K. and Dr. Raghavendra B.S. They stood by me during peak and valley times and I have got great encouragement from them. They were supported in technical and non-technical discussions.

I express my gratitude to Prof. Lakshminidhi T, Head of the department, Electronics and Communication Engineering during my enrollment for the Ph.D. program and Prof. Lakshminidhi T and Prof. Ashvini Chaturvedi, Head of the Department of E& C Engineering during my research work for their support, help, and encouragement. I am grateful to my RPAC members, Dr. Krishnamoorthy K., Department of Electronics and Communication Engineering, and Dr. Y Suresh, Department of E & E Engineering, for giving vital comments and suggestions throughout the research, which helped in improving the quality of research.

I am thankful to my seniors, Sravan Kumar Padala, P Sudhakar Reddy and Geriki Polaiiah for their support for technical discussions and the way they motivate me to prepare for various questions and answers for any technical presentation.

I would like to thank the non-teaching staff of Department of E & C: Sanjeev Pujari, Rathish Kumar Thumbay, B Vasudeva Shettigar, Subrahmanya Karanth, Guruthilak Shriyan, and Amitha Amin help me to simulate the various parameters of UAVs.

I would like to thank all the faculty members and staff of the E & C department, NITK Surathkal, for their assistance. I would like to express my gratitude to all friends and colleagues at NITK for encouraging me in the good and the bad times, making a memorable stay in NITK. Thanks to

Abhishek Kumar, Purushottama T. L., M. Ashoka Chakravarthi, L. Bhargava Kumar, and Pradeep Gorre, and Dipanshu for technical discussions and support during my research work.

I would like to take a moment to my appreciation to Dr. Prashantha Kumar H, Prof. John DSouza, and Dr. Raghavendra Bobbi to provide technical support, which helped me to learn many technical details.

I would like to thank my parents Kutumba rao and venkateswramma, wife Veera Lakshmi, sisters Prashnthi, and Anna mani for their continuous support, love, and encouragement.

I am deeply indebted to all my teachers throughout life, who have guided, encouraged, and inspired me to grow in both technical and personal aspects.

Finally, I would like to thank god for giving me good health, strength, and bliss during my research work.

Dedicated to
My Dear Parents

Abstract

Unmanned aerial vehicles (UAVs) are attractive solutions for current and future wireless communication systems. Radio-frequency (RF)-based UAV growth is projected to be USD 49.0 billion by 2026, and UAVs inherent nature provides a wide range of applications. RF-based UAVs have significant limitations, such as higher data rate, limited RF spectrum, fronthaul/backhaul link, interference, security and latency requirement, inter UAV coordination. UAV-based Free-space optics (FSO) is the alternative solution for such needs. High-altitude platform (HAP)/UAVs play a critical role in connecting terrestrial to satellite networks via FSO communication links to provide services such as 5G, 5G+ networks were hard to reach areas. HAPs/UAVs act as a relay, base stations, and high capacity backhaul/fronthaul links for civilian navy, military, and disaster management applications. Due to alignment issues developing a channel model for inter UAV based FSO communication is a difficult task. The various alignment strategies and channel models that exist in the literature have been studied, and they are complex.

In First work, we proposed and deduced a simple channel model using Meijer's G functions for inter UAV communication. The derived analytical channel model results are verified with Monte-Carlo simulations. We used heterodyne detection (HD) in FSO-based inter-UAV communication for the first time. The proposed systems outage and average bit error rate (BER) performance are evaluated, and the results are compared to existing Intensity modulation direct detection (IM/DD) systems.

The first proposed system has the disadvantage of not being suitable for long-range applications. Inter UAV-based FSO communication systems distance is another performance-limiting factor as the distance increases the systems performance worst, as shown in the literature. We proposed polarization shift keying modulation (POLSK) modulation for long-range inter UAV-based FSO communication systems in our second work. The performance metrics are derived and the results are analysed under different weather conditions. Results indicated that significant performance improvement under POLSK modulation when compared with the exist-

ing On-off-keying (OOK) modulation scheme. We showed optimal values selection under different weather conditions for inter UAVs.

The inherent nature of HAPs provides larger coverage areas with better Line-of-sight (LOS), rapid development, and low maintenance costs. HAP is mainly used to connect the satellite to the ground station via a high-capacity optical backhaul link. Such a high-capacity HAP-based FSO communication link under hovering HAP fluctuations performance analysis is challenging. We addressed this challenge in the third work. Derived the Ground-to-HAP, HAP-to-Ground channel model under hovering state fluctuations. We improved the Ground-to-HAP-based FSO links performance using coding techniques.

The growth of internet of things and 5G networks required convergent systems like, RF, millimetre wave, FSO and Underwater wireless optical communication (UWOC) etc. UWOC links are mainly focused on the applications of underwater ranging and imaging. The drawback of UWOC systems is poor BER performance under absorption and scattering, link misalignment, random movement of the sea surface, and complex environment. In the Fourth work, we proposed the HAP-UWOC communication systems under hovering fluctuations for HAP backhaul to underwater applications. We evaluated the BER performance of HAP, UWOC, and HAP-UWOC links. Evaluated the end-to-end performance of HAP-UWOC under the clear ocean, coastal ocean, Turbid harbor, and HAP hovering fluctuations are considered.

Keywords: Unmanned aerial vehicle; Free-Space Optical; Intensity modulation/direct detection; Heterodyne detection; angle-of-arrival fluctuations; Polarization Shift Keying; Field Of View; High altitude platforms.

Contents

Acknowledgements	i
Abstract	iv
List of figures	x
List of tables	xv
Abbreviations	xvi
Notations	xvi
1 INTRODUCTION	1
1.1 Background and Motivation	1
1.2 Introduction to FSO Communication Systems	2
1.3 Introduction to UAV equipped FSO Communication Systems	3
1.4 UAV equipped FSO Communication System Limitations	5
1.5 Thesis Contributions	8
1.6 Thesis Organization	10
2 CHANNEL MODEL	11
2.1 Introduction to UAV based FSO Channel Model	11
2.1.1 Path Loss	11
2.1.2 Modeling of FSO Atmospheric Turbulence	12
2.1.2.1 Weak Turbulence Channel Model	12
2.1.2.2 Moderate-Strong Turbulence Channel Model	13
2.1.3 Pointing Error Impairments Mathematical Modeling	14
2.1.3.1 Beckmann Distribution	15
2.1.3.2 Rayleigh Distribution	16
2.1.4 Link Interruption due to AOA Fluctuations	16
2.2 Modeling of Composite Channels	18
2.3 Inter UAV-based FSO Communication System Channel Model	20

2.3.1	Inter UAV-based FSO link with Log-normal channel	20
2.3.2	Inter UAV-based FSO link with Gamma-Gamma turbulence channel	20
2.4	Ground-to-HAP Channel Model	21
2.4.1	Atmospheric Loss	21
2.4.1.1	Fog Attenuation	22
2.4.1.2	Rain Attenuation	22
2.4.1.3	Cloud Attenuation	23
2.4.2	Atmospheric Turbulence Channel	23
2.4.3	Misalignment Fading	24
2.4.4	Angle Of Arrival Fluctuations	25
2.4.5	Combined Channel Model	26
2.5	HAP-to-Ground Link Channel Model	26
2.5.1	Path Loss	27
2.5.2	Atmospheric Turbulence Channel	27
2.5.3	Misalignment Fading	28
2.5.4	Angle Of Arrival Fluctuations	29
2.5.5	Combined Channel Model	29
2.6	UWOC Link Channel Model	30

3 INTER UAV-BASED FSO COMMUNICATION SYSTEM PERFORMANCE ANALYSIS WITH DETECTION TECHNIQUES 33

3.1	Introduction	33
3.2	Major contributions	34
3.3	System and received signal model	35
3.4	Channel Model	38
3.4.1	UAV-UAV-FSO link with Log-normal channel	38
3.4.2	UAV-UAV-FSO link with Gamma-Gamma turbulence channel .	39
3.5	Outage Probability for Inter UAV-based FSO Communication System .	39
3.5.1	Outage Probability of a Inter UA-based FSO link with Log- normal channel	39
3.5.2	Outage Probability of a UAV-UAV-FSO link with Gamma- Gamma turbulence channel	41
3.6	Average Bit-error rate	42

3.7	Results and Discussions	43
3.8	Summary	51
4	POLSK MODULATION INTER UAV-BASED FSO COMMUNICATION UNDER DIFFERENT WEATHER CONDITIONS.	52
4.1	Introduction	52
4.2	Main Contributions	53
4.3	System model	53
4.4	Channel Model	55
4.4.1	Atmospheric Loss	55
4.4.1.1	Fog	55
4.4.1.2	Rain	56
4.4.2	Combined Channel Model	56
4.5	Performance Analysis	57
4.5.1	Average Bit Error Rate	57
4.6	Results and Discussions	58
4.7	Summary	65
5	CODED GROUND-TO-HAP BASED FSO COMMUNICATION SYSTEM USING POLSK MODULATION	66
5.1	Introduction	66
5.2	Main Contributions	67
5.3	System Model	67
5.4	Channel Model	70
5.5	Coded Ground-to-HAP FSO Link	71
5.6	Average BER	72
5.6.1	BCH Code	72
5.6.2	Repetition Code	73
5.7	Results and Discussions	73
5.8	Summary	80
6	CONVERGENT FSO BASED HAP COMMUNICATION SYSTEM WITH UWOC COMMUNICATION SYSTEM	81
6.1	Introduction	81
6.2	Main Contributions	82

6.3	System Model	82
6.4	Channel Model	83
6.4.1	HAP-to-Ground Channel Model	83
6.4.2	UWOC Channel Model	85
6.5	Performance Analysis	85
6.5.1	Outage Performance Analysis	86
6.5.2	Average BER	86
6.5.3	HAP-to-Ground BER	87
6.5.4	UWOC BER	88
6.6	Results and Discussions	88
6.7	Summary	93
7	CONCLUSIONS AND FUTURE DIRECTIONS	95
7.1	Conclusions	95
7.2	Future Directions	97
	APPENDICES	98
I:	UAV-UAV FSO	98
A-1	Derivation Of UAV-UAV-FSO Over Gamma-Gamma Channel	98
A-2	Derivation Of HD Detection Over Log-normal Channel	100
	Publications based on the thesis	111

List of Figures

2.1	Zero boresight: no misalignment:	15
2.2	Bi-Directional misalignment: zero bore sight and identical jitters	17
3.1	Ground-UAV-UAV-Ground Links.	35
3.2	UAV-UAV FSO link two UAV's are in hovering state with out and with Misalignment.	37
3.3	UAV-UAV FSO link two UAV's are in hovering state with out and with Misalignment.	37
3.4	Outage probability of UAV-UAV-FSO LINK versus average SNR over Gamma-Gamma turbulence model for $\sigma_{to} = \sigma_{ro} = 3mrad$, $W_z = 2m$, $Z = 250m$ with both detection techniques under different turbulence conditions.	43
3.5	Outage probability of UAV-UAV-FSO LINK versus average SNR over Gamma-Gamma turbulence model for $\sigma_{to} = \sigma_{ro} = 3mrad$, $W_z = 2m$, $Z = 250m$, different values of θ_{FOV} with both detection techniques under moderate to strong turbulence condition.	44
3.6	Outage probability of UAV-UAV LINK-FSO versus average SNR over Gamma-Gamma turbulence model for $\sigma_{tp} = \sigma_{rp} = 30cm$, $W_z = 2m$, $Z = 250m$, different values of σ_{to}, σ_{ro} with both detection techniques under moderate to strong turbulence condition.	45
3.7	Outage probability of UAV-UAV-FSO LINK versus average SNR over Log-normal turbulence model for $\sigma_{to} = \sigma_{ro} = 2mrad$, $W_z = 2m$, $Z = 250m$, $\sigma_R = 0.1$ different values of θ_{FOV} with both detection techniques under weak to moderate turbulence condition.	46

3.8	Outage probability of UAV-UAV-FSO LINK versus average SNR over Log-normal turbulence model for $\sigma_{to} = \sigma_{ro} = 2mrad, W_z = 2m, Z = 500m, \sigma_R = 0.1$ different values of θ_{FOV} with both detection techniques under weak to moderate turbulence condition.	47
3.9	Outage probability of UAV-UAV-FSO LINK versus average SNR over Log-normal turbulence model for $\sigma_{to} = \sigma_{ro} = 2mrad, FOV = 11mrad, Z = 250m, \sigma_R = 0.1$ different values of W_z with both detection techniques under weak to moderate turbulence condition.	48
3.10	Outage probability of UAV-UAV-FSO LINK versus average SNR over Log-normal turbulence model for $\sigma_{to} = \sigma_{ro} = 2mrad, FOV = 11mrad, Z = 500m, \sigma_R = 0.1$ different values of W_z with both detection techniques under weak to moderate turbulence condition.	49
3.11	Average BER of UAV-UAV-FSO LINK versus average SNR over moderate to strong turbulence model for $\sigma_{to} = \sigma_{ro} = 3mrad, FOV = 20mrad, Z = 250m$, different values of σ_R with Heterodyne Detection technique.	49
3.12	Average BER of UAV-UAV-FSO LINK versus average SNR over moderate to strong turbulence channel model for $\sigma_{to} = \sigma_{ro} = 3mrad, Z = 250m, \sigma_R = 10$ different values of FOV with Heterodyne Detection technique.	50
4.1	Two UAV's are in hovering state with misalignment and different weather conditions	54
4.2	Average BER versus average SNR under very clear weather conditions for various σ_{to}, σ_{ro} values.	59
4.3	Average BER versus average SNR under very clear weather conditions various θ_{FOV} values.	59
4.4	Average BER versus average SNR under very clear weather conditions for various W_z values.	60
4.5	Average BER versus average SNR under very clear weather conditions for various Z values.	60
4.6	Average BER versus average SNR under different fog conditions for various σ_{to}, σ_{ro} values.	61
4.7	Average BER versus average SNR under different fog conditions different values of θ_{FOV}	61

4.8	Average BER versus average SNR under different rain conditions for different values of θ_{FOV}	62
4.9	Average BER versus average SNR under different rain conditions for different values of σ_{to}, σ_{ro}	62
5.1	Graphical illustration of Ground-to-HAP optical communication link.	68
5.2	The schematic of Ground-to-HAP optical communication link with length L with HAP hovering state parameter values are given in table II [Safi <i>et al.</i> (2020), Fig.(2)]	70
5.3	Average BER versus transmitted power $P_t(dBm)$ over very clear sky condition for $W_z=2, \sigma_{ro} = 0.4, \sigma_{rd} = 16\text{mrad}$, different values of θ_{FOV} with POLSK modulation	75
5.4	Analytical Average BER versus receiver FOV (θ_{FOV}) over very clear sky condition for $W_z=2, \sigma_{ro} = 0.4$, different values of σ_{rd} with POLSK modulation	75
5.5	Average BER versus transmitted power $P_t(dBm)$ over very clear sky condition for $W_z=2, \sigma_{ro} = 0.4, \theta_{FOV} = 75\text{mrad}$, different values of σ_{rd} with POLSK modulation.	76
5.6	Average BER versus transmitted power $P_t(dBm)$ over very clear sky condition for $\sigma_{rd}=13\text{mrad}, \sigma_{ro} = 0.4, \theta_{FOV} = 75\text{mrad}$, different values of W_z with POLSK modulation.	77
5.7	Average BER versus Average SNR under different Fog conditions for $W_z=2, \sigma_{ro} = 0.4, \theta_{FOV} = 15\text{mrad}$, different values of σ_{rd} with POLSK modulation.	77
5.8	Average BER versus average SNR under different fog conditions for $W_z = 2, \sigma_{ro} = 0.4, \sigma_{rd} = 5\text{mrad}$, different values of θ_{FOV} with POLSK modulation.	78
5.9	Average BER versus average SNR under different rain conditions for $W_z = 2, \sigma_{ro} = 0.4, \sigma_{rd} = 3\text{mrad}$, different values of θ_{FOV} with POLSK modulation.	78
5.10	Average BER versus average SNR under different rain conditions for $W_z = 2, \sigma_{ro} = 0.4, \theta_{FOV} = 30\text{mrad}$, different values of σ_{rd} with POLSK modulation.	79
5.11	Analytical and simulation results for coded Ground-to-HAP Optical Link with POLSK modulation.	79

6.1	schematic diagram of Dual-hop HAP-UWOC System that consist of source (S) in hovering state, relay (R), and a destination (D).	84
6.2	Outage Probability of HAP LINK versus Reveiver FOV over Gamma-Gamma turbulence model for different values of σ_{rd}	88
6.3	Outage Probability of HAP LINK versus Transmitted power over Gamma-Gamma turbulence model for $\sigma_{rd} = 11, 10, 9$ mrad.	89
6.4	Outage Probability of HAP-UWOC LINK versus Transmitted power over Coastal ocean under hovering fluctuations	89
6.5	Average BER of HAP-UWOC LINK versus Transmitted power over Coastal ocean under hovering fluctuations.	90
6.6	Average BER of HAP-UWOC LINK versus Transmitted power over Coastal ocean for strong-to-weak turbulence conditions under hovering fluctuations.	91
6.7	Average BER of HAP-UWOC LINK versus Transmitted power over Clear ocean for strong-to-weak turbulence conditions under hovering fluctuations.	91
6.8	Average BER of HAP-UWOC LINK versus Transmitted power over Turbid harbor ocean for strong-to-weak turbulence conditions under hovering fluctuations.	92
6.9	Average BER of HAP-UWOC LINK versus Transmitted power over Turbid harbor ocean for strong-to-weak pointing($\gamma_2 = 1, 2, 6$) error under hovering fluctuations.	93

List of Tables

2.1	Attenuation Coefficients at 1550 nm between Ground-to-HAP FSO Link	23
2.2	Path loss of 10m UWOC link [Kumar and Krishnan (2020)], [Kaymak <i>et al.</i> (2018)].	32
3.1	Optimal values of θ_{FOV} to achieve minimum outage probability over GG Turbulence Model for $SNR = 40dB, \sigma_{tp} = \sigma_{rp} = 30cm$, and different values of Z	48
3.2	Optimal values of $\sigma_{to} = \sigma_{ro}$ to achieve minimum outage probability over GG Turbulence Model for $SNR = 35dB, \sigma_{tp} = 30cm, \theta_{FOV} = 13mrad$ and different values of Z	50
4.1	Attenuation coefficients at 1550 nm between UAV-UAV FSO Link	57
4.2	Optimal values of θ_{FOV} to achieve Average BER over GG Turbulence Model for $SNR = 50dB, \sigma_{to} = \sigma_{ro} = 30cm$, and different fog conditions.	63
4.3	Optimal values of θ_{FOV} to achieve Average BER over GG Turbulence Model for $SNR = 40dB, \sigma_{to} = \sigma_{ro} = 30cm$ and different rain conditions.	63
5.1	Analytical and Simulation Parameters	74
6.1	Turbulence conditions for UWOC link [Zeng <i>et al.</i> (2016)].	94
6.2	Parameters for HAP and UWOC link.	94

Abbreviations

5G	Fifth-Generation
6G	Sixth-Generation
AoA	Angle-of-Arrival
AWGN	Additive White Gaussian Noise
BER	Bit Error Rate
BPSK	Binary Phase-Shift Keying
CDF	Cumulative Distribution Function
DF	Decode-and-Forward
DPSK	Differential Phase-Shift Keying
FOV	Filed Of View
FSO	Free Space Optical
GG	Gamma-Gamma
HAP	High altitude platform
HD	Heterodyne Detection
IM/DD	Intensity Modulation / Direct Detection
LOS	Line-Of-Sight
MIMO	Multiple-Input Multiple-Output
NLOS	Non-Line-Of-Sight
OOK	On-Off Keying
PD	Photo Detector
PDF	Probability Density Function
POLSK	Polarization Shift Keying
SISO	Single-Input Single-Output
SNR	Signal-to-Noise Ratio
UAVs	Unmanned Aerial Vehicles
UWOC	Under Water Optical Communication

Notations

η	Responsivity
B_o	Optical bandwidth
B_e	Receiver electrical bandwidth
$N_b(\lambda)$	Spectral radiance
ς	HAP zenith angle
V_m	wind speed
$1.7 * 10^{-13} m^{-2/3}$	Refractive index structure at the ground $C_n^2(0)$
λ	Wavelength
r_a	Aperture Radius
σ_{to}	Transmit orientation deviations
σ_{ro}	Receiver orientation deviations
σ_{tp}	Transmit position deviations
σ_{rp}	Receiver position deviations
d_f	Focal length
r_p	radius of circular photo detector
Z	Link length
θ_{FOV}	FOV angle
R	PD responsivity
h	Over all channel effect
h_{pl}	Path loss
h_{at}	Atmospheric turbulence
h_{pp}	Pointing error
h_{AOA}	Angle of arrival fluctuations
$\Gamma(\cdot)$	Gamma random variable
$K_v(\cdot)$	Modified Bessel function of second kind
h_{th}	Threshold SNR
ς	AWGN noise
σ_R	Rytov variance
α	Large scale turbulent eddies
β	Small scale turbulent eddies
μ_{HD}	Average SNR of HD detection
$\mu_{IM/DD}$	Average SNR of IM/DD detection

Chapter 1

INTRODUCTION

1.1 Background and Motivation

The higher data rate, cost-effective, easy to develop fronthaul/backhaul FSO communication systems gained considerable attention in 5G+ and beyond networks. Existing RF-based backhauling/fronthauling links provide service between the SSBs to a central hub. These RF-based links have limitations of low data rate, limited spectrum, security, privacy, and more interference. Proposed FSO based backhauling/fronthauling overcame these limitations and provided additional benefits. FSO communication links have higher data transfer capacity with point-to-point communication and maintain the greater LOS. 5G+ networks SSBs have placed disaster management application scenarios where LOS path doesn't exist. In such scenarios, UAVs/HAPs provided end-to-end cellular services to hard-to-reach areas. Due to the availability of UAVs/HAPs recently introduced as base stations for cellular networks. 5G+ and beyond networks equipped with UAVs/HAPs to provide the service with higher capacity hard-to-reach areas and end-to-end communication through FSO backhaul/fronthaul link.

Future communication networks equipped with the swarm of UAVs/HAPs to deliver services to several applications. This swarm of UAVs/HAPs provides services from ground station to satellite station to full fill the criteria of future wireless communications networks. The capacity of the FSO based backhaul/fronthaul link influences the total end-to-end communication system performance. UAVs/HAPs equipped FSO fronthaul/backhaul communication links more significant role in 5G+ and beyond networks. The primary performance limiting factors of the swarm of UAVs/HAPs

equipped FSO links are alignment, weather effects, blockages, hovering state fluctuations, and turbulence effects. Considering all these limitations, designing an effective communication system has more advantages for 5G+ and beyond networks. Considering fully equipped 5G+ network communication system link performance mainly depends on the Inter UAV equipped FSO communication system.

In this introduction, we discuss the benefits and the limitations of using UAVs/HAPs equipped FSO fronthaul/backhaul communication links for 5G+ and beyond networks

1.2 Introduction to FSO Communication Systems

Free space optical is license-free, secure, point-to-point narrow beam communications, wider bandwidth, and immune to jamming and interference, making it suitable for wireless communication applications. Still, Free space optics (FSO) It is possibly extremely sensitive to transceiver orientation and environmental conditions. The distance increases turbulence-induced scintillation increases, and performance loss of FSO link increases. By adopting a relay system between source and destination, path loss decreases, and FSO link capacity improves. One of the challenging tasks in relay communication systems is that relay transfers the data even if the relay link under the worst channel conditions because of blockages and weather conditions [Khalighi and Uysal \(2014\)](#), [Ghassemlooy *et al.* \(2019\)](#). FSO systems under different modulation techniques and channel models are proposed in [Pham *et al.* \(2014\)](#), [Elsayed and Yousif \(2020\)](#), [Singh and Malhotra \(2019b\)](#), [Anandkumar and Sangeetha \(2021\)](#), [Rahman *et al.* \(2020\)](#). Performance analysis of different FSO systems under different weather conditions by considering weak to moderate turbulence channels is studied in [Jha *et al.* \(2018\)](#), [Majumdar \(2014\)](#). Serial-relay FSO systems by considering atmospheric attenuation and signal-dependent shot noise under moderate to strong turbulence were derived in [Djordjevic \(2018\)](#), [Kaushal *et al.* \(2017\)](#), [Bhowal and Kshetrimayum \(2021\)](#).

Performance improvement by considering the distance of data transmission and BER for Hybrid fiber/FSO communication system is presented in [Elsayed and Yousif \(2020\)](#). Orthogonal Frequency Division Multiplexing (OFDM) based FSO Link under different link distances and weather conditions successfully presented in [Singh and Malhotra \(2019b\)](#). Demonstration of nanosatellite laser downlink and optimal beam pointing is explained in [Amphawan *et al.* \(2020\)](#).

Multi-hop DF FSO system by considering different turbulence conditions and different path loss is analyzed in [Singh *et al.* \(2020\)](#), [Lei *et al.* \(2018\)](#), [Djordjevic \(2018\)](#).

Performance analysis of Multiple Input Single Output(MISO) - FSO system over M-ary Modified Pulse-Position Modulation(MPPM) and Spatial Pulse-Position Modulation (SPPM) modulation schemes were studied in [Bhowal and Kshetrimayum \(2021\)](#), [Uysal and Nouri \(2014\)](#). Multiple-Input Multiple-Output(MIMO)-FSO communication system performance over correlated fading channel under different channel effects are considered in [Kumbhani and Kshetrimayum \(2017\)](#), [Singh and Malhotra \(2019a\)](#), [Zhang *et al.* \(2020\)](#), [Abaza *et al.* \(2015\)](#).

1.3 Introduction to UAV equipped FSO Communication Systems

The potential applications, challenges, critical issues, growth of UAVs in wireless networks are studied in [Gupta *et al.* \(2015\)](#). An accurate channel model is required to get the full benefits of UAVs, and designing accurate channel models between Ground-to-air, air-to-Ground, air-to-air is another critical task. A detailed literature review of channel models for UAV communication under various scenarios, link loss and channel fading effects, multi-antenna aided UAV communications, and some of the open issues and challenges regarding the analytical channel model designs are presented in [Yan *et al.* \(2019\)](#). Studied detailed literature survey of FSO communication systems advantages, disadvantages, applications, the role of UAV equipped FSO communication systems between Ground-to-UAV based FSO experimental and simulation results presented in [Harris *et al.* \(2005\)](#).

Alignment and tracking is the fundamental limitation of Ground-to-UAV based FSO link. Active alignment and tracking was improve with three-wavelength in the presence of atmospheric fading presented in [Harris *et al.* \(2006\)](#). Another important aspect of interest in UAV-based FSO is the UAV-to-UAV-based FSO channel model (air-to-air). Where two UAVs are hovering, so the alignment of two UAVs are difficult; such novel alignment model proposed and analyzed in [Kaadan *et al.* \(2013\)](#). Multirotor-based FSO systems are the best suitable option for current communication systems in terms of alignment/ stability. Two multirotor in hovering states with open-loop alignment/ stability theoretical and optical geometrical intersection models are simulated and compared with other ground-to-air, air-to-ground, and air-to-air models. This model is validated with previous models performance is improved with existing mathematical models [Kaadan *et al.* \(2014\)](#). Closed-form analytical expres-

sions for optical transmitter array with a spherically curved optical receiver array in different configurations to improve coverage and alignment proposed in [Kaadan *et al.* \(2016\)](#). In this part of the literature survey, we studied the wireless UAVs and its applications, UAV-based FSO Communication systems and their challenges, alignment and coverage models of different UAV-based FSO link configurations.

Alignment and Design of more tractable channel models between UAVs are Major challenges. The performance analysis of inter UAVs-based FSO communication systems under different weather conditions is another challenge. Alignment is the major technical challenge in inter-UAV-based FSO Communication systems, and this alignment is not only in inter UAVs which is present in FSO Communication systems. UAV-based FSO communication systems for Ground-to-UAV, UAV-to-UAV link performance is analyzed experimentally with alignment under clear weather conditions investigated [Leitgeb *et al.* \(2007\)](#). UAV based FSO initially proposed high data rate applications such as military and civil with a data rate of 2.5 Gbit/s. It highlighted the UAV-to-UAV based FSO link for different wireless networks [Chlestil *et al.* \(2006\)](#). Conventional relay-FSO systems replaced with UAV's and their performance evaluation in [Fawaz *et al.* \(2018\)](#).

The critical enabler for 5G+ wireless networks is the small cell concept. This higher number of small cells requires a high data rate backhauling/front hauling link, which increases cost and difficult to establish a link. Swarm of UAVs based FSO is proposed for such backhauling/front hauling link [Alzenad *et al.* \(2018a\)](#). All the above UAV-based FSO applications are enabled with tractable channel models. Such a channel model between Ground-to-UAV, UAV-to-Ground, and UAV-to-UAV are proposed in [Dabiri *et al.* \(2018a\)](#). The tractable and more efficient UAV-to-UAV based FSO channel model is proposed in [Dabiri *et al.* \(2019a\)](#). The UAV based FSO system's performance under hovering fluctuations of the UAV by considering blind data detection proposed in [Safi *et al.* \(2019a\)](#). Source relay(SR) and relay to destination(RD) channel models of the UAV based FSO system where UAV as a relay with DF is relaying proposed in [Dabiri and Sadough \(2019a\)](#). UAV based FSO channel with Nonzero Boresight pointing error and Statistical channel modeling proposed in [Dabiri *et al.* \(2020\)](#).

Another important challenge is even we designed a more tractable analytical channel model between UAVs, ground-to-UAV, and UAV-to-ground, the Horizontal/Vertical links are mainly affected by weather conditions. Literature studies stud-

ied on UAV-based FSO in this synopsis are related to short-distance communication links. The performance of the UAV-based FSO system is limited by distance. Improving the performance with distance under the worst weather conditions scenario is another important challenge. The performance improvement is made with a suitable modulation scheme under different weather conditions presented in [Nallagonda and Krishnan \(2021a\)](#). The simple mathematical model for inter UAV-based FSO communication systems under different detection techniques and comparative study was present for weak to strong turbulence cases. HD detection is the best suitable detection for mitigating the turbulence effect, and random hovering fluctuations are presented [Nallagonda and Krishnan \(2021b\)](#).

APD based UAV-assisted FSO communication system, and its performance analysis studied in [Khankalantary *et al.* \(2020\)](#). Ground-to-UAV, UAV-to-Ground UAV-based FSO communication system with Amplify-and-Forward Relaying and its performance analysis under hovering fluctuations studied in [Dabiri *et al.* \(2021\)](#). The capacity and outage of Ground-to-UAV UAV-based FSO link with closed-form expression was derived and performance analysis studied in [Dabiri *et al.* \(2019c\)](#), [Dabiri and Sadough \(2019c\)](#)

1.4 UAV equipped FSO Communication System Limitations

It is useful to take advantage of UAV-based FSO's benefits. It's suitable for various 5G+ and beyond communication networks applications. Due to the propagation of UAV-based FSO communication systems through the atmosphere, the losses generated by the environment are unavoidable. The losses are inevitable since these UAV-based FSO communication links are travel from air-to-ground, ground-to-air, and air-to-air. These limitations are briefly explained below.

- **Atmospheric Weather Conditions:** One of the main limiting factors that degrade the performance of UAV-based FSO communication systems is weather conditions. Generally, these UAV-based FSO horizontal/vertical links are placed where the infrastructure is unavailable, hard to reach areas, disaster management, or rural/urban areas. Depending on the application area environment, the weather attenuation loss is increased. Many researchers have done experimental and theoretical work to evaluate the performance of the fog effect on FSO links. Depending on the fog density, the loss increases. Rain is another limiting

factor, and it depends on the heavy rain or weak rain condition. Depending on the environment and areas, the loss can be described as fog, rain, cloud, haze, dust, smock, Sandstrom, and clear sky weather. Performance analysis of different wavelengths under different weather conditions based on research has been done. Many researchers proposed mitigation techniques to reduce the weather conditions effects. Different attenuation functions are proposed for different weather effects. These attention factors are used to find the estimation of the correct link budget for UAV-based FSO systems. In this thesis, we evaluated the performance of Inter UAV-equipped FSO communication system under different weather conditions. We mitigated the weather effect by increasing the receiver FOV for Inter UAV-based FSO communication system.

- **Optimal Placement Of UAVs:** In practical scenarios, the UAVs flying to provide the services to different applications. Such flying UAVs have many tall buildings obstacles which leads to the interpretation of services. The optimal location of flying UAV is designing is a limitation. This problem was nicely addressed in the literature survey. More research is required to address this problem based on the application scenarios.
- **Alignment of Inter UAV FSO systems:** The misalignment has mainly occurred in Inter UAV communication systems. Inter UAV-based FSO communication's main limiting factor is alignment. As the distance increases, the alignment is more severe. Different alignment models are proposed based on the geometric intersection methods with optical arrays. The FSO communication alignment models design was presented in the literature.
- **Position and Orientation fluctuations of UAVs:** Position and Orientation deviations are present inside or outside of the UAVs. This position and orientation are present because of the propellers imbalance, motor and mechanical variations, air turbulence, and others. These position and orientation fluctuations are random variables that are rayleigh distribution and independent of others. The position and orientation fluctuations depend on the link type, i.e., Ground-to-UAV, UAV-to-Ground, and UAV-to-UAV. In the case of UAV-to-UAV, the orientation and position fluctuations are more. We analyzed the performance effect on position and orientation fluctuation in this thesis. These fluctuations are generally measured in mrad.

- **Atmospheric turbulence:** The light beam travels through the atmosphere. Most of the signal parameters are affected by atmospheric turbulence. The source of atmospheric turbulence consists of gases, particles, molecules. Temperature, humidity, pressure has mostly affected atmospheric turbulence in both time and space. These parameters are random, so random variations of the refractive index are known as turbulence. This turbulence is different for different environments, i.e., air-water, saltwater, and space. Based on the severity of turbulence, they are categorized as weak, moderate, and strong turbulence. For medium to strong Gamma-Gamma distribution and for weak to moderate turbulence, Lognormal is proposed in this thesis.
- **Misalignment or pointing error+:** Pointing error is defined as misalignment between two nodes. In this thesis, two nodes are UAV-Ground, Ground-UAV, and UAV-UAV. FSO link performance degradation is mainly due to pointing errors. Horizontal and vertical displacement of the optical laser beam is defined as pointing error. Many researchers experimentally and theoretically analyzed the performance under pointing errors. Several mathematical models are proposed for pointing errors. In this thesis, the pointing error is mainly due to the position and orientation deviations of UAVs/HAPs. The severity of pointing error mainly depends on the position and orientation of UAVs/HAPs. Pointing error has two components: bore-sight and jitter. Bore-sight represents the displacement between the beam and aperture lens center. On the other hand, jitter defines the amount of offset randomness between the beam center and the receiver aperture.
- **Beam spreading and path losses:** Path loss is defined as the loss along with the path distance. Light beam spreads between the transmitter and receiver, and spreading loss severity depends on the distance; as the distance increases, the loss is more, and it also depends on the weather conditions. In this particular thesis, performance analysis is done concerning path loss.
- **Blockages:** These air-to-ground, ground-to-air, and air-to-air type communication systems have more obstacles, such as birds, planes, trees, tall buildings, and other factors. Especially this UAV-based FSO communications have more blockages when compared to regular FSO communications. The placing of UAV is another critical challenge with clear blockages.

1.5 Thesis Contributions

It is inferred from the above literature survey that RF-based UAVs are not suitable for high-capacity scenarios. UAVs/HAPs-based FSO Communication systems full file high capacity requirements, license-free, high security, privacy. The designing of UAV-based FSO communication systems has fundamental limitations such as weather conditions, channel modeling, UAV alignment, and blockages. Alignment is a significant limitation in FSO communications. This problem is more severe in the case of inter UAV communication systems. Different approaches are proposed to deal with this problem. Performance improvement of UAVs/HAPs-based FSO communication systems under these limitations is another important research area.

Based on the above requirements and limitations, we framed the four objectives to design and analyze UAVs/HAPs-based FSO communication systems. With proper alignment multi-rotor, Inter UAV-based FSO communication system complex channel model presented in the literature. We proposed Inter-UAV based FSO communication system channel model with simple Meijer's G functions. We proposed the HD detection technique for Inter UAV-based FSO communication system. HD detection technique is compared with existing IM/DD detection techniques. The performance of HD detection is improved by taking pointing errors into account. From this analysis, we identified that the current system has a limitation of distance. As the distance increase, the performance of the system decreases.

The goal is to design the Inter UAV-based FSO communication link for the long-range application. The current and existing proposed systems are for short-range applications is about 500m range. We Introduced the POLSK modulation for Inter UAV-based FSO communication systems. POLSK modulation is the best option for long-distance Inter UAV -based FSO communication systems. POLSK modulation-based inter UAV FSO communication system performance analysis is evaluated under different weather conditions. The results show that the performance improvement is improved under different weather conditions with increasing the receiver FOV. Inter UAV-based FSO communication system performance analysis with POLSK modulation under different weather conditions presents its results in chapters 2, 3, and 4.

In this thesis, we also presented a HAP-equipped FSO communication system performance analysis under a hovering state. First, we introduced POLSK modulation for the ground-to-HAP optical link. We improved this optical link performance by considering coding(Repetitive and BCH) schemes. This optical link performance was

validated under different weather conditions. The first time we proposed the HAP-UWOC communication system for underwater applications. In this work, we proposed a HAP-to-Ground FSO link under hovering fluctuations. Proposed link performance is evaluated under a hovering state. End-to-end link performance evaluated with DF relay. From the objectives, first, we derived the analytical channel model with Meijer's G functions. we also derived analytical expressions for the Outage probability and Average BER. We compared the analytical results with Monte-Carlo simulations.

1.6 Thesis Organization

The rest of the thesis is organized as follows.

- In chapter 2, Presents the Designed the analytical channel Model for Inter UAV-based FSO communication system using simple Meijer's G functions.
- In chapter 3, Presents the Performance analysis of Inter UAV-based FSO communication system with Different Detection techniques with pointing errors. Comparison of different detection techniques with pointing error are present in results section.
- Chapter 4 Presents the POLSK modulation based Inter UAV-based FSO communication under different weather conditions. Mitigation of different weather conditions effects by increasing Receiver FOV and its performance analysis is presented in results section proposed in 4.
- Chapter 5 Proposed the Ground-to-HAP based FSO communication system under hovering fluctuations. Performance is improved Ground-to-HAP link with suitable coding techniques under different weather conditions. coded verses uncoded system performance analysis was shown in results section of chapter 5.
- Chapter 6 Proposed the HAP-UWOC optical communication system. End-to-end performance is evaluated with DF relaying. Proposed system performance is evaluated under different channel parameters.
- Chapter 7 We concluded the thesis by identifying future directions that an interested researcher could pursue.

Chapter 2

CHANNEL MODEL

There are three basic FSO communications link scenarios with UAV platform. They are (i) Ground-UAV, (ii) UAV-Ground, and (iii) UAV-UAV or between UAVs (UAV swarm).

2.1 Introduction to UAV based FSO Channel Model

In this section, we discuss the system and channel models used throughout this thesis. Mathematical modeling is crucial in the performance analysis of UAV-based FSO communication systems. It enables the prediction of the capabilities of the system before real employment. In particular, we first present Ground-UAV-based FSO systems channel models over log-normal. Then, we describe general Gamma-Gamma distribution for optical atmospheric turbulence channel. Moreover, we introduce the general pointing error impairment model as well as its special cases.

2.1.1 Path Loss

Path loss is a crucial propagation effect as it quantifies the fluctuation in the power of a transmitted optical signal over long propagation distances [Ghassemlooy *et al.* \(2019\)](#). Path loss is a deterministic quantity and is typically represented as a function of distance d . Path loss can be modeled using Beers law as is $h_{pl} = \exp(-\beta d)$ where β is the attenuation coefficient exponent, defined as a summation of absorption and the scattering coefficients. The signal power is decaying rapidly due to path loss.

2.1.2 Modeling of FSO Atmospheric Turbulence

The irradiance of the received optical wave h is defined as

$$h = h_{pl}h_{al}h_{pp}h_{A0A} \quad (2.1)$$

where h_{pl} is the path loss effect and it is assumed to be normalized to 1, while h_{al} and h_{pp} reflect the turbulence-induced fading and the pointing error effect, respectively [Taghi Dabiri *et al.* \(2020\)](#). The fading due to the atmospheric turbulence conditions It can be viewed as the modulation of large-scale (refractive) and small-scale (diffractive) fluctuations (i.e. if the turbulence cells are larger than the beam diameter and vice versa). Mathematically, it can be written as

$$h_{al} = h_x h_y \quad (2.2)$$

where h_x and h_y are statistically independent unit mean processes representing large scale and small-scale effects, respectively. In this section, various turbulence models are visited. In specific, the irradiance h_{al} which is considered as a random variable (RV) can follow different distributions according to the turbulence conditions.

2.1.2.1 Weak Turbulence Channel Model

For weak turbulence conditions, in which large-scale fluctuations dominate, h_{al} is modeled as [Awan *et al.* \(2009\)](#)

$$h_{al} = \exp(2X), \quad (2.3)$$

where $X \sim N(\mu_X, \sigma_X^2)$ is the log-amplitude of the optical intensity such that $\sigma_X^2 \approx \frac{\sigma_R^2}{4} \approx 0.30545k^{\frac{7}{6}}C_n^2 z^{\frac{7}{6}}$. Where σ_R^2 is the Rytov variance¹ C_n^2 is the index of refraction structure parameter of atmosphere and $k = \frac{2\pi}{\lambda}$ is the optical wavenumber with λ being the wavelength then the PDF of h_{al} can be given as

$$f_{h_{al}}(h) = \frac{1}{h} \frac{1}{\sqrt{2\pi\sigma_I^2}} \exp\left(-\frac{(\ln(h) - \mu_h)^2}{2\sigma_h^2}\right) \quad (2.4)$$

where $\mu_h = 2\mu_X$ and $\sigma_h^2 = 4\sigma_X^2$ are the mean and standard deviation of h_{al} . To ensure that the average power is not amplified by fading, the irradiance is normalized.

2.1.2.2 Moderate-Strong Turbulence Channel Model

Moderate-to-strong turbulence conditions result from combined effect of the large scale and small-scale fluctuations. Hence, the second moment of irradiance can be defined as

$$\mathbb{E}[h_{al}^2] = \mathbb{E}[h_x^2]\mathbb{E}[h_y^2] \quad (2.5)$$

Since h_x and h_y are assumed to be unit mean independent random variables, then Eq. (2.5) can be written as

$$\mathbb{E}[h_{al}^2] = (1 + \sigma_{h_x}^2)(1 + \sigma_{h_y}^2) \quad (2.6)$$

where $\sigma_{h_x}^2$ and $\sigma_{h_y}^2$ are normalized variances of h_x h_y , respectively. Then, the scintillation index is expressed as

$$\sigma_{h_{al}}^2 = (1 + \sigma_{h_x}^2)(1 + \sigma_{h_y}^2) - 1 = \sigma_{h_x}^2 + \sigma_{h_y}^2 + \sigma_{h_x}^2 \sigma_{h_y}^2 \quad (2.7)$$

According to the novel work by [Taghi Dabiri *et al.* (2020)], h_x and h_y are generally modeled as Gamma random variables leading to h_{al} modeled as a Gamma-Gamma RV with a PDF given by [Al-Habash *et al.* (2001), Eq. (13)]

$$f_{h_{al}}(h) = \frac{2(\alpha\beta h)^{\frac{\alpha+\beta}{2}}}{\Gamma(\alpha)\Gamma(\beta)h} k_{\alpha-\beta}(2\sqrt{\alpha\beta h}), \quad (2.8)$$

By considering the Eq. (2.8) and from [Adamchik and Marichev (1990), Eq.(14)], we simplify as follows

$$K_v(x) = \frac{1}{2} G_{2,0}^{0,2} \left(\begin{matrix} -, - \\ \frac{v}{2}, -\frac{v}{2} \end{matrix} \middle| \frac{x^2}{4} \right), \quad (2.9)$$

The PDF in Eq. (2.8) can be rewritten as

$$f_{h_i}(h) = \frac{(\alpha_i\beta_i h)^{\frac{\alpha_i+\beta_i}{2}}}{\Gamma(\alpha_i)\Gamma(\beta_i)h} G_{0,2}^{2,0} \left(\begin{matrix} -, - \\ \frac{\alpha_i-\beta_i}{2}, -\frac{\beta_i-\alpha_i}{2} \end{matrix} \middle| \alpha_i\beta_i h \right) \quad (2.10)$$

where $G_{m,n}^{p,q}[\cdot]$ is the Meijers G-function as defined in [Jeffrey and Zwillinger (2007)], Eq.(9.301)], $\Gamma(\cdot)$ is the Gamma function defined in [Jeffrey and Zwillinger (2007), Eq.(8.310)], $K_i(\cdot)$ is the modified Bessel function of order i , α and β are the fading parameters of large-scale and small-scale fluctuations.

The nth moment of h_{al} can be derived by utilizing [Wolfram (2001), Eq. 07.34.21.0009.01] as

$$\mathbb{E}[h_{al}^n] = \frac{\Gamma(\alpha + n)\Gamma(\beta + n)}{(\alpha\beta)^n\Gamma(\alpha)\Gamma(\beta)}, \quad (2.11)$$

and the second moment can be written as

$$\mathbb{E}[h_{al}^2] = \left(1 + \frac{1}{\alpha}\right)\left(1 + \frac{1}{\beta}\right). \quad (2.12)$$

Comparing Eq. (2.6) and Eq. (2.12), the following relations are trivial

$$\alpha = \frac{1}{\sigma_{h_x}^2}, \beta = \frac{1}{\sigma_{h_y}^2}, \quad (2.13)$$

$$\sigma_{al}^2 = \frac{1}{\alpha} + \frac{1}{\beta} + \frac{1}{\alpha\beta}, \quad (2.14)$$

The variances of small-scale and large-scale fluctuations are expressed in terms of the Rytov variance in [Al-Habash *et al.* (2001), Eqs. (18) and Eq. (19)]. In the case of plane wave as an example, the turbulence parameters α and β can

$$\alpha = \left[\exp\left(\frac{0.94\sigma_R^2}{(1 + 1.11\sigma_R^{12/5})7/6}\right) - 1 \right]^{-1}$$

$$\beta = \left[\exp\left(\frac{0.51\sigma_R^2}{(1 + 0.69\sigma_R^{12/5})7/6}\right) - 1 \right]^{-1}$$

2.1.3 Pointing Error Impairments Mathematical Modeling

Assuming Gaussian beam with initial beam waist, w_0 , and radius of curvature, F_0 , propagating through atmospheric turbulence of distance z , the beam waist at the receiver of radius a in long term, w_z , can be defined [Andrews and Phillips (2005), Eq. 45, p.238]. Given a radial displacement r , the fraction of collected power at distance z can be approximated by

$$h_{pp}(r : z) \approx A_0 \exp\left(-\frac{2r^2}{W_{Zeq}^2}\right), \quad (2.15)$$

where W_{Zeq}^2 is bandwidth of the receiver is the equivalent beamwidth defined, $W_{Zeq}^2 = W_z^2 \frac{\sqrt{A_0\pi}}{2v \exp(-v^2)}$ such that $A_0 = [\text{erf}(v)]^2$ is the maximum fraction of the collected

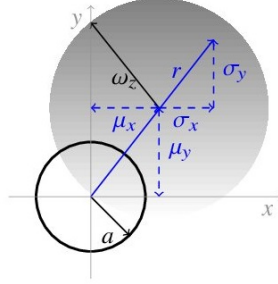


Figure 2.1: Zero boresight: no misalignment:
Farid and Hranilovic (2007)

power (i.e. the fraction of power at $r = 0$), $v = \sqrt{\frac{a^2\pi}{2W_z}}$, is the ratio between the aperture radius a and the beamwidth W_z . It is important to note that the approximation in Eq. (2.15) is valid when $W_z > 6a$ [Andrews and Phillips (2005)]. At the receiver, the radial displacement vector can be expressed as $r = [xy]^T$, where x and y represent the vertical and horizontal displacements of the beam in the detector plane. Thus, the distribution of $r = |r| = \sqrt{x^2 + y^2}$. Depends on the distribution of x and y . Assuming independent Gaussian displacements along the horizontal and elevation axes, then r can be distributed according to the following distributions.

2.1.3.1 Beckmann Distribution

The Beckmann distribution is a versatile model that includes many distributions as special cases. It is a four-parameter distribution modeling the envelope of two independent Gaussian RVs. In our case, if both displacements are nonzero mean Gaussian RVs with different jitters, i.e. $x \sim \mathcal{N}(\mu_x, \sigma_x)$ and $y \sim \mathcal{N}(\mu_y, \sigma_y)$ then $r = |r| = \sqrt{x^2 + y^2}$ follows the Beckmann distribution [Simon and Alouini (2005), Eq. 2.37], [Ghassemlooy *et al.* (2019), Eq. (31)], with PDF given by

$$f_r(r) = \frac{r}{2\pi\sigma_x\sigma_y} \int_0^{2\pi} \exp\left(-\frac{(r\cos\theta - \mu_x)^2}{2\sigma_x^2} - \frac{(r\sin\theta - \mu_y)^2}{2\sigma_y^2}\right) d\theta \quad (2.16)$$

With the PDF of r , we can calculate the n th moment of h_{pp} defined in Eq. (2.15) as

$$\mathbb{E}[h_{pp}^n] = A_0^n \mathcal{M}_{r,2} \left(-\frac{2r}{W_{zeq}^2} \right), \quad (2.17)$$

where $\mathcal{M}_{r^2}(\cdot)$ is the moment-generating function of the random variable r^2 and given by [Ghassemlooy *et al.* (2019), Eq. (2.38)]

$$\mathcal{M}_{r^2}(s) = \frac{1}{\sqrt{(1 - \sigma_x s)(1 - \sigma_y s)}} \exp\left(\frac{\mu_x^2 s}{1 - 2\sigma_x^2 s} + \frac{\mu_y^2 s}{1 - 2\sigma_y^2 s}\right), \quad (2.18)$$

Therefore, the n th moment of h_{pp} becomes in this case

$$\mathbb{E}[h_{pp}^n] = \frac{A_0^n \tau_x \tau_y}{\sqrt{(n + \tau_x^2)(n + \tau_y^2)}} \exp\left(-\frac{2n}{W_{zeq}^2} \left[\frac{\mu_x^2}{1 + \frac{n}{\tau_x^2}} + \frac{\mu_y^2}{1 + \frac{n}{\tau_y^2}}\right]\right). \quad (2.19)$$

where $\mu_x^2 = \frac{W_{zeq}}{2\sigma_x}$ and $\mu_y^2 = \frac{W_{zeq}}{2\sigma_y}$, are the ratio between the equivalent beam width and the jitter variance for each direction.

2.1.3.2 Rayleigh Distribution

When both displacements have zero mean and common variance, i.e. $\mu_x = \mu_y = 0$ and $\sigma_x = \sigma_y = \sigma$ as illustrated in Fig.2.2, r is a Rayleigh distributed RV whose PDF is given by

$$f_r(r) = \frac{r}{\sigma^2} \exp\left(-\frac{r^2}{2\sigma^2}\right), \quad (2.20)$$

The PDF of h_{pp} reduces in this case to [Farid and Hranilovic (2007)].

$$f_{h_{pp}}(h_{pp}) = \frac{\tau^2}{A_0^{\tau^2}} h_{pp}^{\tau^2-1}, \quad (2.21)$$

where $\tau = \frac{W_{zeq}}{2\sigma}$ The n th moment can be deduced from Eq. (2.19) as

$$\mathbb{E}[h_{pp}^n] = \frac{A_0^n \tau^2}{n + \tau^2}. \quad (2.22)$$

2.1.4 Link Interruption due to AOA Fluctuations

We are able to assume that h_{pp} takes two discrete values 1 and 0 to determine if the incident optical signal is located on the receivers FOV or not and hence, it can be formulated as

$$h_{AoA} = \begin{cases} 1 & \text{for } \theta_a \leq \theta_{FOV} \\ 0 & \text{for } \theta_a \geq \theta_{FOV} \end{cases} \quad (2.23)$$

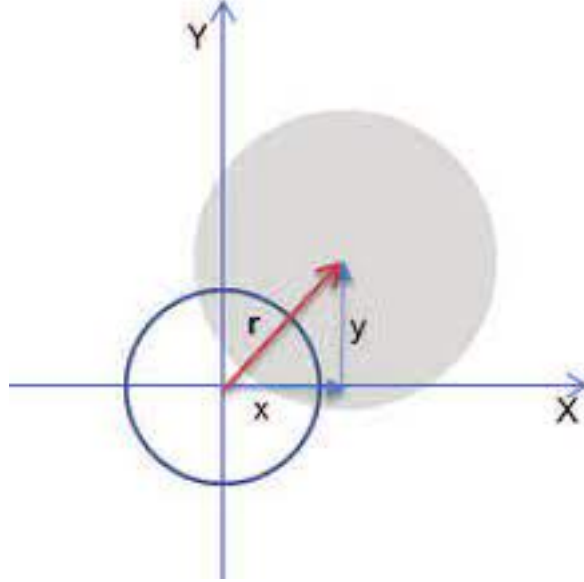


Figure 2.2: Bi-Directional misalignment: zero bore sight and identical jitters
Farid and Hranilovic (2007)

where θ_a is The incidence angle relative to the receiver axis is called the AoA of the signal and it is obtained as $\theta_a = \sqrt{(\theta_{tx} + \theta_{rx})^2 + (\theta_{ty} + \theta_{ry})^2}$ which has a Rayleigh distribution a

$$f_{\theta_a}(\theta_a) = \frac{\theta_a}{\sigma_{to}^2 + \sigma_{ro}^2} \exp\left(-\frac{\theta_a^2}{2(\sigma_{to}^2 + \sigma_{ro}^2)}\right), \theta_a \geq 0. \quad (2.24)$$

When an incident beam with small value of θ_a is passed through a lens, the outside angle of beam will be approximately unaltered [Gagliardi and Karp (1976)]. Moreover, the fraction of power in the side lobes of Airy pattern (beam footprint at the PD has an Airy Pattern) is much smaller than that in the main lobe. Hence, ignoring the effect of power from the side lobes of Airy pattern can be a reasonable assumption [Gagliardi and Karp (1976)]. The width of the main lobe of the Airy pattern is approximately equal to 2.4λ and it is much smaller than the conventional sizes of the PD radius that is commonly in order of mm [Gagliardi and Karp (1976)]. This highly permits us to ignore the effects at boundary condition From Eq. (2.23) and Eq. (2.24), the PDF of

h_{pa} is obtained as

$$f_{h_{AoA}} = \exp\left(\frac{-\theta_{FOV}}{2(\sigma_{to}^2 + \sigma_{ro}^2)}\right)\delta(h_{AoA}) + \left[1 - \exp\left(\frac{-\theta_{FOV}}{2(\sigma_{to}^2 + \sigma_{ro}^2)}\right)\right]\delta(h_{AoA} - 1). \quad (2.25)$$

2.2 Modeling of Composite Channels

In this section, the combined effect of pathloss, turbulence and pointing errors is presented. the turbulence is modeled by GG and the pointing error is modeled by the Rayleigh distribution. In specific, the joint distribution of $h' = h_{pl}h_{al}h_{pp}$ Here, h_{pl} stands for path loss. It depends on the distance, which is a deterministic term, h_{pp} pointing error due to UAV's position and orientation deviations due to hovering state and h_{al} represents the turbulence-induced fading which is a random variable. The combined effect of weak turbulence h' Can be represented as [Safi *et al.* (2019b), Alzenad *et al.* (2018b)] with respect to UAV-UAV-FSO was derived in [Adamchik and Marichev (1990)]. h' is defined and it's PDF is

$$f_{h'}(h') \approx \int \frac{1}{h_{pl}h_{al}} f_{h_{pp}}\left(\frac{h'}{h_{pl}h_{al}}\right) f_{h_{al}}(h_{al}) dh_{al}, \quad (2.26)$$

Using [Farid and Hranilovic (2007)] and [Dabiri *et al.* (2018b), Eqs. (11)], h_{pp} is given as

$$h_{pp} \approx A_0 e^{-\frac{2(x_t+x_r+Z\theta_{tx})^2+(y_t+y_r+Z\theta_{ty})^2}{w_{zeq}^2}}, \quad (2.27)$$

From Eq. (2.27), the PDF of h_{pp} is obtained as

$$f_{h_{pp}}(h_{pp}) = \frac{\tau}{A_0^\tau} h_{pp}^{\tau-1} \quad (2.28)$$

Where $A_0 = [erf(\nu)]^2$ is received optical power. ν is defined by $\nu = \sqrt{\frac{\pi}{2}} \frac{a}{w_z}$, a is receiver radius and w_z is the beam width at the distance L , effective beam width at the link end. $w_{zeq} = \left[\frac{\sqrt{\pi} erf(\nu) w_z^2}{2\nu e^{-\nu^2}}\right]^{\frac{1}{2}}$. Here, $\tau = \frac{w_{zeq}^2}{4(L^2\sigma_{to}^2 + \sigma_{rp}^2 + \sigma_{tp}^2)}$. is due to position, orientations fluctuations of UAV. Erfc(.) is the complementary error function. Here, $\mu = 2\sigma_R^2(1 + 2\tau)$, Here, h' denotes the channel attenuation due to path loss, atmospheric turbulence, and misalignment fading for weak turbulence case.

For moderate to strong turbulence conditions, the channel can be expressed and derived in [Farid and Hranilovic \(2007\)](#), concerning the Inter UAV-based FSO link was derived in [[Dabiri *et al.* \(2019b\)](#)].

$$f_{h'}(h') \approx \int \frac{1}{h_{pl}h_{al}} f_{h_{pp}}\left(\frac{h'}{h_{pl}h_{al}}\right) f_{h_{al}}(h_{al}) dh_{al} \quad (2.29)$$

from [Dabiri and Sadough \(2019b\)](#) it is defined as

$$f_{h'}(h') = \frac{2\tau(\alpha\beta)^{\frac{\alpha+\beta}{2}} h'^{\tau-1}}{A_0^\tau h_{pl}^\tau \Gamma(\alpha)\Gamma(\beta)} \int_{\frac{h'}{h_{pl}A_0}}^{\infty} h_{al}^{\frac{\alpha+\beta}{2}-\tau-1} k_{\alpha-\beta}(2\sqrt{\alpha\beta h_{al}}) dh_{al} \quad (2.30)$$

By considering the Eq. (2.30) and from [[Adamchik and Marichev \(1990\)](#), Eq.(14)] we simplify as follows

$$K_v(x) = \frac{1}{2} G_{2,0}^{0,2} \left(\begin{matrix} -, - \\ \frac{v}{2}, -\frac{v}{2} \end{matrix} \middle| \frac{x^2}{4} \right) \quad (2.31)$$

$$f_{h'}(h') = \frac{2\tau(\alpha\beta)^{\frac{\alpha+\beta}{2}} h'^{\tau-1}}{A_0^\tau h_{pl}^\tau \Gamma(\alpha)\Gamma(\beta)} \int_{\frac{h'}{h_{pl}A_0}}^{\infty} h_{al}^{\frac{\alpha+\beta}{2}-\tau-1} * \frac{1}{2} G_{0,2}^{2,0} \left(\begin{matrix} -, - \\ \frac{\alpha-\beta}{2}, -\frac{\beta-\alpha}{2} \end{matrix} \middle| \alpha\beta h_a \right) dh_{al} \quad (2.32)$$

From [[Wolfram \(2001\)](#), eq.(07.34.21.0085.01)] and after simplifications

$$f_{h'}(h') = \frac{\tau\alpha\beta}{A_0 h_{pl} \Gamma(\alpha)\Gamma(\beta)} \left(\frac{\alpha\beta h'}{A_0 h_{pl}} \right)^{\frac{\alpha+\beta}{2}-1} G_{1,3}^{3,0} \left(\begin{matrix} 1 + \tau - \frac{\alpha+\beta}{2} \\ \tau - \frac{\alpha+\beta}{2}, \frac{\alpha-\beta}{2}, \frac{\beta-\alpha}{2} \end{matrix} \middle| \frac{\alpha\beta h'}{A_0 h_{pl}} \right). \quad (2.33)$$

This can be further simplified by considering [[Wolfram \(2001\)](#), eq.(07.34.16.0001.01)] along with some mathematical simplifications the PDF of h' for weak to moderate turbulence case the PDF of h' derived as

$$f_{h'}(h') \approx \frac{\tau}{2(A_0 h_{pl})^\tau} h'^{\tau-1} \operatorname{erfc} \left(\frac{\ln\left(\frac{h'}{A_0 h_{pl}} + \mu\right)}{\sqrt{8}\sigma_R} \right) e^{2\sigma_R^2 \tau(1+\tau)}. \quad (2.34)$$

In this thesis, the channel model h is taken as product of h_{pl} , h_{al} , h_{pp} , and h_{AOA} so

we have h' and h_{AOA} both are independent and it's PDF approximated as.

$$f_h(h) \approx \int \frac{1}{h'} f_{h_{AOA}}(h/h') f_{h'}(h') dh', \quad (2.35)$$

2.3 Inter UAV-based FSO Communication System Channel Model

2.3.1 Inter UAV-based FSO link with Log-normal channel

To derive the complete channel model with weak to moderate turbulence (Log-normal distribution) case by substituting Eq. (2.25) and Eq. (2.34) in Eq. (2.35), thus we get After solving the Eq. (2.35), the closed-form channel model between the Inter UAV-based FSO link under log-normal fading channel function of θ_{FOV} can be expressed below.

$$f_h(h) \approx a_1 \delta(h) + f_h(h > 0), \quad (2.36)$$

where

$$a_1 = \exp\left(\frac{-\theta_{FOV}^2}{2(\sigma_{to}^2 + \sigma_{ro}^2)}\right),$$

$$f_h(h > 0) = \left[1 - \exp\left(\frac{-\theta_{FOV}^2}{2(\sigma_{to}^2 + \sigma_{ro}^2)}\right)\right] D1$$

$$h'^{\tau-1} \operatorname{erfc}\left(\frac{\ln\left(\frac{h'}{A_o h_{pl}} + \mu\right)}{\sqrt{8}\sigma_R}\right),$$

where

$$D1 = e^{2\sigma_R^2\tau(1+\tau)} \frac{\tau}{2(A_o h_{pl})^\tau},$$

2.3.2 Inter UAV-based FSO link with Gamma-Gamma turbulence channel

By considering Eq. (2.32), we derived closed-form expression using Meijer's G functions. By considering the reference [Taghi Dabiri *et al.* (2020)], [Sandalidis *et al.* (2009a)-Farid and Hranilovic (2007)], the result in Eq. (2.33) and the Eq. (2.34) by substituting in Eq. (2.35), we get below.

α and β are the fading parameters. After simplifying the above Eq. (2.35), we get result is

$$f_h(h) \approx a_1 \delta(h) + f_h(h > 0), \quad (2.37)$$

where

$$a_1 = \exp\left(\frac{-\theta_{FOV}^2}{2(\sigma_{to}^2 + \sigma_{ro}^2)}\right),$$

$$f_h(h > 0) = \left[1 - \exp\left(\frac{-\theta_{FOV}^2}{2(\sigma_{to}^2 + \sigma_{ro}^2)}\right)\right] * D2 * G_{1,3}^{3,0}\left(\tau \left| \frac{\alpha\beta h'}{A_0 h_l} \right.\right),$$

where

$$D2 = \frac{\alpha\beta\tau}{A_0 h_{pl} \Gamma(\alpha) \Gamma(\beta)},$$

2.4 Ground-to-HAP Channel Model

The channel state consider to be the product of four factors and briefly explained as

$$h = h_l h_a h_p h_f. \quad (2.38)$$

where $h' = h_l h_a h_p$. Here, h_l stands for loss of direction, which is a deterministic term. h_p pointing error, which is a random quantity and is distributed by Rayleigh. In particular, we presume that the pointing error is due to the random HAP movement. The random attenuation between Ground-to-HAP due to atmospheric turbulence is h_a . The h_f is the Rayleigh distributed random variable which depends on the receiver FOV.

2.4.1 Atmospheric Loss

The atmospheric loss follows the exponential Beers-Lambert law as path loss, described as below, with a Length of L

$$h_l = \exp(-LF) \quad (2.39)$$

Where the path-loss is h_l . F is the coefficient of attenuation, which depends on the visibility range in meters.

2.4.1.1 Fog Attenuation

Several experimental and theoretical results showed that Fog is the main limiting factor in FSO communication systems. Evaluating the performance of Ground -HAP based FSO communication system under different weather conditions is an important research direction. Under dense Fog condition, the loss around 350dB/km, and we evaluated under moderate to light fog conditions. The availability of this link is mainly dependent on Fog and rain. In this chapter, we evaluated the system performance by considering mitigation techniques under moderate to light fog conditions. The performance of the system improved under Moderate to light Fog condition by considering optimal values of Reciever FOV. The new results are shown in this chapter for vertical Ground-to-HAP link under varying weather conditions. Different analytical models are proposed to evaluate the performance of the system under Fog's condition. In this chapter, we consider the Mie scattering attenuation coefficient, which depends on visibility, as shown below [Kaushal and Kaddoum \(2016\)](#), [Ghassemlooy *et al.* \(2019\)](#)

$$F = 4.34 \left[\frac{3.91}{V} \left(\frac{\lambda}{550} \right)^{-q} \right] S, \quad (2.40)$$

Where visibility is V , λ means wavelength. S represents the distance along which the scattering phenomena occurs in km. $S = \Delta S_{fog} / \sin \phi$ q is the scattering distribution coefficient of size that can be found by the model of Kim, which gives the values below. Eq. (2.41) is the same as one obtained in [[Alzenad *et al.* \(2018b\)](#), Eq. (1)],

$$h_f = \begin{cases} 1.6, & \text{for } V > 50km \\ 1.3, & \text{for } 6km < V < 50km \\ 0.585V^{1/3}, & \text{for } V < 6km \end{cases} \quad (2.41)$$

2.4.1.2 Rain Attenuation

Rain is another important limiting factor for optical links, and it depended on the rainfall rate M [mm/h]. The Eq. (2.41) is the same as one obtained in [[Alzenad *et al.* \(2018b\)](#), Rain Attenuation section]. Rain attenuation in dB is follows as

$$\beta_{rain} = 1.076 * M^{0.67} b_{rain}, \quad (2.42)$$

where $b_{rain} = \Delta * b_{rain} / \sin(\phi)$, $\Delta * b_{rain}$ is the rain layer thickness and ϕ is the elevation angle. In the Ground-to-HAP-based FSO link, its loss ranges from 2dB /

Table 2.1: Attenuation Coefficients at 1550 nm between Ground-to-HAP FSO Link

Weather condition	Attenuation F (dB/km)	Visibility(m)
Dense fog	271.66	50
Thick fog	59.57	200
Moderate fog	20.99	500
Light fog	12.65	770
Very Light fog	4.22	1900

km to 10dB / km. By considering the adequate receiver FOV under rain conditions, we improved the Ground-to-HAP-based FSO link's performance. The rain attenuation parameters based on adapted analytical methods proposed for FSO communication by the International Telecommunication Union-Radio communication Sector (ITU-R) have been evaluated. We have modified the same Ground-to-HAP-based FSO link parameter, as shown below. This chapter adopted the parameter values for light rain and strong rain conditions, shown in Table 2.1. Here Weather constituents (mm/h) are for strong rain 25 and light rain 2.5 based on reference [Ghassemlooy *et al.* \(2019\)](#).

2.4.1.3 Cloud Attenuation

Cloud is another affecting factor for HAP optical link. Cloud visibility can be obtained as $V = 1.002/(LWC * N)^{0.6473}$, where height, number density (N), liquid water contents(LWC), water droplet size and horizontal distribution extent. Based on cloud visibility, we can estimate the cloud attenuation with the help of Eq. (2.39) for different layers. In this chapter, we adapted the reference [Awan *et al.* \(2009\)](#).

2.4.2 Atmospheric Turbulence Channel

This chapter analysis Ground-to-HAP channel modeled as GG turbulence-induced fading for moderate to strong turbulence conditions, and its PDF is defined as

$$f_{GG}(h_a) = \frac{2(\alpha\beta)^{\frac{\alpha+\beta}{2}}}{\Gamma(\alpha)\Gamma(\beta)} h_a^{\frac{\alpha+\beta}{2}-1} k_{\alpha-\beta}(2\sqrt{\alpha\beta h_a}), \quad (2.43)$$

where α , β are small scale and large scale fluctuations. $\Gamma(\cdot)$ well know gamma random variable and $K_v(\cdot)$ modified Bessel function of order two. α and β defined as below

$$\alpha = \left[\exp\left(\frac{0.49\sigma_{rs}^2}{(1 + 0.56\sigma_{rs}^2)^{12/6}}\right) - 1 \right]^{-1}$$

$$\beta = \left[\exp\left(\frac{0.51\sigma_{rs}^2}{(1 + 0.69\sigma_{rs}^2)^{12/6}}\right) - 1 \right]^{-1}$$

where σ_{rs}^2 is Rytov variance. In this Ground-to-HAP model, transmitter and receiver are not at the same heights, and it's Rytov variance defined as

$$\begin{aligned} \sigma_{rs}^2 &= 2.25 \left(\frac{2\pi}{\lambda}\right)^{\frac{7}{6}} \left(H - h_0\right)^{\frac{5}{6}} \sec(\zeta)^{\frac{11}{6}} \\ &\int_{h_0}^H C_n^2(k) \left(1 - \frac{k - h_0}{H - h_0}\right)^{\frac{5}{6}} \left(\frac{k - h_0}{H - h_0}\right)^{\frac{5}{6}} dk . \end{aligned} \quad (2.44)$$

2.4.3 Misalignment Fading

Consider the Gaussian beam is propagated through the channel with an optical beamwidth of W_z . Optical beam received at the receiver with a circular detector aperture of radius r_a and collecting area with an angle θ_s . In this Ground-HAP link, we considered both beam wandering effects and it's instantaneous position, Orientation fluctuations taken into account. Based on the reference the PDF of pointing error loss h_p conditions on θ_s can be given below [Dabiri *et al.* \(2018b\)](#), [Yang *et al.* \(2014\)](#), [Jung *et al.* \(2020\)](#).

$$f_{h_p/\theta_s}(h_p) = \left[2\left(\frac{r_a}{W_z^2}\right)^2\right]^{-\gamma^2} \gamma^2 h_p^{\gamma^2-1} \cos(\theta_s) \quad (2.45)$$

where, $\gamma = \frac{W_z}{2\sigma_{ro}}$, W_z is the beam radius, $\sigma_{ro} = \sigma_w + \sigma_p$ HAP beam wandering and instantaneous position fluctuations. $W_z = w_0 \left[1 + \epsilon \left(\frac{\lambda L}{\pi w_0^2}\right)^2\right]^{\frac{1}{2}}$, where w_0 is beam width at $Z = 0$, $w_0 = \frac{D}{\sqrt{2\pi}}$, D is transmitter aperture diameter. $\epsilon = (1 + 2w_0^2/\rho_0^2)$, $\rho_0^2 = \int_{h_0}^H (0.55C_n^2(k)(\frac{2\pi}{\lambda})^2 k)^{-3/5} dk$ is the coherence length.

The combined channel model PDF of $h' = h_l h_a h_p$ conditioned on θ_s can be repre-

sented as

$$\begin{aligned} f_{h'/\theta_s}(h') &= \int f_{h'/\theta_s, h'}(h') f_{h_a}(h_a) dh_a \\ &= \int \frac{1}{h_l h_a} f_{h'/\theta_s}(h'/h_l h_a) f_{h_a}(h_a) dh_a. \end{aligned} \quad (2.46)$$

By substituting Eq. (2.43) and Eq. (2.45) in Eq. (2.46) and after some mathematical manipulations, the analytical expression for GG atmospheric turbulence model is derived by using Meijer's G functions. The closed-form expression for $f_{h'/\theta_s}(h')$ is given by

$$f_{h'/\theta_s}(h') = \frac{\left[2\left(\frac{r_a}{W_z^2}\right)^2\right]^{-\gamma^2} \alpha \beta \gamma^2 \cos(\theta_s)}{h_l \Gamma(\alpha) \Gamma(\beta)} G_{1,3}^{3,0} \left(\begin{matrix} \gamma^2 \\ \gamma^2 - 1, \alpha - 1, \beta - 1 \end{matrix} \middle| \frac{\alpha \beta h'}{h_l} \right), \quad (2.47)$$

2.4.4 Angle Of Arrival Fluctuations

The received optical beam is collected by a circular photodetector(PD). by the inherent nature of the aerial node, the angle of arrival of the optical beam deviated from their mean position due to random orientation deviations of the aerial node. These orientation deviations of an aerial node are approximated as Rayleigh distributed and detail derivation is derived in [Kaaan *et al.* \(2014\)](#). Total optical power received if the Optical beam within the receiver FOV, i.e., $\theta_z \leq FOV$. By neglecting the effect of side lobes the approximated h_f can be defined as follows. [Dabiri *et al.* \(2018b\)](#), [Dabiri *et al.* \(2019b\)](#)

$$h_f = \begin{cases} 1, & \text{if } \theta_z \leq FOV. \\ 0, & \text{if } \theta_z > FOV. \end{cases} \quad (2.48)$$

$$\begin{aligned} f_{h_f} &= \exp\left(\frac{-\theta_{FOV}^2}{2\sigma_{rd}^2}\right) \delta(h_f) \\ &+ \left[1 - \exp\left(\frac{-\theta_{FOV}^2}{2\sigma_{rd}^2}\right)\right] \delta(h_f - 1), \end{aligned} \quad (2.49)$$

where $\delta(\cdot)$ is the Dirac delta function, σ_{rd} is the variance of the orientation deviations of the UAV, θ_{FOV} is the receiver Field-of-view (FOV) respectively.

2.4.5 Combined Channel Model

The combined analytical channel model was obtained by substituting Eq. (2.47) and Eq. (2.49) into Eq. (2.50) and assuming $\cos(\theta_s) \approx 1$. By simplifying the above equation, the closed-form channel model between ground-to-HAP link can be derived with Meijer's G functions as follows

$$f_h(h) \approx \int \frac{1}{h'} f_{h_f}(h/h') f_{h'}(h') dh', \quad (2.50)$$

$$f_h(h) \approx d_2 \delta(h) + f_h(h > 0), \quad (2.51)$$

where

$$d_2 = \exp\left(\frac{-\theta_{FOV}^2}{2\sigma_{rd}^2}\right),$$

$$f_h(h > 0) = \left[1 - \exp\left(\frac{-\theta_{FOV}^2}{2\sigma_{rd}^2}\right)\right] * b_2 * G_{1,3}^{3,0}\left(\begin{matrix} \gamma^2 \\ \gamma^2 - 1, \alpha - 1, \beta - 1 \end{matrix} \middle| \frac{\alpha\beta h}{h_l}\right),$$

$$b_2 = \frac{\left[2\left(\frac{r_a}{W_z}\right)^2\right]^{-\gamma^2} \alpha\beta\gamma^2}{h_l \Gamma(\alpha)\Gamma(\beta)}.$$

2.5 HAP-to-Ground Link Channel Model

In this section, we explored the end-to-end channel models used for HAP and UWOC links, respectively. The HAP-to-Ground channel model under hovering fluctuations by considering four factors into account is defined as

$$h_{s,r} = h_{pl} h_{al} h_{pp} h_{AoA} \quad (2.52)$$

Here $h' = h_{pl} h_{al} h_{pp}$, Where h_{pl} stands for slant path link path loss coefficient. It mainly depends on the different weather conditions, which is not a random quantity. h_{pp} is the pointing error due to HAP fluctuations at the hovering state. h_{al} represents the turbulence-induced fading which is a random variable GG distributed S-R node

link.

2.5.1 Path Loss

The path loss for slant path by exponential Beers-Lambert law as

$$h_l = \exp(-L_1 F) \quad (2.53)$$

Where L_1 distance S-R node link length, F is the attenuation coefficient.

2.5.2 Atmospheric Turbulence Channel

A more tractable and analytical channel model between Ground-to-HAP by using the GG turbulence channel model was proposed in [Safi *et al.* (2020)]. Here we adapted the same analysis and proposed HAP-to-Ground channel model as GG turbulence-induced fading, and its PDF is defined as

$$f_{GG}(h_a) = \frac{2(\alpha_1 \beta_1)^{\frac{\alpha_1 + \beta_1}{2}}}{\Gamma(\alpha_1) \Gamma(\beta_1)} h_a^{\frac{\alpha_1 + \beta_1}{2} - 1} K_{\alpha_1 - \beta_1}(2\sqrt{\alpha_1 \beta_1 h_a}), \quad (2.54)$$

where α_1, β_1 are turbulence fluctuations. $\Gamma(\cdot)$ gamma random variable, and $K_v(\cdot)$ Bessel function of order two. α and β defined as below

$$\alpha_1 = \left[\exp\left(\frac{0.49\sigma_{rs}^2}{(1 + 1.11\sigma_{rs}^{12/6})^{7/6}}\right) - 1 \right]^{-1}$$

$$\beta_1 = \left[\exp\left(\frac{0.51\sigma_{rs}^2}{(1 + 0.69\sigma_{rs}^{12/6})^{5/6}}\right) - 1 \right]^{-1}$$

where σ_{rs}^2 is Rytov variance. In this HAP-to-Ground model, S and R are not at the same heights, and its Rytov variance defined as

$$\sigma_{rs}^2 = 2.25 \left(\frac{2\pi}{\lambda}\right)^{\frac{7}{6}} \left(H - h_0\right)^{\frac{5}{6}} \sec(\varsigma)^{\frac{11}{6}} \int_{h_0}^H C_n^2(k) \left(\frac{k - h_0}{H - h_0}\right)^{\frac{5}{6}}. \quad (2.55)$$

2.5.3 Misalignment Fading

The pointing error mainly depends on HAP instantaneous position, Orientation fluctuations, and beam wandering effect. In the HAP-to-Ground channel, we considered Gaussian beam with an optical beamwidth of W_z . An optical beam is propagated through S to R. This optical beam is received at R and a detector aperture of radius r_a with an angle θ_s . Based on results in [Safi *et al.* (2020)], [Dabiri *et al.* (2019b)], [Dabiri and Sadough (2019b)], pointing loss h_p condition on θ_s its PDF of HAP-to-Ground can be written as

$$f_{h_p/\theta_s}(h_p) = \left[2 \left(\frac{r_a}{W_z^2} \right)^2 \right]^{-\gamma_1^2} \gamma_1^2 h_p^{\gamma_1^2 - 1} \cos(\theta_s) \quad (2.56)$$

where, $\gamma_1 = \frac{W_z}{2\sigma_{ro}}$, W_z is the beam radius, $\sigma_{ro} = \sigma_w + \sigma_{tp} + L\sigma_{to}$, HAP beam wandering, instantaneous position and orientation fluctuations variance of the HAP. $W_z = w_0 \left[1 + \epsilon \left(\frac{\lambda L}{\pi w_0^2} \right)^2 \right]^{\frac{1}{2}}$, where w_0 is beam width at $Z = 0$, $w_0 = \frac{D}{\sqrt{2\pi}}$, D is transmitter aperture diameter. $\epsilon = (1 + 2w_0^2/\rho_0^2)$, $\rho_0^2 = \int_{h_0}^H (0.55C_n^2(k)(\frac{2\pi}{\lambda})^2 k)^{-3/5} dk$ is the coherence length.

The HAP-to-Ground channel PDF of $h' = h_l h_a h_p$ conditioned on θ_s can be written as

$$f_{h'/\theta_s}(h') = \int f_{h'/\theta_s, h'}(h') f_{h_a}(h_a) dh_a \quad (2.57)$$

$$= \int \frac{1}{h_l h_a} f_{h'/\theta_s}(h'/h_l h_a) f_{h_a}(h_a) dh_a.$$

By substituting Eq. (2.54), Eq. (2.56) in Eq. (2.57) and by simplifying above Eq. (2.57) the analytical expression for HAP-to-Ground channel model GG atmospheric turbulence is derived by using Meijer's G functions. The results expression for $f_{h'/\theta_s}(h')$ is follows as

$$f_{h'/\theta_s}(h') = \frac{\left[2 \left(\frac{r_a}{W_z^2} \right)^2 \right]^{-\gamma_1^2} \alpha_1 \beta_1 \gamma_1^2 \cos(\theta_s)}{h_l \Gamma(\alpha_1) \Gamma(\beta_1)} G_{1,3}^{3,0} \left(\begin{matrix} \gamma_1^2 \\ \gamma_1^2 - 1, \alpha_1 - 1, \beta_1 - 1 \end{matrix} \middle| \frac{\alpha_1 \beta_1 h'}{h_l} \right), \quad (2.58)$$

2.5.4 Angle Of Arrival Fluctuations

The HAP is hovering above the earth; the optical beam is received at the R node by a circular PD. The received beam is highly affected by the orientation deviation of the S node. Due to this orientation deviation, the AOA of the optical beam deviated from the there mean position of the detector at the R node. Due to the high stability of the S node, orientation deviations are assumed to be the order of mrad. This orientation deviation of the S node to R node is modeled as Rayleigh distributed, and its brief explanation is given in [Dabiri *et al.* (2020)], [Dabiri and Sadough (2019b)], [Kaymak *et al.* (2018)]. The optical power received at the R node within the R node FOV, i.e., $\theta_z \leq FOV$ then the total power captured by the R node. If R node received optical beam is outside the R node FOV, i.e., $\theta_z > FOV$ and the fading at R node approximated h_f as

$$h_f = \begin{cases} 1, & \text{if } \theta_z \leq FOV. \\ 0, & \text{if } \theta_z > FOV. \end{cases} \quad (2.59)$$

$$f_{h_f} = \exp\left(\frac{-\theta_{FOV}^2}{2\sigma_{rd}^2}\right)\delta(h_f) + \left[1 - \exp\left(\frac{-\theta_{FOV}^2}{2\sigma_{rd}^2}\right)\right]\delta(h_f - 1), \quad (2.60)$$

where $\delta(\cdot)$ is the Dirac delta function, HAP node orientation deviations variance σ_{rd} , θ_{FOV} is the R node Field-of-view (FOV) respectively.

2.5.5 Combined Channel Model

The composite analytical channel model was obtained by substituting Eq. (2.58) and Eq. (2.60) into Eq. (6.3) and assuming $\cos(\theta_s) \approx 1$. For Ground-to-HAP link Outage probability analytical expression is derived in [Safi *et al.* (2020)]. After some mathematical manipulations, the closed-form PDF between S node to R node-link can be derived with Meijer's G functions as

$$f_{h_1}(h) \approx \int \frac{1}{h'} f_{h_f}(h/h') f_{h'}(h') dh', \quad (2.61)$$

$$f_{h_1}(h) \approx d_2 \delta(h) + f_h(h > 0), \quad (2.62)$$

where

$$d_2 = \exp\left(\frac{-\theta_{FOV}^2}{2\sigma_{rd}^2}\right),$$

$$f_h(h > 0) = [1 - d_2] * b_2 * G_{1,3}^{3,0}\left(\gamma_1^2 \gamma_1^2 - 1, \alpha_1 - 1, \beta_1 - 1 \left| \frac{\alpha_1 \beta_1 h_{s,r}}{h_l}\right.\right),$$

$$b_2 = \frac{\left[2\left(\frac{r_a}{W_z^2}\right)^2\right]^{-\gamma_1^2} \alpha_1 \beta_1 \gamma_1^2}{h_l \Gamma(\alpha_1) \Gamma(\beta_1)}.$$

By using [[Adamchik and Marichev (1990)], Eq.26] and [[Jeffrey and Zwillinger (2007)], section.9.31] After simplifying The cumulative distribution function (CDF) of Eq. (6.4) is expressed as

$$F_{h1}(h) \approx d_3 + f_h(h > 0), \quad (2.63)$$

$$d_3 = \exp\left(\frac{-\theta_{FOV}^2}{2\sigma_{rd}^2}\right),$$

$$F_h(h > 0) = [1 - d_3] * b_3 * G_{2,4}^{3,1}\left(\frac{\alpha_1 \beta_1 h_{th}}{h_l} \left| \begin{array}{l} \gamma_1^2 + 1, 1 \\ \gamma_1^2, \alpha_1, \beta_1, 0 \end{array} \right.\right)$$

$$b_3 = \frac{\left[2\left(\frac{r_a}{W_z^2}\right)^2\right]^{-\gamma_1^2} \gamma_1^2}{\Gamma(\alpha_1) \Gamma(\beta_1)}.$$

This analysis is true for lower values of 'h,' and the same analysis for Ground-to-HAP was derived with finite integral equations [Safi *et al.* (2020)]. Here we approached with Meijer G-functions.

2.6 UWOC Link Channel Model

In this section, the UWOC channel model considering the effects of link attenuation, geometric misalignment, and turbulence.

Compared with the HAP-to-Ground Communication channel model, the performance of the UWOC channel is more attenuated by absorption, scattering, and turbulence. This absorption and scattering two parameters limit link distance, optical

light beam spread, and multi-path dispersion. A simple model under different effects in UWOC channel link with log-normal(LN) distribution was derived in[Zeng *et al.* (2016)],[Liu *et al.* (2015)]. In this chapter, we considered GG distributed channel model between R node to D node. The received optical signal at the R node is transmitted through the UWOC channel to the destination. The received optical beam at the D node is modeled as

$$h_{r,d} = h_{pu}h_{au}h_{tu} \quad (2.64)$$

where h_{pu} , is the attenuation effect of absorption and scattering for underwater optical links. h_{tu} is the underwater optical GG turbulence distribution. h_{au} is the intensity of the transmitted signal.

absorption and scattering are two main factors that affect the UWOC link, which is modeled as

$$c(\lambda) = a(\lambda) + b(\lambda) \quad (2.65)$$

Where $c(\lambda)$ is extinction coefficient, $a(\lambda)$ is absorption coefficient, $b(\lambda)$ is scattering coefficient. λ is the transmitted optical beam wavelength, this parameters values different for different water and source wavelengths. for UWOC links, the attenuation coefficient is modeled by using Beer-Lambert's law with link distance L and wavelength λ as

$$h_{pu} = e^{-c(\lambda)L_2} \quad (2.66)$$

Here $c(\lambda)$, is the four water types such as Pure seawater, Clear ocean, Coastal ocean, and Turbid harbor water. More details regarding the absorption and scattering coefficients under different water types were highlighted in [Kaymak *et al.* (2018)], [Liu *et al.* (2015)], [Johnson *et al.* (2014)]. In this chapter, the Path loss and extinction coefficient calculated for the UWOC link L_2 of 10m performance is evaluated.

The UWOC channel model from R node to D node by considering combined effect into account GG distributed Link PDF is defined as

$$f_{h_2}(h) = \frac{\alpha_2\beta_2\gamma_2^2}{A_0h_{pu}\Gamma(\alpha_2)\Gamma(\beta_2)} G_{1,3}^{3,0} \left(\frac{\alpha_2\beta_2h}{A_0h_{pu}} \left| \begin{matrix} \gamma_2^2 \\ \gamma_2^2 - 1, \alpha_2 - 1, \beta_2 - 1 \end{matrix} \right. \right) \quad (2.67)$$

$A_0 = [erf(v)]^2$ received optical power at destination at D node, $v = \frac{a_r}{w_z} \sqrt{(\frac{\pi}{2})}$. The

Table 2.2: Path loss of 10m UWOC link [Kumar and Krishnan (2020)], [Kaymak *et al.* (2018)].

Water type	$c(\lambda)$	h_{pu}
Clear ocean	0.151	0.7063
Coastal ocean	0.399	0.3990
Turbid harbor	2.195	0.0064

parameter γ_2 indicates pointing errors caused by the misalignment between the R node and D node. By utilizing [Adamchik and Marichev (1990), Eq.26] and [[Jeffrey and Zwillinger (2007), section.9.31] After some mathematical manipulations The CDF of Eq. (6.6) is expressed as

$$F_{h_2}(h) = \frac{\gamma_2^2}{\Gamma(\alpha_2)\Gamma(\beta_2)} G_{2,4}^{3,1} \left(\frac{\alpha_2 \beta_2 h_{th}}{A_0 h_{pu}} \left| \begin{array}{l} \gamma_2^2 + 1, 1 \\ \gamma_2^2, \alpha_2, \beta_2, 0 \end{array} \right. \right) \quad (2.68)$$

Chapter 3

INTER UAV-BASED FSO COMMUNICATION SYSTEM PERFORMANCE ANALYSIS WITH DETECTION TECHNIQUES

3.1 Introduction

Alignment and Design of more tractable channel models between UAVs are Major challenges. The performance analysis of inter UAVs-based FSO communication systems under different weather conditions is another challenge. Alignment is the major technical challenge in inter-UAV-based FSO Communication systems, and this alignment is not only in inter UAVs which is present in FSO Communication systems. UAV-based FSO communication systems for Ground-to-UAV, UAV-to-UAV link performance is analyzed experimentally with alignment under clear weather conditions investigated [Leitgeb *et al.* \(2007\)](#). UAV based FSO initially proposed high data rate applications such as military and civil with a data rate of 2.5 Gbit/s. It highlighted the UAV-to-UAV based FSO link for different wireless networks [Chlestil *et al.* \(2006\)](#).

Conventional relay-FSO systems replaced with UAV's and their performance evaluation in [Fawaz *et al.* \(2018\)](#). The critical enabler for 5G+ wireless networks is the small cell concept. This higher number of small cells requires a high data rate back-

hauling/front hauling link, which increases cost and difficult to establish a link. swarm of UAVs based FSO is proposed for such backhauling/front hauling link [Alzenad *et al.* \(2018a\)](#). All the above UAV-based FSO applications are enabled with tractable channel models. Such a channel model between Ground-to-UAV, UAV-to-Ground, and UAV-to-UAV are proposed in [Dabiri *et al.* \(2018a\)](#). The tractable and more efficient UAV-to-UAV based FSO channel model is proposed in [Dabiri *et al.* \(2019a\)](#).

The UAV based FSO system's performance under hovering fluctuations of the UAV by considering blind data detection proposed in [Safi *et al.* \(2019a\)](#). Source relay(SR) and relay to destination(RD) channel models of the UAV based FSO system where UAV as a relay with DF is relaying proposed in [Dabiri and Sadough \(2019a\)](#). UAV based FSO channel with Nonzero Boresight pointing error and Statistical channel modeling proposed in [Dabiri *et al.* \(2020\)](#). First, we derived the analytical expressions for the inter UAV-based FSO communication system using Meijer's G functions. We derived the closed-form expression under hovering fluctuations. Derived analytical expressions results are compared with Monte-Carlo simulations. The performance analysis was done with two different detection techniques; we introduced heterodyne detection (HD) in FSO based inter UAV communication. The outage and average bit error rate (BER) performance of the proposed system is analyzed, and the results are compared with the existing Intensity modulation direct detection (IM/DD). We studied the impact of turbulence and pointing errors on BER and the outage performance of the proposed system. The results are plotted for different system parameters such as Rytov Variance, field-Of-view, Transmitter UAV orientation, receive UAV orientation, link range, and Beamwidth.

3.2 Major contributions

The major contributions in the Chapter 3 are as follows,

- First time we introduced heterodyne detection (HD) in FSO based inter UAV communication. The outage and average bit error rate (BER) performance of the proposed system is analyzed and the results are compared with the existing Intensity modulation direct detection (IM/DD).
- We studied the impact of turbulence and pointing errors on BER and outage performance of the proposed system. The results are plotted for different system parameters such as Rytov Variance, field-Of-view, Transmitter UAV orientation ; receive UAV orientation, link range, and Beam width.

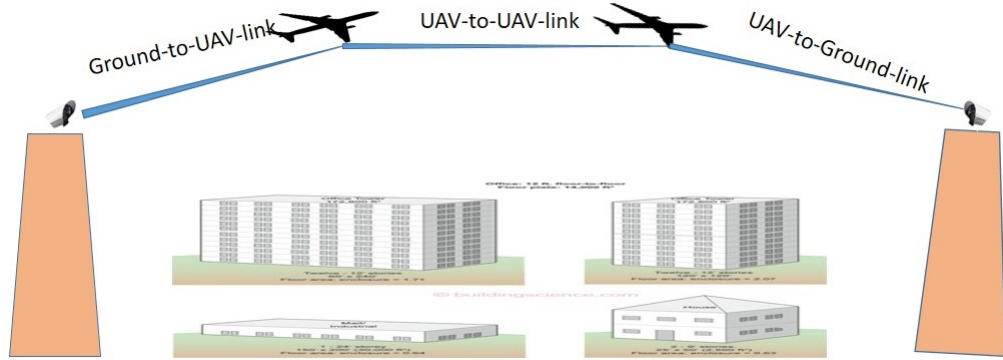


Figure 3.1: Ground-UAV-UAV-Ground Links.

- The analytical results are validated with the monte-carlo simulations.

The rest of the chapter is structured as follows: In Section 3.3, the framework subtleties have been discussed, and Section 3.4 depicts the UAV-UAV FSO Link channel model. The outage probability of the UAV-UAV FSO link has been inferred in Section 3.5 closed-form numerical expressions. The average BER of Inter UAV-based FSO link has been discussed in Section 3.6. In Section 3.7, numerical outcomes are introduced with pointing error for different turbulence Conditions, θ_{FOV} , σ_{ro} , σ_{to} , distance. Toward the end of Section 3.8, the conclusion of this work has been summed up.

3.3 System and received signal model

To model the UAV-UAV FSO link, we assume the following assumptions. Both UAV's are hovering in one place with clear weather conditions. Due to the random movement of UAV's in hovering state position, and orientation deviation exist. $B_{Tx} = \begin{bmatrix} 0 & 0 & 0 \end{bmatrix}$, $B_{Rx} = \begin{bmatrix} 0 & 0 & z \end{bmatrix}$, in the Cartesian coordinate system $\begin{bmatrix} x & y & z \end{bmatrix} \in R^{(1 \times 3)}$. $B'Tx = \begin{bmatrix} x_t & y_t & z_t \end{bmatrix}$, are instantaneous position deviations of transmits UAV. $B'Rx = \begin{bmatrix} x_r & y_r & z_r \end{bmatrix}$, are instantaneous position deviations of receiver UAV. Transmit and receiver orientation deviation respectively are θ_{tx} , θ_{ty} , θ_{rx} and θ_{ry} . On the z-axis orientation deviation of transmitter and receiver are presented. for ground-UAV and UAV-ground the orientation deviation minimal values which are negligible. The derived equation also applicable for Ground-UAV and UAV-Ground link.

A typical UAV-UAV FSO Connection is shown in Fig.3.1, where one UAV goes around as a transmitter and another acts as a UAV receiver. Both UAVs communicate with the FSO link and effectively align, with no position and orientation deviations present, i.e., they are within the θ_{FOV} . The alignment coefficient A range between

$0 \leq A \leq 1$ if $A = 0$ misalignment if it is $A = 1$ perfectly alignment. Both UAV's are hovering with a separation of L [Rahman *et al.* (2020)]. Fig.3.2, shows a single UAV-UAV FSO link with a Misalignment state with a misalignment angle of σ_{to}, σ_{ro} . Two UAV's are hovering; due to the hovering state, the position and orientation of UAVs deviated from their mean positions; these deviations are random and modeled as gaussian distribution. The position and orientation deviations of transmitter and receiver variance are equal to $\sigma_{tp}, \sigma_{to}, \sigma_{ro}$ and σ_{rp} respectively and the detailed explanation is given in [Schulz *et al.* (2016)-Dabiri *et al.* (2020)].

We consider detection technique with binary modulation used for optical transmission in UAV-FSO systems. The transmitted beam propagated through the UAV-UAV-FSO link and received at the surface of the photo detector(PD). The PD convert the optical signal to electrical signal. The received signal mathematically modeled as [Dabiri *et al.* (2019b)]

$$r = RhX + \varsigma \quad (3.1)$$

h is the combined UAV-UAV FSO channel model which is demonstrated as Eq. (3.3) R is Photo detector responsivity and X is transmitted optical beam ς is the Gaussian noise with Variance $\sigma_n^2 = 2eB_eRP_b$ e is electron charge B_e is the photo detector band width P_b back ground power which is defined as $P_b = A_a B_o N_b(\lambda) \Omega_{FOV}$, where $N_b(\lambda)$ is the spectral radiance of the background radiations at wavelength λ , B_o is the bandwidth of the optical filter at the Rx and A_a is the lens area. Moreover, Ω_{FOV} denotes the Rx FOV that can be represented as $\Omega_{FOV} = \frac{\pi \theta_{FOV}^2}{4}$. here, $\theta_{FOV} = \frac{2r_p}{d_f}$ denote the FOV angle, where d_f and r_p are the focal length radius of circular PD, respectively.

The probability of outage for UAV-UAV FSO link under weak, moderate, and strong turbulence conditions can work out utilizing $f_h(h)$. The probability of an outage is evaluated at h_{th} by the CDF of h . Outage probability is defined as the probability that the instant SNR drops under a given threshold. The threshold is the protective value of the above-mentioned SNR, where the quality of the UAV-UAV FSO relation is acceptable. The Outage probability can be specified by the context under consideration mathematically represented as follows [Sandalidis *et al.* (2009a)-Farid and Hranilovic (2007)].

$$p_{out}(h_{th}) = pr(h \leq h_{th}) = \int_0^{h_{th}} f_h(h) d(h), \quad (3.2)$$

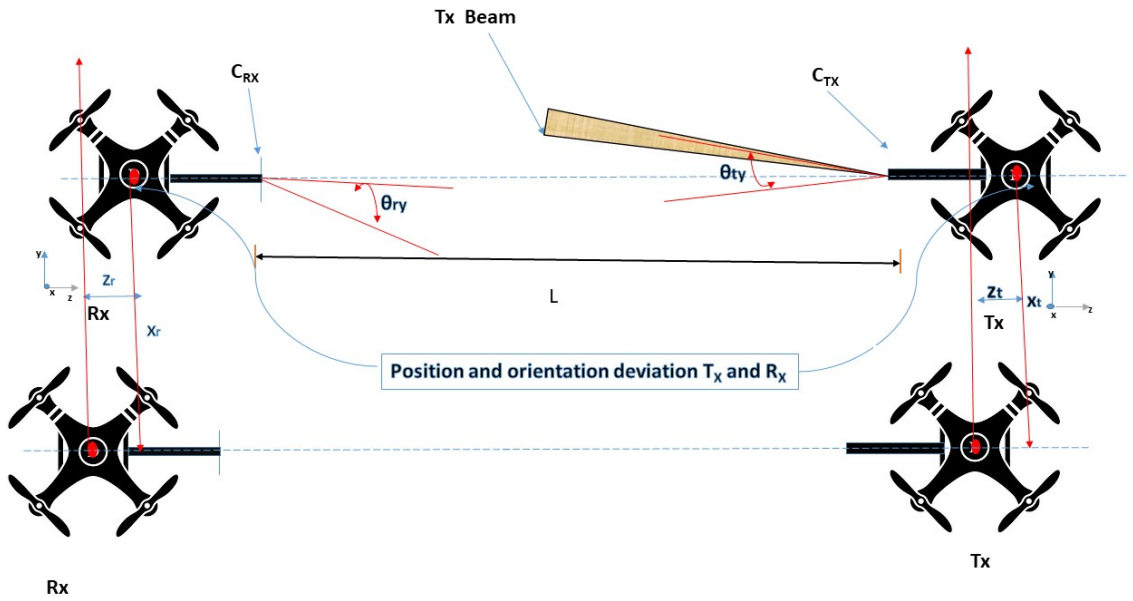


Figure 3.2: UAV-UAV FSO link two UAV's are in hovering state with out and with Misalignment.

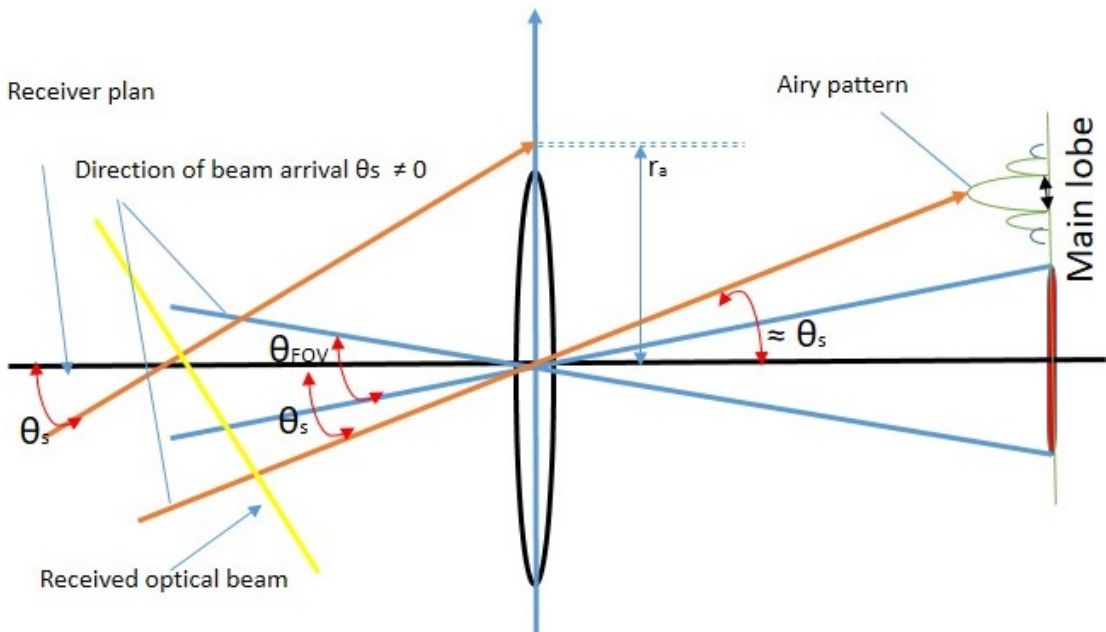


Figure 3.3: UAV-UAV FSO link two UAV's are in hovering state with out and with Misalignment.

where, h_{th} is threshold SNR

3.4 Channel Model

The combined channel model between UAV-UAV-FSO link involving many random variables and it's brief explanation is given below. Channel model can be defined as follows,

$$h = h_{pl}h_{al}h_{pp}h_{AOA}. \quad (3.3)$$

where $h' = h_{pl}h_{al}h_{pp}$ Here h_{pl} stands for path loss. It depends on the distance, which is a deterministic term, h_{pp} pointing error due to UAV's position and orientation deviations due to hovering state and h_{al} represents the turbulence-induced fading which is a random variable. For a UAV-UAV FSO link with distance Z , the path loss represented by the Beers-Lambert law as $h_{pl} = \exp(-Z\zeta)$ where ζ is the path-loss coefficient which depends on the visibility. here we consider the path loss is clear sky weather condition.

3.4.1 UAV-UAV-FSO link with Log-normal channel

Channel model for inter UAV-based FSO link under log-normal channel fading was derived below [Chapter 2, Eq. (2.36)]

$$f_h(h) \approx a_1\delta(h) + f_h(h > 0), \quad (3.4)$$

where

$$a_1 = \exp\left(\frac{-\theta_{FOV}^2}{2(\sigma_{to}^2 + \sigma_{ro}^2)}\right),$$

$$f_h(h > 0) = \left[1 - \exp\left(\frac{-\theta_{FOV}^2}{2(\sigma_{to}^2 + \sigma_{ro}^2)}\right)\right] D1$$

$$h'^{\tau-1} \text{erfc}\left(\frac{\ln\left(\frac{h'}{A_o h_{pl}} + \mu\right)}{\sqrt{8}\sigma_R}\right),$$

where

$$D1 = e^{2\sigma_R^2\tau(1+\tau)} \frac{\tau}{2(A_o h_{pl})^\tau},$$

3.4.2 UAV-UAV-FSO link with Gamma-Gamma turbulence channel

We derived closed-form expression using Meijer's G functions. The derived Inter UAV-based FSO GG turbulence fading channel model as below.

$$f_h(h) \approx a_1 \delta(h) + f_h(h > 0), \quad (3.5)$$

where

$$a_1 = \exp\left(\frac{-\theta_{FOV}^2}{2(\sigma_{to}^2 + \sigma_{ro}^2)}\right),$$

$$f_h(h > 0) = \left[1 - \exp\left(\frac{-\theta_{FOV}^2}{2(\sigma_{to}^2 + \sigma_{ro}^2)}\right)\right] * D2 * G_{1,3}^{3,0} \left(\begin{matrix} \tau \\ \tau - 1, \alpha - 1, \beta - 1 \end{matrix} \middle| \frac{\alpha\beta h'}{A_0 h_l} \right),$$

where

$$D2 = \frac{\alpha\beta\tau}{A_0 h_{pl} \Gamma(\alpha) \Gamma(\beta)},$$

3.5 Outage Probability for Inter UAV-based FSO Communication System

In this section, Derived the analytical expressions for Inter UAV-based FSO link with IM/DD and HD techniques. We considered Log-normal distribution for weak-to-moderate turbulence and Gamma-Gamma distribution for moderate-to-strong turbulence.

3.5.1 Outage Probability of a Inter UA-based FSO link with Log-normal channel

Outage probability derived in this section by considering the IM / DD with pointing error in the case of weak to moderate turbulence modeled as Log-normal distribution. The average SNR in case of IM/DD Can be composed as $\mu_{IM/DD} = \frac{\eta^2 E_h^2 \{h\}}{N_0}$, by considering the pointing error into account in UAV-UAV-FSO link with IM/DD $\mu_{IM/DD} = \frac{\eta^2 A_0^2 h_{pl}^2 \tau^2}{(\tau+1)^2 N_0}$. The instantaneous SNR $\gamma = \frac{\eta^2 h^2}{N_0}$, the received beam $h = \frac{\sqrt{\gamma N_0}}{\eta} = \frac{A_0 h_{pl} \tau}{(1+\tau)} \sqrt{\frac{\gamma}{\mu_{IM/DD}}}$, SNR = $(\frac{1+\tau}{\tau})^2 \frac{\mu_{IM/DD}}{h_{pl}^2 A_0^2} h^2$. finding its simple derivative using simple Power transformation of the random variable h the result UAV-UAV-FSO link with

weak to moderate turbulence with IM/DD, the resulting PDF can be composed as [21-22]

$$f_\gamma(\gamma) = f_h(h(\gamma)) \left| \frac{dh}{d\gamma} \right|$$

$$f_\gamma(\gamma) = a1\delta(h) + (1 - a1)D1 \frac{A_0^\tau h_{pl}^\tau \tau^\tau}{(1 + \tau)^\tau 2\mu_{IM/DD}} \left(\sqrt{\frac{\gamma}{\mu_{IM/DD}}} \right)^{\tau-2} \text{erfc} \left(\frac{\ln\left(\frac{\tau\sqrt{\gamma}}{(1+\tau)\sqrt{\mu_{IM/DD}}} + \mu\right)}{\sqrt{8}\sigma_R} \right), \quad (3.6)$$

After simplifying the Eq. (3.6) with [45, Eq.(06.27.21.0011.01)], closed-form expression under the link with weak to moderate turbulence channel outage probability can be represented by

$$p_{out.IM/DD} = a1 + \left[\frac{(1 - a1)}{2} e^{\tau\psi - 2\sigma_R^2\tau^2} \text{erfc}\left(\frac{\psi}{\sqrt{8}\sigma_R}\right) + \text{erfc}\left(\frac{4\sigma_R^2\tau - \psi}{\sqrt{8}\sigma_R}\right) \right]. \quad (3.7)$$

where

$$\psi = \mu + \ln\left(\frac{\tau^2\sqrt{h_{th}}}{(1+\tau)\sqrt{\mu_{HD}}}\right),$$

Presently considering the UAV-UAV-FSO link under weak to moderate turbulence condition with HD detection, the average SNR can be composed as $\mu_{HD} = \frac{\eta(E_h\{h\})}{N_0}$, by considering the pointing error into account in UAV-UAV-FSO link with HD $\mu_{HD} = \frac{\eta A_0 h_{pl} \tau}{(\tau+1)N_0}$. The instantaneous SNR $\gamma = \frac{\eta h}{N_0}$, the received beam $h = \frac{\gamma N_0}{\eta} = \frac{A_0 h_{pl} \tau \gamma}{(1+\tau)\mu_{HD}}$, SNR = $\left(\frac{1+\tau}{\tau}\right) \frac{\mu_{HD}}{A_0 h_{pl}} h$. By finding its basic derivate utilizing simple Power transformation of the random variable h the result UAV-UAV-FSO link with weak to moderate turbulence with HD, the resulting PDF can be composed as

$$f_\gamma(\gamma) = f_h(h(\gamma)) \left| \frac{dh}{d\gamma} \right|$$

$$f_\gamma(\gamma) = a1\delta(h) + (1 - a1)D1 \left[\frac{h_{pl}^\tau A_0^\tau \tau^\tau}{(1 + \tau)^\tau \mu_{HD}^\tau} \right] \gamma^{\tau-1} \text{erfc} \left(\frac{\ln\left(\frac{\gamma^\tau}{\mu_{HD}(1+\tau)} + \mu\right)}{\sqrt{8}\sigma_R} \right), \quad (3.8)$$

Similarly, using [Wolfram (2001), Eq.(06.27.21.0011.01)], under weak to moderate turbulence, the UAV-UAV-FSO channel with HD Detection outage probability can be derived as below.

$$p_{out.HD} = a1 + \left[\frac{(1 - a1)}{2} e^{\tau\psi - 2\sigma_R^2\tau^2} \text{erfc}\left(\frac{\psi}{\sqrt{8}\sigma_R}\right) + \text{erfc}\left(\frac{4\sigma_R^2\tau - \psi}{\sqrt{8}\sigma_R}\right) \right]. \quad (3.9)$$

3.5.2 Outage Probability of a UAV-UAV-FSO link with Gamma-Gamma turbulence channel

For considering the moderate to strong turbulence between UAV-UAV-FSO link with IM/DD detection using simple random variable transformation, the resultant PDF can be composed as

$$f_\gamma(\gamma) = f_h(h(\gamma)) \left| \frac{dh}{d\gamma} \right|$$

Similarly, by utilizing [Wolfram (2001), Eq.(07.34.21.0084.01)], and after simplification, The outage probability of Eq. (3.5) can be composed as

$$p_{out.IM/DD} = a1 + (1 - a1) \frac{\alpha\beta\tau^2 2^{\alpha+\beta-3}}{4\pi\Gamma(\alpha)\Gamma(\beta)(1 + \tau)} \sqrt{\frac{h_{th}}{\mu_{IM/DD}}} G_{3,7}^{6,1} \left(X1 \left[\frac{(\alpha\beta\tau)^2 h_{th}}{(4(1 + \tau))^2 \mu_{IM/DD}} \right] \right) \quad (3.10)$$

where $X1 = 1/2, \tau/2, \tau + 1/2, X2 = \tau - 1/2, \tau/2, \alpha - 1/2, \alpha/2, -1/2, \beta - 1/2, \beta/2$.

For considering the moderate to strong turbulence between UAV-UAV-FSO link with HD detection using simple random variable transformation, the resultant PDF can be composed as

$$f_\gamma(\gamma) = f_h(h(\gamma)) \left| \frac{dh}{d\gamma} \right|$$

$$f_\gamma(\gamma) = a1\delta(h) + ((1 - a1)\frac{\alpha\beta\tau^2}{(1 + \tau)\Gamma(\alpha)\Gamma(\beta)\mu_{HD}}G_{1,3}^{3,0}\left(\begin{matrix} \tau \\ \tau - 1, \alpha - 1, \beta - 1 \end{matrix} \middle| \frac{\alpha\beta\tau\gamma}{(1 + \tau)\mu_{HD}}\right)) \quad (3.11)$$

By utilizing [Adamchik and Marichev (1990), eq.26], The outage probability of Eq. (3.11), Can be composed as.

$$p_{out.HD} = a1 + \left[((1 - a1)\frac{\tau}{\Gamma(\alpha)\Gamma(\beta)}G_{2,4}^{3,1}\left(\begin{matrix} 1, \tau + 1 \\ \tau, \alpha, \beta, 0 \end{matrix} \middle| \frac{\alpha\beta\tau h_{th}}{(1 + \tau)\mu_{HD}}\right) \right]. \quad (3.12)$$

3.6 Average Bit-error rate

The average BER for the considered UAV-based FSO communication link with BPSK modulation closed-form expression was derived. In this Inter UAV communication link, performance is analyzed over the moderate to strong turbulence condition under HD detection with Meijer's G is derived as [Sandalidis *et al.* (2009b)]

$$P_e = \frac{1}{2} \int_0^\infty \text{erfc}\left(\frac{R\gamma}{2\sigma_R^2}\right) f_\gamma(\gamma) d\gamma \quad (3.13)$$

Eq. (3.13) can modified With the help of $\text{erfc}(\sqrt{x})$, which is given below and is as

$$\text{erfc}(\sqrt{x}) = \frac{1}{\sqrt{\pi}} G_{1,2}^{2,0}\left(\begin{matrix} 1 \\ 0, 0.5 \end{matrix} \middle| x\right)$$

$$P_e = \frac{a1}{2} + \frac{(1 - a1)}{2\sqrt{\pi}} \int_0^\infty G_{1,2}^{2,0}\left(\begin{matrix} 1 \\ 0, 0.5 \end{matrix} \middle| \frac{R^2\gamma^2}{4\sigma_R^2}\right) * G_{1,3}^{3,0}\left(\begin{matrix} \gamma^2 \\ \gamma^2 - 1, \alpha - 1, \beta - 1 \end{matrix} \middle| \frac{\alpha\beta h}{h_l}\right) d\gamma \quad (3.14)$$

where, $D3 = \frac{\alpha\beta\tau^2}{(1+\tau)\Gamma(\alpha)\Gamma(\beta)\mu_{HD}}$ using [Wolfram (2001), Eq.(07.34.21.0013.01)], and after some mathematical manipulations, the expression for BER between UAV-UAV communication link performance is derived as

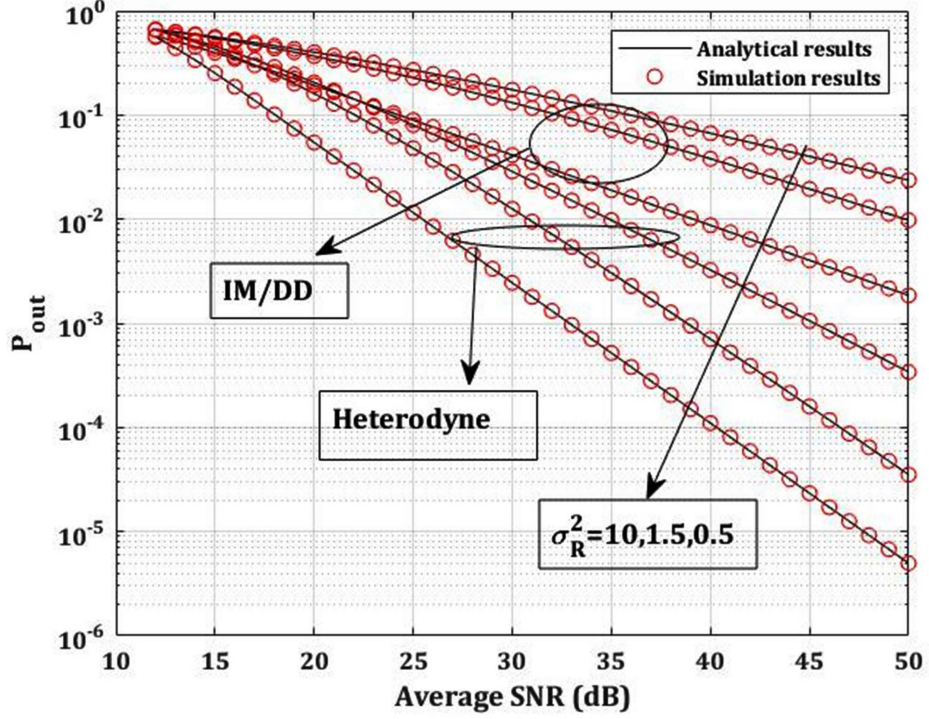


Figure 3.4: Outage probability of UAV-UAV-FSO LINK versus average SNR over Gamma-Gamma turbulence model for $\sigma_{t_o} = \sigma_{r_o} = 3mrad$, $W_z = 2m$, $Z = 250m$ with both detection techniques under different turbulence conditions.

$$P_e = \frac{a1}{2} + \frac{\tau(1-a1)2^{\alpha+\beta-2}}{4\pi^{3/2}\Gamma(\alpha)\Gamma(\beta)} G_{2,6}^{7,4} \left(\begin{matrix} X1 \\ X2 \end{matrix} \middle| \frac{4R^2(1+\tau)^2\mu_{HD}^2}{2\sigma_n^2(\alpha\beta)^2\tau^2} \right) \quad (3.15)$$

Where, $X1 = 1, (1-\tau)/2, (2-\tau)/2, (1-\beta)/2, (2-\beta)/2, (1-\alpha)/2, (2-\alpha)/2$
 $X2 = 0, 0.5, -\tau/2, (1-\tau)/2$

3.7 Results and Discussions

This section examines the performance of the UAV-UAV-FSO Link with detection techniques under the constraints of weak, moderate, and strong turbulence derived from in this work Eq. (3.7), Eq. (3.9), Eq. (3.10), and Eq. (3.12). As follows, we consider the parameters of the analytical result, the distance we have taken between two UAVs as $L=250m$; we assumed that the UAV aperture of the receiver is having the radius $r_a=5cm$, responsivity $R=0.8$, for weak to moderate turbulence (log-normal) $\sigma_R=0.1$, for moderate turbulence (Gamma-Gamma turbulence) $\sigma_R = 0.5$ to 1.5 and

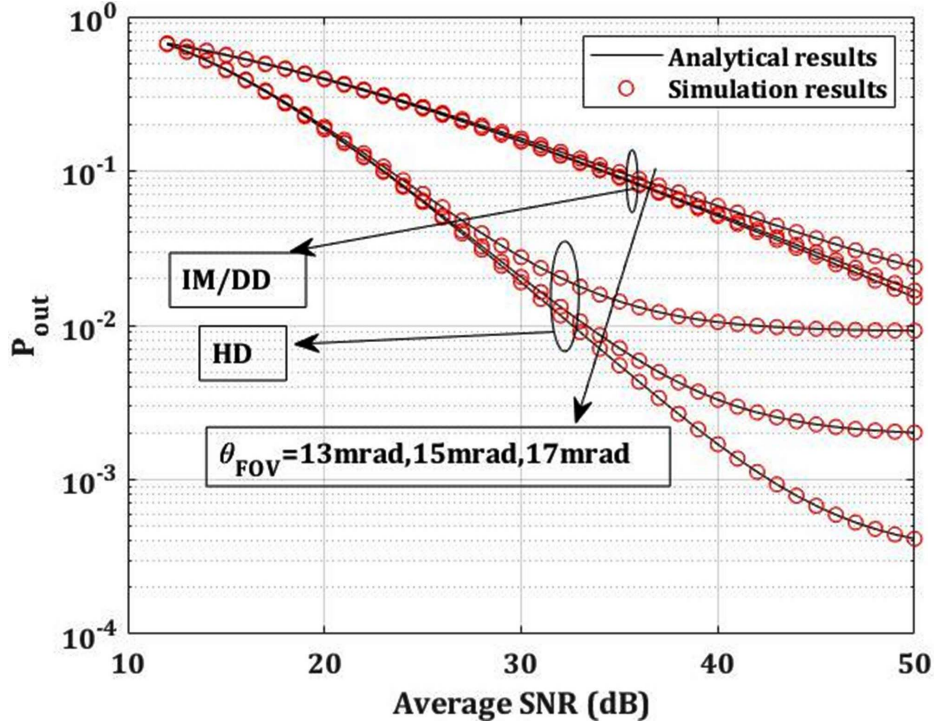


Figure 3.5: Outage probability of UAV-UAV-FSO LINK versus average SNR over Gamma-Gamma turbulence model for $\sigma_{to} = \sigma_{ro} = 3\text{mrad}$, $W_z = 2\text{m}$, $Z = 250\text{m}$, different values of θ_{FOV} with both detection techniques under moderate to strong turbulence condition.

for strong turbulence (Gamma-Gamma turbulence) 2 to 10. The position standard deviations of transmitting and receive UAV given as σ_{tp}, σ_{rp} are equal to 30cm. Orientation standard deviations of transmitting and receive UAV given as σ_{to}, σ_{ro} are equal to 3mrad, W_z is beam width varying from 1-30m, $h_{pl} = 1$ is for very clear weather condition, receiver FOV is from 1-50mrad, and the threshold SNR is 11.8 dB in case of binary detection. The parameter is the same in the case of both the detection techniques.

Detection is one of the important parameters to improve the performance of the UAV-UAV-FSO. The improvement is shown concerning pointing error for both the detection techniques. The P_{out} is presented in Fig.3.4, For both the detection techniques across the average SNR at σ_R . From Fig.3.4, as σ_R decreases, performance increases, which was shown for both the detection techniques. Another important observation is that at point 10^{-2} with $\sigma_R = 0.5$, the average SNR for HD is 25dB at the same point the Average SNR for IM/DD is 40dB from this HD has higher performance when

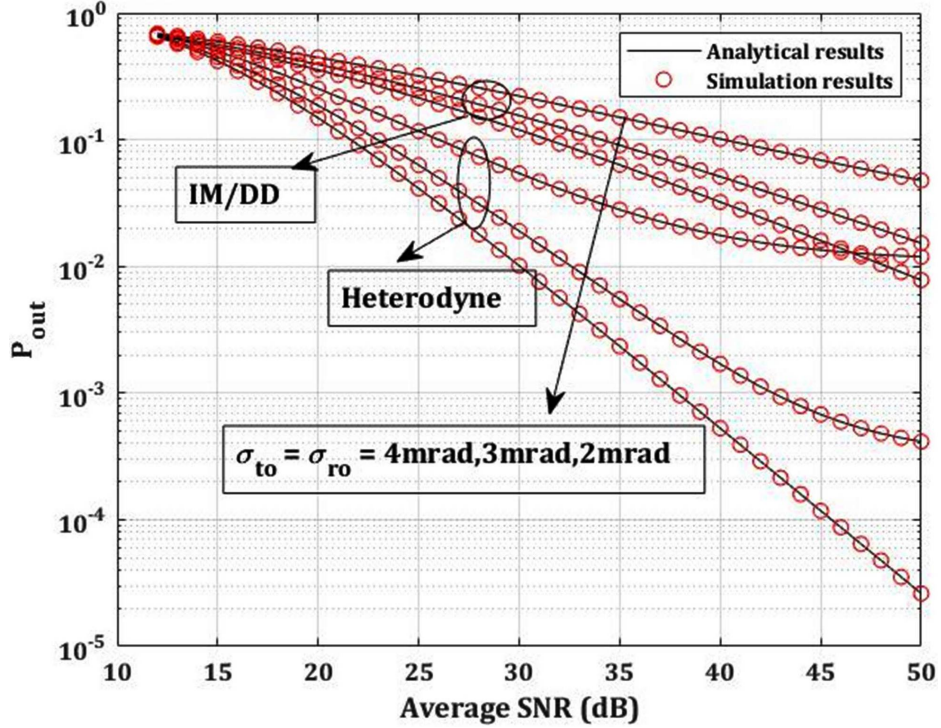


Figure 3.6: Outage probability of UAV-UAV LINK-FSO versus average SNR over Gamma-Gamma turbulence model for $\sigma_{tp} = \sigma_{rp} = 30cm$, $W_z = 2m$, $Z = 250m$, different values of σ_{to} , σ_{ro} with both detection techniques under moderate to strong turbulence condition.

compared to the IM/DD Technique, by 15dB, with increasing the system complexity. Both analytical and simulation results are verified.

Similarly, Fig.3.5 represents Outage Probability for varying the effect of θ_{FOV} under IM/DD and HD detection techniques. From the above Fig.3.5, it is observed that for lower values of θ_{FOV} , the performance is worst for large values of θ_{FOV} the performance increase which was shown in Fig.3.5, for both detection techniques. Large FOV leading to background noise will increase. Similarly Fig.3.6, represents Outage Probability for varying the effect of σ_{to} , σ_{ro} under IM/DD and HD detection techniques. observed that for lower values of σ_{to} , σ_{ro} the performance increases. Small deviations in orientation lead to significant performance deviations shown for both detection techniques. From the above Fig.3.5, Fig.3.6, it is observed that both detection techniques performance depends on the θ_{FOV} , σ_{to} , σ_{ro} it is the actual results which shown in this section. Fig. 3.7. We considered the UAV-UAV-FSO link performance under IM/DD and HD detection techniques with weak to moderate turbulence conditions. the outage

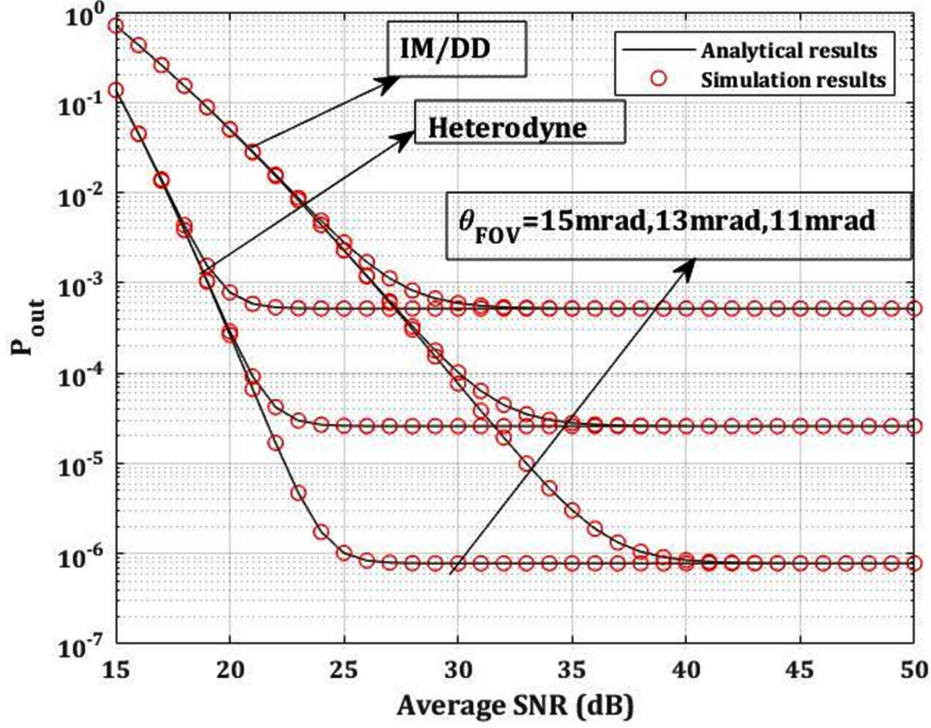


Figure 3.7: Outage probability of UAV-UAV-FSO LINK versus average SNR over Log-normal turbulence model for $\sigma_{to} = \sigma_{ro} = 2mrad$, $W_z = 2m$, $Z = 250m$, $\sigma_R = 0.1$ different values of θ_{FOV} with both detection techniques under weak to moderate turbulence condition.

probability were analyzed by varying the θ_{FOV} . As θ_{FOV} increases, the performance of the link improves in the case of both the detection techniques. The difference between Fig. 3.7, Fig. 3.8 is only the link length.

The link length is one of the important parameters in UAV-UAV-FSO systems. Suppose link length increases outage probability increase, $Z = 250m$, and $Z = 500m$ because of the UAVs' orientation deviations. Finding the optimal beam width UAV-UAV-FSO link is an important parameter, shown in this Fig.3.9. In Fig.3.9, we plotted the outage probability of the UAV based FSO link as a function of average SNR. We observed the optimal value of SNR as a function of beam width (w_z). For different values of (w_z) outage probability improvement was shown for IM/DD and HD detection. Optimal values under worst channel conditions also analyzed in Fig.3.9, Fig.3.10, by taking suitable beamwidth (w_z). In this chapter we derived the analytical expression for Average BER and plotted in Fig.3.11. We plotted the graph between Average BER verses Average SNR by varying the σ_R . The σ_R value ranging from 0 to

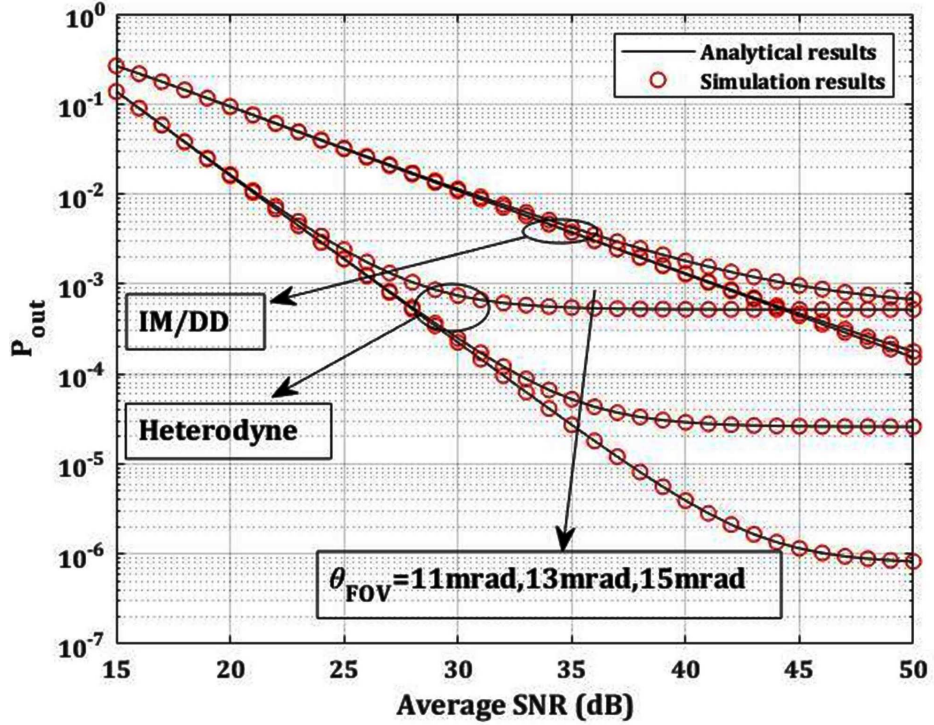


Figure 3.8: Outage probability of UAV-UAV-FSO LINK versus average SNR over Log-normal turbulence model for $\sigma_{to} = \sigma_{ro} = 2\text{mrad}$, $W_z = 2\text{m}$, $Z = 500\text{m}$, $\sigma_R = 0.1$ different values of θ_{FOV} with both detection techniques under weak to moderate turbulence condition.

10. For lower values σ_R takes weak turbulence, mid-range value moderate turbulence, and for higher range values it takes strong turbulence. Here we considered 0.6 for weak turbulence, 4.0 for moderate turbulence, and 10 for strong turbulence. From the Fig 3.11 strong to weak turbulence significant performance improvement was observed. In Fig.3.12 we plotted the graph between Average BER versus Average SNR by varying the receiver θ_{FOV} ranging from 1-50mrad. From the Fig.3.12 as the θ_{FOV} increases the BER curve improvement was observed.

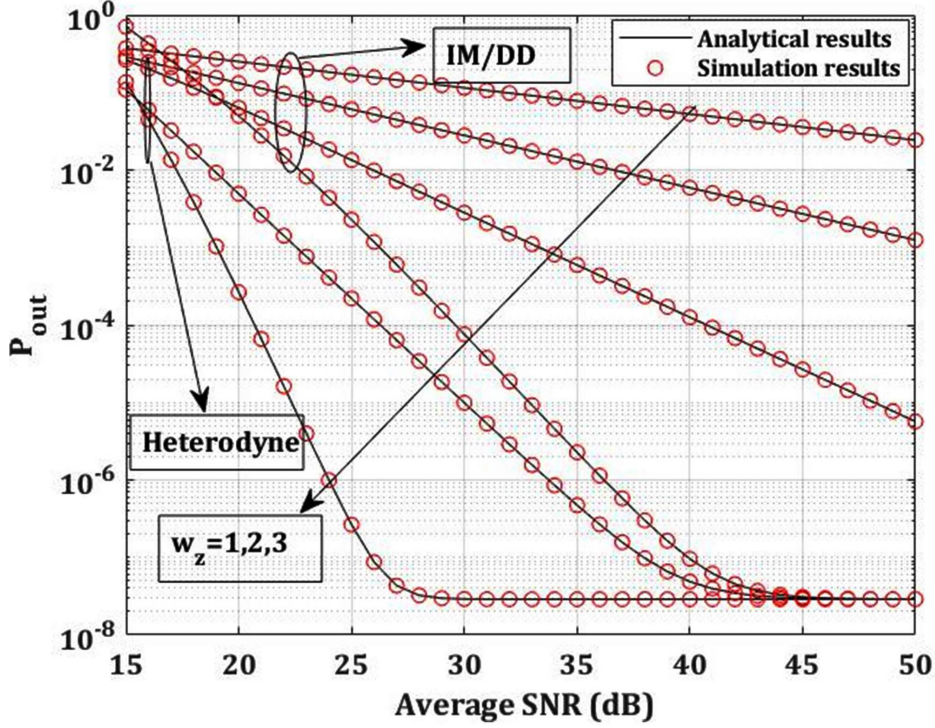


Figure 3.9: Outage probability of UAV-UAV-FSO LINK versus average SNR over Log-normal turbulence model for $\sigma_{to} = \sigma_{ro} = 2mrad$, $FOV = 11mrad$, $Z = 250m$, $\sigma_R = 0.1$ different values of W_z with both detection techniques under weak to moderate turbulence condition.

Table 3.1: Optimal values of θ_{FOV} to achieve minimum outage probability over GG Turbulence Model for $SNR = 40dB$, $\sigma_{tp} = \sigma_{rp} = 30cm$, and different values of Z

$Z(m)$	$\theta_{FOV}(mrad)$	$P_{out/IMDD}$	$P_{out/HD}$
250	13	6×10^{-2}	1×10^{-2}
250	15	6.5×10^{-2}	3×10^{-3}
250	17	5×10^{-2}	2.5×10^{-3}
500	13	1×10^{-1}	5×10^{-1}

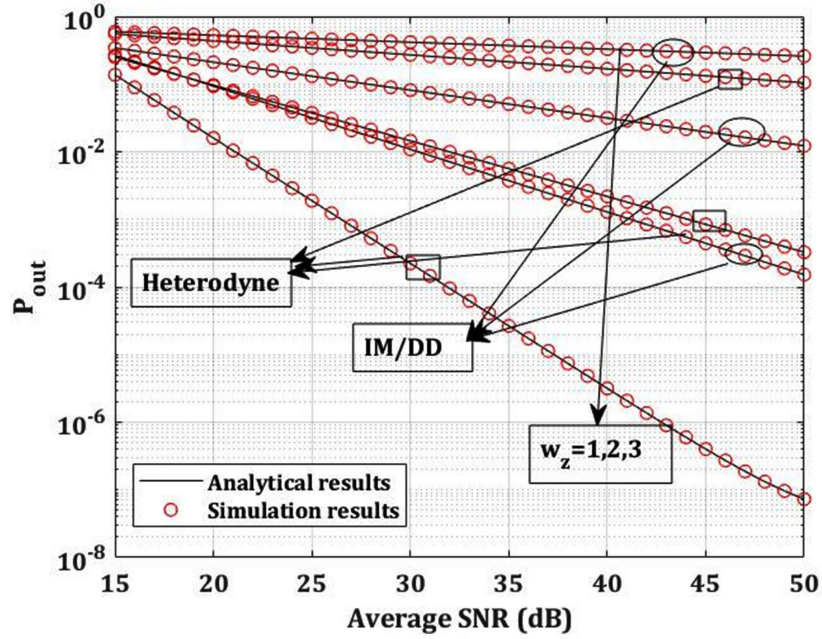


Figure 3.10: Outage probability of UAV-UAV-FSO LINK versus average SNR over Log-normal turbulence model for $\sigma_{to} = \sigma_{ro} = 2mrad$, $FOV = 11mrad$, $Z = 500m$, $\sigma_R = 0.1$ different values of W_z with both detection techniques under weak to moderate turbulence condition.

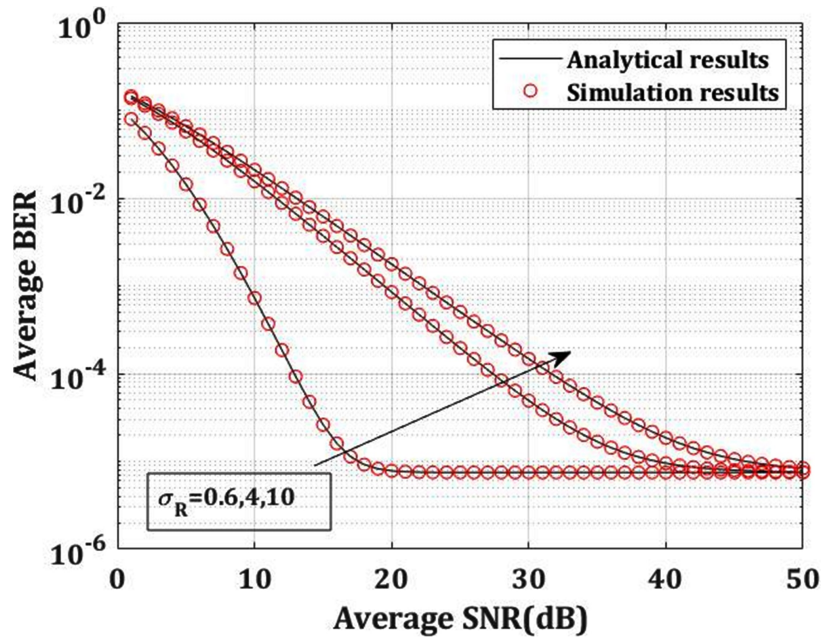


Figure 3.11: Average BER of UAV-UAV-FSO LINK versus average SNR over moderate to strong turbulence model for $\sigma_{to} = \sigma_{ro} = 3mrad$, $FOV = 20mrad$, $Z = 250m$, different values of σ_R with Heterodyne Detection technique.

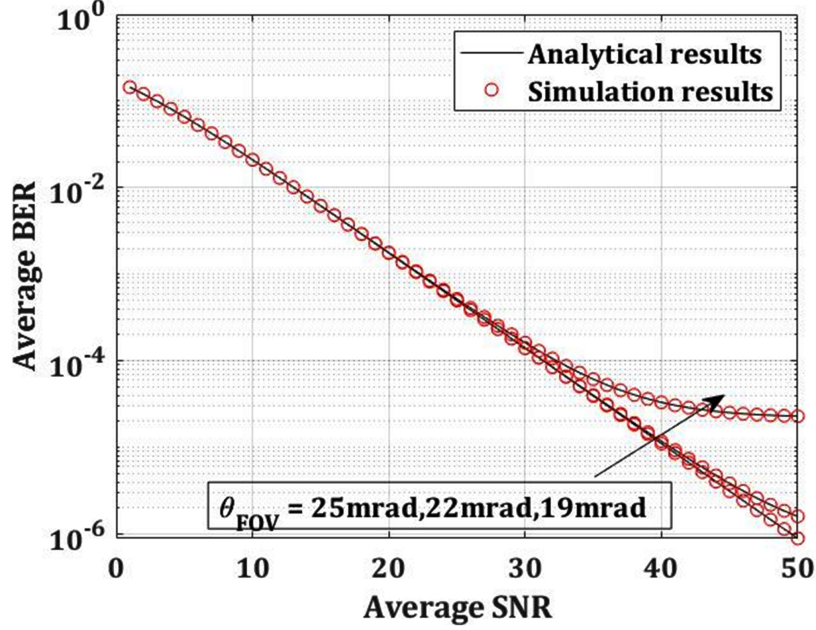


Figure 3.12: Average BER of UAV-UAV-FSO LINK versus average SNR over moderate to strong turbulence channel model for $\sigma_{to} = \sigma_{ro} = 3\text{mrad}$, $Z = 250\text{m}$, $\sigma_R = 10$ different values of FOV with Heterodyne Detection technique.

Table 3.2: Optimal values of $\sigma_{to} = \sigma_{ro}$ to achieve minimum outage probability over GG Turbulence Model for $SNR = 35\text{dB}$, $\sigma_{tp} = 30\text{cm}$, $\theta_{FOV} = 13\text{mrad}$ and different values of Z

$Z(\text{m})$	$\sigma_{to} = \sigma_{ro}(\text{mrad})$	$P_{out/IMDD}$	$P_{out/HD}$
250	4	2×10^{-1}	5×10^{-2}
250	3	1.5×10^{-1}	2×10^{-2}
250	2	1×10^{-1}	1×10^{-3}
500	4	1	1×10^{-2}

3.8 Summary

In this Chapter, we derived the UAV-based FSO System's analytical expressions for both IM / DD and HD Detection with a pointing error. The derived analytical Results are for weak to strong turbulence channel cases. Performance analysis metrics such as outage and BER analyzed for various channel parameters such as W_Z , Average SNR, θ_{FOV} , σ_{to} , σ_{ro} and other channel parameters. The above results show that HD compensates UAV's orientation deviations and overcome the turbulence effect compared to IM/DD detection. The proposed system is highly useful in 5G beyond, IoT, and disaster management applications.

Chapter 4

POLSK MODULATION INTER UAV-BASED FSO COMMUNICATION UNDER DIFFERENT WEATHER CONDITIONS.

4.1 Introduction

FSO communication systems performance is limited by weather conditions. The performance of a UAV-based FSO communication system horizontal/vertical path link mainly depends on weather conditions and distance. By considering these two effects consideration, we derived the analytical expressions by using Meijer's G functions. Compared the analytical expression with simulation results. We examine the effect of different weather conditions such as rain, fog on the bit error rate (BER) performance of the proposed system. Novel closed-form expressions for inter UAV-based FSO propagation channels are derived, and BER performance is investigated under different weather conditions.

Fog and rain are the main limiting factors mitigated by suitable mitigation techniques by increasing receiver FOV. We improved the performance of inter UAV-based FSO communication link by considering POLSK modulation. Polarization Shift Keying (PolSK) is an alternative technique to improve the Inter UAV based FSO commu-

nication systems. It is used for long distance outdoor FSO communication systems. Compared to other modulation schemes, PolSK provides immunity to atmospheric scintillation, higher data rates and lower BER. It has high immunity to laser phase noise and the light intensity is more uniform when propagating through atmospheric turbulences. In PolSK, the States of Polarizations (SOPs) of an optical signal are used as information carrying parameters. The information is encoded with different SOPs using an external modulator. PolSK uses intensity modulation, where two orthogonal polarization directions are used for the transmission of 0 and 1 data bits. The Transmitting Laser (TL) beam is linearly polarized and has a $/4$ polarization with respect to the principle axe of the external Phase Modulator (PM). We also improved the link range by considering this modulation scheme. Results are verified with existing link ranges, and the proposed system is suitable for long-range air-to-air links. We improved the receiver FOV to considerably mitigate the rain and cloud effect, which are presented in the results section. The main limiting factor is fog. Even we increase the receiver FOV, the performance UAV based FSO remains the same.

4.2 Main Contributions

The major contributions in the Chapter 4 are as follows,

- Fog and rain are the main limiting factors mitigated by suitable mitigation techniques by increasing receiver FOV.
- We improved the performance of inter UAV-based FSO communication link by considering POLSK modulation.
- We also improved the link range by considering this modulation scheme.

In the Inter UAV-based FSO system, Section 4.3 demonstrates the design and receives a signal model, while Section 4.4 details the channel model between UAV-UAV. Section 4.5, mainly novel Closed-Form expression, was derived under various weather conditions. Section 4.6 presents the results and discussion of the UAV-UAV FSO link under multiple weather conditions and the POLSK modulation study between UAV-UAV. Section 4.6 conclusion of UAV-UAV FSO link performance analysis described.

4.3 System model

The laser beam propagated through the UAV-UAV-based FSO system at a distance of Z meters along the horizontal direction. The UAV-UAV FSO link with the digital

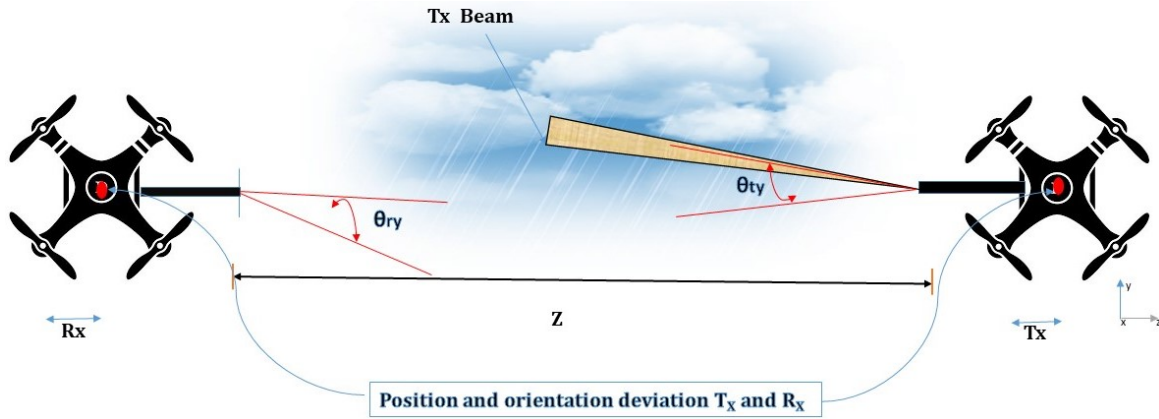


Figure 4.1: Two UAV's are in hovering state with misalignment and different weather conditions

POLSK modulation is used for transmission taken into account. Recently, POLSK has developed considerable interest in optical communication research for long-range applications. Where both UAVs communicate at a distance of Z meters with each other under hovering state with misalignment and it's weather effect link shown in Fig.4.1. Here, different weather conditions are presumed, and the resulting channel model is provided by [Taghi Dabiri *et al.* \(2020\)](#), [Dabiri and Sadough \(2019b\)](#)

$$r = Rhs + n \quad (4.1)$$

h is the over all atmospheric loss coefficient and it is the combined effects of all the loss between UAV-UAV and the R is Responsivity. Here s is the number of symbols transmitted between UAV-UAV FSO link with transmitted power P_t . n is photo noise and which is signal independent zero mean Gaussian noise with variance $\sigma_n^2 = 2eB_eRP_b$ e is electron charge B_e is the photo detector band width P_b back ground power which is defined as $P_b = A_a B_o N_b(\lambda) \Omega_{FOV}$, where $N_b(\lambda)$ is the spectral radiance of the background radiations at wavelength λ , B_o is the bandwidth of the optical filter at the Rx and A_a is the lens area. Moreover, Ω_{FOV} denotes the Rx FOV that can be represented as $\Omega_{FOV} = \frac{\pi \theta_{FOV}^2}{4}$, here, $\theta_{FOV} = \frac{2r_p}{d_f}$ denote the FOV angle, where d_f and r_p are the focal length radius and radius of circular photo detector.

4.4 Channel Model

The channel state consider to be the product of four factors and it can be expressed as [Taghi Dabiri *et al.* \(2020\)](#), [Dabiri and Sadough \(2019b\)](#),

$$h = h_l h_a h_p h_f. \quad (4.2)$$

where $h' = h_l h_a h_p$ Here, h_l stands for loss of direction, which is a deterministic term. h_p pointing error, which is a random quantity and is distributed by Rayleigh. In particular, we presume that the pointing error is due to the random UAV movement. The random attenuation between UAV-UAVs due to atmospheric turbulence is h_a . h_f is the Angle of arrival (AOA) fluctuations, which are explained briefly in section 3.4.

4.4.1 Atmospheric Loss

The exponential law of Beers-Lambert as a path loss, as described below, with a length Z [Tsiftsis \(2008\)](#), [Farid and Hranilovic \(2007\)](#)

$$h_l = \exp(-Z\zeta) \quad (4.3)$$

Where the path-loss is h_l . ζ is the coefficient of attenuation, which depends on the visibility in terms of meters.

4.4.1.1 Fog

The main performance-limiting factor is fog. The loss may be above 350dB/km during a dense fog, and this link may not be available. In this chapter, analyzed for moderate to very light fog conditions under the mitigation technique to reduce the fog effect by considering a large field of view. Consider for dense fog to medium fog condition performance improvement negligible even if it increases the field of view. The mitigation technique we adapted here is receiver FOV. Based on reference [Kaushal and Kaddoum \(2016\)](#), as the receiver FOV increases, we can considerably mitigate the fog effect. Here we considered the Mie scattering attenuation coefficient for fog condition [Ghassemlooy *et al.* \(2019\)](#).

$$\zeta = \frac{3.91}{V} \left(\frac{\lambda}{550} \right)^{-q} \quad (4.4)$$

Where visibility is V , λ means wavelength. Where q is the scattering distribution coefficient of size that can be found by the model of Kim, which gives the values below

Ghassemlooy *et al.* (2019)

$$h_f = \begin{cases} 1.6, & \text{for } V > 50km \\ 1.3, & \text{for } 6km < V < 50km \\ 0.16V + 0.34, & \text{for } 1km < V < 6km \\ V - 0.5, & \text{for } 0.5km < V < 1km \\ 0, & \text{for } V < 0.5km \end{cases} \quad (4.5)$$

4.4.1.2 Rain

In the UAV-UAV FSO link, rain is another limiting factor and its loss ranges from 2dB / km to 10dB / km. By considering the adequate receiver FOV under rain conditions, we improved the performance of the UAV-UAV FSO link. The rain attenuation parameters based on adapted analytical methods proposed for FSO communication by the International Telecommunication Union- Radio communication Sector (ITU-R) have been evaluated here. We have modified the same UAV-UAV FSO link parameter as shown below [Alzenad *et al.* \(2018b\)](#), [Grabner and Kvicera \(2010\)](#).

$$\beta_{rain} = s_1 * K^{s_2} \quad (4.6)$$

Here K is the rain rate in mm/km, s_1 and s_2 are parameters and it's value's are depend on the rain drop size and temperature. In this chapter, adapted the parameter values for light and strong rain conditions which are shown in Table 4.1 and performance of UAV-UAV-FSO under different weather conditions. Brief explanation is given in results and discussions section. Here weather constituents (mm/h) are for strong rain 25 and for light rain 2.5 based on reference [Alzenad *et al.* \(2018b\)](#), [Ghassemlooy *et al.* \(2019\)](#).

4.4.2 Combined Channel Model

Based on previous derived PDFs such as turbulence-induced fading, pointing error, and AOA fluctuations, the combined PDF is derived below. Here we consider gamma-gamma turbulence channel for moderate to strong turbulence case [Nallagonda and Krishnan \(2021b\)](#). Considering PDF's Eqs. 2.25 and 2.33 in 2.35 and after some mathematical manipulations, the resultant channel model is

Table 4.1: Attenuation coefficients at 1550 nm between UAV-UAV FSO Link

Weather condition	Attenuation ζ (dB/km)
Moderate fog	33.9618
Light fog	16.0041
Very light fog	10.4251
Strong rain	6.8567
Light rain	2.0692
Haze	0.7360
Very clear air	0.0647

$$f_h(h) \approx d_2\delta(h) + f_h(h > 0), \quad (4.7)$$

where

$$d_2 = \exp\left(\frac{-\theta_{FOV}}{2(\sigma_{to}^2 + \sigma_{ro}^2)}\right),$$

$$f_h(h > 0) = \left[1 - \exp\left(\frac{-\theta_{FOV}}{2(\sigma_{to}^2 + \sigma_{ro}^2)}\right)\right] b_2$$

$$G_{1,3}^{3,0}\left(\gamma^2\gamma^2 - 1, \alpha - 1, \beta - 1 \left| \frac{\alpha\beta h'}{A_0 h_l}\right.\right),$$

where

$$b_2 = \frac{\alpha\beta\gamma^2}{A_0 h_l \Gamma(\alpha)\Gamma(\beta)},$$

4.5 Performance Analysis

4.5.1 Average Bit Error Rate

The average BER of POLSK modulation can be expressed by considering the UAV-UAV FSO link as [Tsiftsis \(2008\)](#),

$$P_e = \frac{1}{2} \int_0^\infty \operatorname{erfc}\left(\sqrt{\frac{R\xi_{Lo}h}{2\sigma_R^2}}\right) f_h(h) dh \quad (4.8)$$

Above Eq. (4.8) can be simplified with the help of [Weisstein *et al.* (2004), Eq.(07.34.03.0619.01)],and resultant as follows

$$\operatorname{erfc}(\sqrt{x}) = \frac{1}{\sqrt{\pi}} G_{1,2}^{2,0} \left(\begin{matrix} 1 \\ 0, 0.5 \end{matrix} \middle| x \right)$$

$$P_e = \frac{a1}{2} + \frac{(1-a1)b2}{2\sqrt{\pi}} \int_0^\infty G_{1,2}^{2,0} \left(\begin{matrix} 1 \\ 0, 0.5 \end{matrix} \middle| \frac{R\xi_{Lo}h}{2\sigma_R^2} \right) * G_{1,3}^{3,0} \left(\begin{matrix} \gamma^2 \\ \gamma^2 - 1, \alpha - 1, \beta - 1 \end{matrix} \middle| \frac{\alpha\beta h}{(A_0 h_l)} \right) (4.9)$$

Similarly, by utilizing [Weisstein *et al.* (2004), Eq.(07.34.21.0013.01)], and after simplification, The BER of Eq. (4.9) can be composed as

$$P_e = \frac{a1}{2} + \frac{(1-a1)\gamma^2}{2\sqrt{\pi}\Gamma(\alpha)\Gamma(\beta)} G_{4,3}^{2,3} \left(\begin{matrix} 1, 1 - \gamma^2, 1 - \beta, 1 - \alpha \\ 0, 0.5, -\gamma^2 \end{matrix} \middle| \frac{R\xi_{Lo}A_0h_l}{2\sigma_R^2\alpha\beta} \right) (4.10)$$

4.6 Results and Discussions

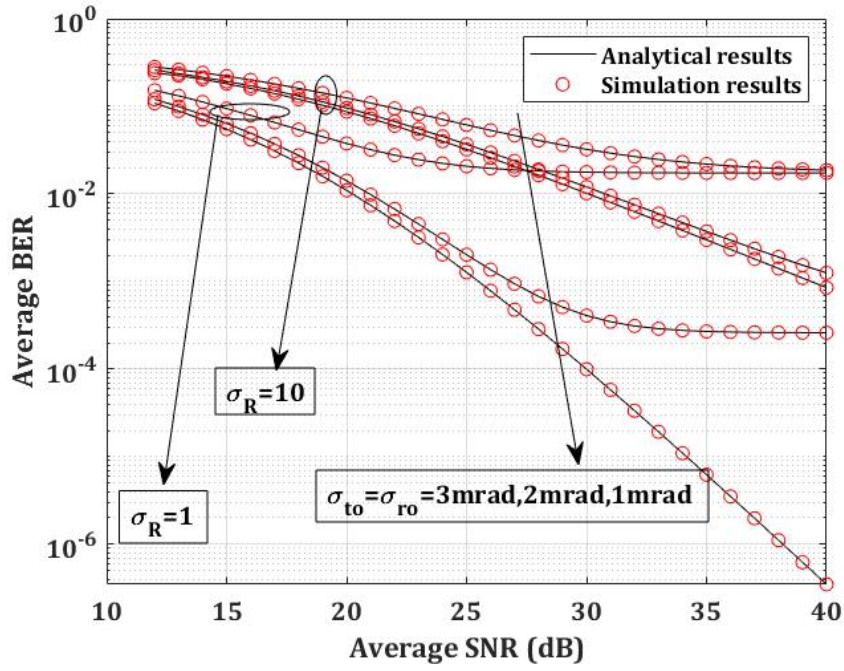


Figure 4.2: Average BER versus average SNR under very clear weather conditions for various σ_{to}, σ_{ro} values.

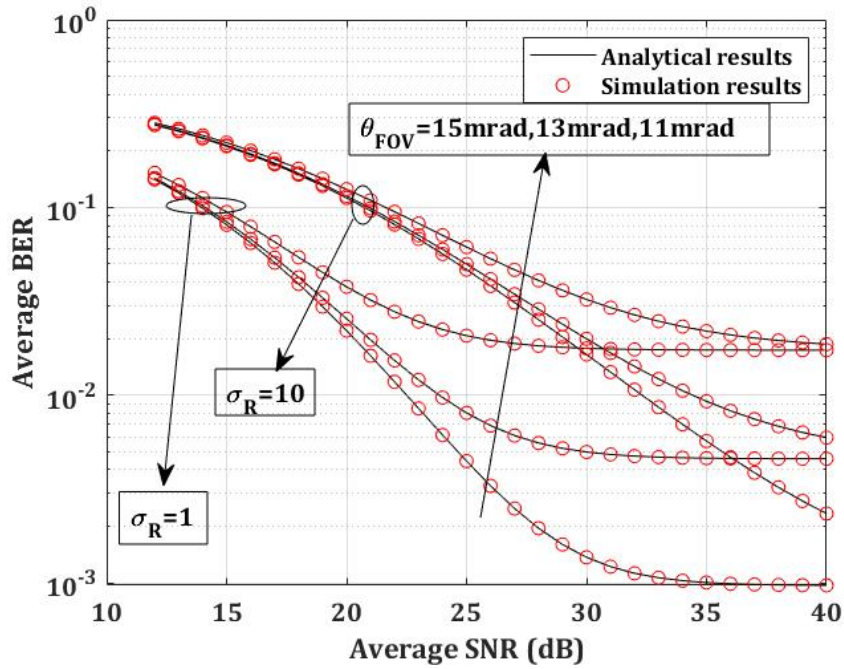


Figure 4.3: Average BER versus average SNR under very clear weather conditions for various θ_{FOV} values.

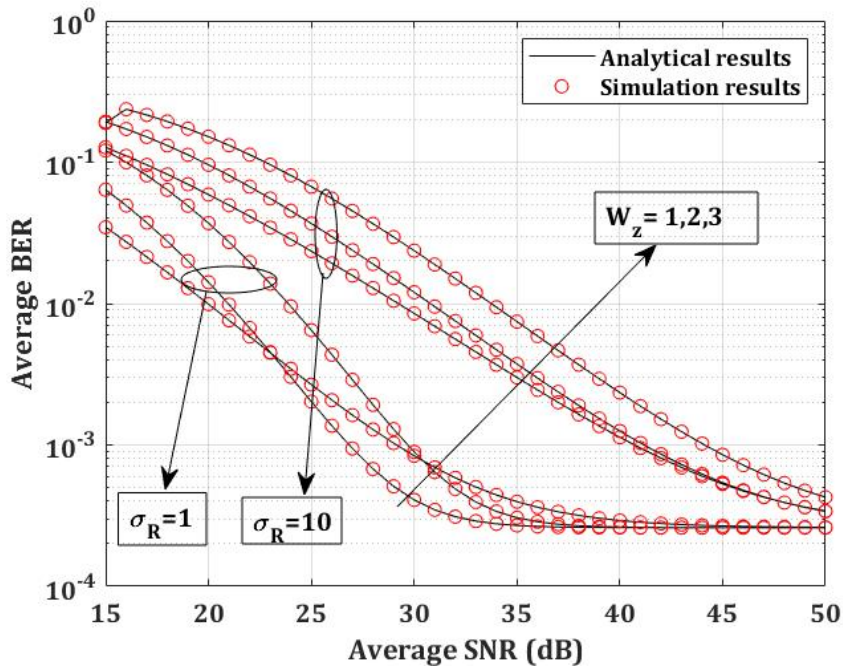


Figure 4.4: Average BER versus average SNR under very clear weather conditions for various W_z values.

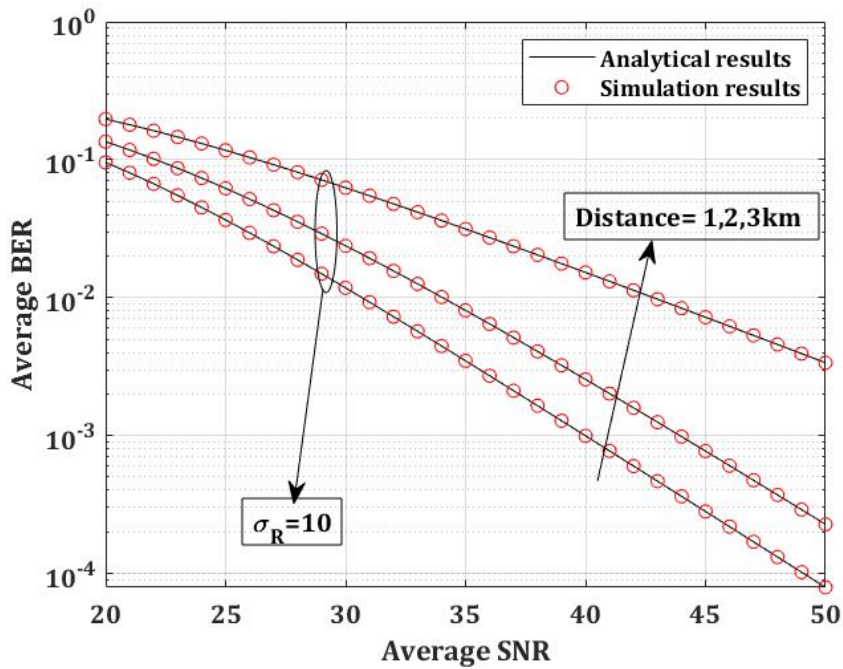


Figure 4.5: Average BER versus average SNR under very clear weather conditions for various Z values.

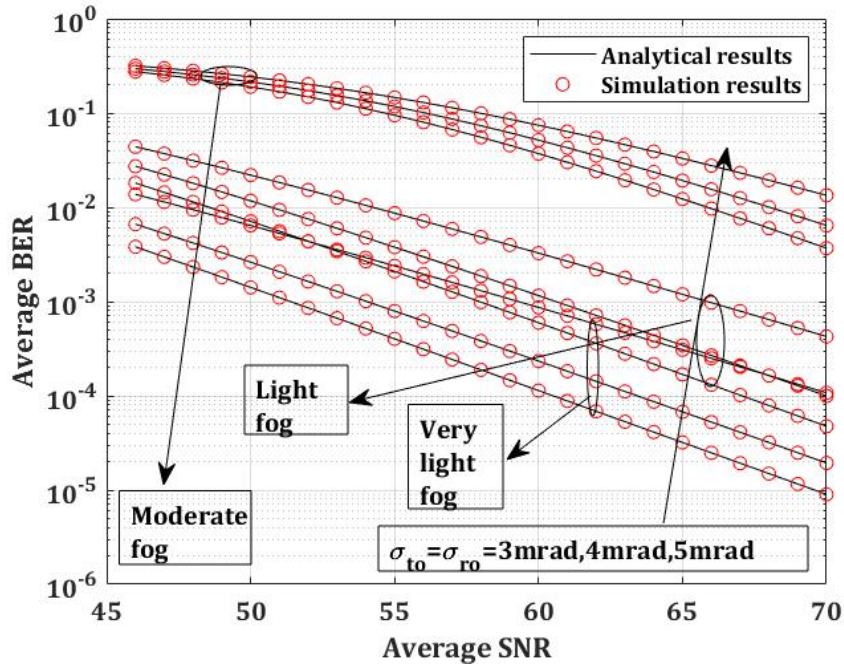


Figure 4.6: Average BER versus average SNR under different fog conditions for various σ_{to}, σ_{ro} values.

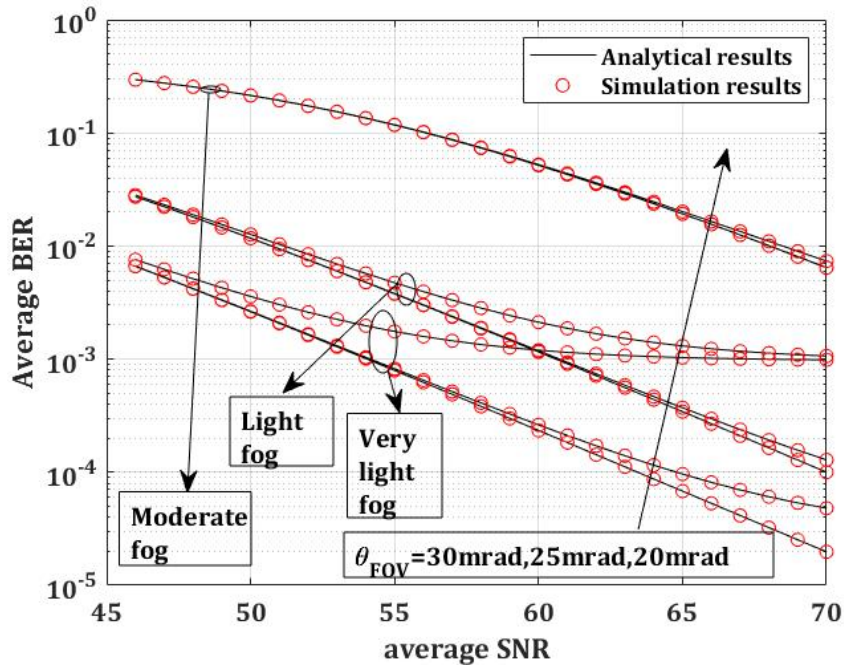


Figure 4.7: Average BER versus average SNR under different fog conditions different values of θ_{FOV} .

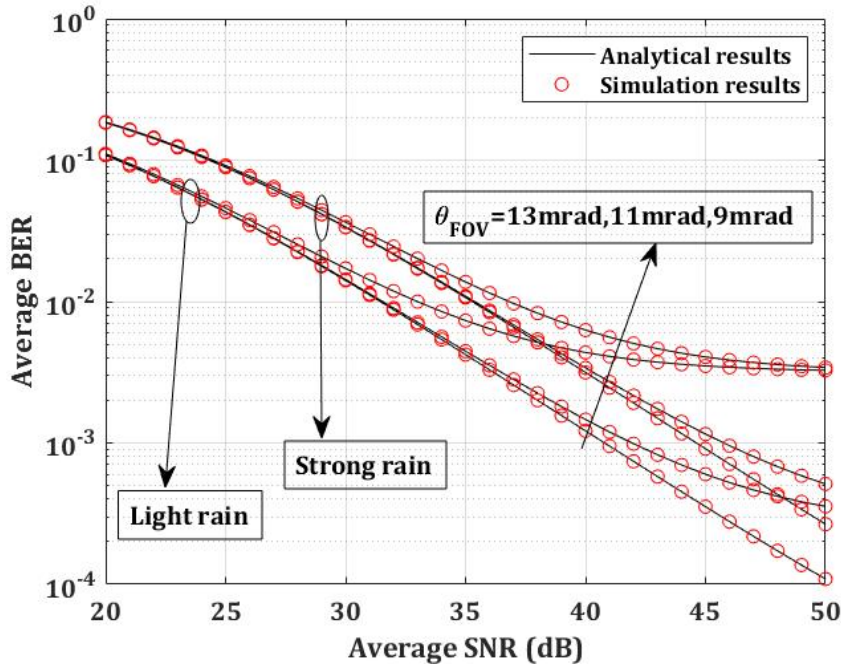


Figure 4.8: Average BER versus average SNR under different rain conditions for different values of θ_{FOV} .

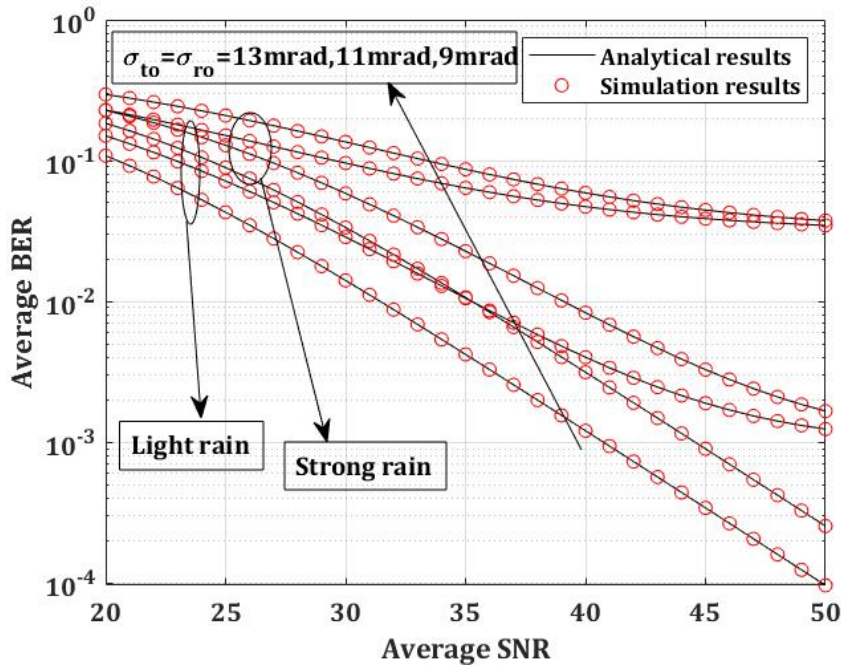


Figure 4.9: Average BER versus average SNR under different rain conditions for different values of σ_{to}, σ_{ro} .

The table 4.2 and 4.3 for Analytical and Simulation results of Fig.4.6 and Fig.4.7.

Table 4.2: Optimal values of θ_{FOV} to achieve Average BER over GG Turbulence Model for $SNR = 50dB, \sigma_{t_o} = \sigma_{r_o} = 30cm$, and different fog conditions.

Weather condition	$\theta_{FOV}(mrad)$	Average BER
Moderate fog	20	0.2
Light fog	20	2.8×10^{-2}
very Light fog	20	4.7×10^{-3}

Table 4.3: Optimal values of θ_{FOV} to achieve Average BER over GG Turbulence Model for $SNR = 40dB, \sigma_{t_o} = \sigma_{r_o} = 30cm$ and different rain conditions.

Weather condition	$\theta_{FOV}(mrad)$	Average BER
Strong rain	13	7×10^{-3}
	11	3.5×10^{-3}
	9	3×10^{-3}
Light rain	13	5×10^{-3}
	11	1.5×10^{-3}
	9	1.2×10^{-3}

In this section, compared the derived analytical expressions with computer simulations between UAV-UAV FSO link under different weather conditions. Considered fixed computer simulations parameter's as follows lens radius $r_a = 5cm$, photo detector responsivity $R = 0.5$, distance between UAV-UAV $Z = 1km$, optical bandwidth $B_o = 10nm$, Rytov variance $\sigma_R = 0.5$ to 10 for moderate to strong turbulence fading channel, field of view(θ_{FOV}) = 20mrad, and $\sigma_{t_o} = \sigma_{r_o} = 3mrad$ orientation fluctuations of UAV, and $\sigma_{t_p} = \sigma_{r_p} = 30mrad$ position fluctuations of UAV.

By consider a UAV-UAV FSO link in Fig.4.2; the average BER versus average SNR for different values of turbulence-induced fading σ_R , here showed the results for moderate to strong turbulence fading channel for POLSK modulation. Whereas in Fig.4.3, the average BER showed for different values of θ_{FOV} against the average SNR, if sufficient θ_{FOV} available the performance of POLSK improvement was shown in Fig.4.5. It is revealed in Fig.4.4, the optimal value for the beam width section for

minimizes required SNR under moderate and strong turbulence fading between the UAV-UAV FSO link shown. In Fig.4.5, by comparing the POLSK modulation performance by varying the distance for long-range air-to-air applications, and it concluded that based on Fig.4.5, results showed significant performance improvement between UAV-UAV FSO link under strong turbulence conditions and this POLSK modulation best suitable modulation for air-to-air, ground-to-air, and air-to-ground links.

In Fig.4.6, plotted the average SNR versus average BER under different fog conditions, where we considered moderate, light, and very light fog conditions into account. By varying different σ_{to}, σ_{ro} from Fig.4.6 as σ_{to} and σ_{ro} increases the performance become worst between UAV-UAV FSO links which was shown for different fog conditions. From Fig.4.6 find the optimal values under different fog conditions and identified that for lower values of σ_{to}, σ_{ro} performance improves. UAV-UAV FSO link with sufficient θ_{FOV} and lower value of σ_{to}, σ_{ro} with POLSK modulation greater link improvement and mitigate by selecting optimal values as shown in this chapter. Similarly, Fig.4.7, shows the important results to mitigate the fog by improving the receiver θ_{FOV} , which was shown in this chapter and cited in reference [3].

Selecting the optimal values based on results shown in this chapter Fig.4.7. Here, considered for lower values of θ_{FOV} and σ_{to}, σ_{ro} performance is evaluated. For higher values θ_{FOV} the performance remains constant due to increased background noise power. In Fig.4.8, and Fig.4.9, showed the performance of the UAV-UAV FSO link under rain conditions. Here, considered performance analysis of UAV-UAV FSO link under light to strong rain for different values of θ_{FOV} , σ_{to} , and σ_{ro} results showed that considerable performance deviation by increasing the θ_{FOV} to mitigate the rain effect by considering optimal values.

The performance of UAV-based FSO system mainly depends on Different fog conditions, which are shown in Table 4.2 and Table 4.3 and different values of θ_{FOV} , σ_{ro} , σ_{to} respectively. We notice from Table 4.3 that a fixed value of θ_{FOV} the minimum average BER is achieved under very light fog conditions and which shows low link attenuation. On the other hand, θ_{FOV} increases average BER decreases, which is shown in Fig.4.7, and the performance mainly depends on the optimal values of θ_{FOV} . From Table 4.3, we observe that as the θ_{FOV} increases, minimum average BER is achieved under strong rain conditions. Compared to strong rain conditions, light rain conditions minimum BER is achieved for optimal values of θ_{FOV} , σ_{ro}, σ_{to} and very low link interpretation is possible under light rain conditions.

4.7 Summary

POLSK modulation was suggested as an alternative for UAV-based FSO communication systems to other modulation techniques. This chapter analysed the BER performance of UAV-based FSO communication systems under various weather effects that are taken into account and described in this chapter as a closed-form expression for BER performance analysis. Optimal values are also provided for the FOV to achieve the minimum BER for different SNR values. In terms of long-distance applications such as air-to-air, ground-to-air, and air-to - ground links, POLSK modulation is the best solution for next-generation wireless communication, and the corresponding results are shown in this chapter. Distance evaluation proposed through POLSK modulation for the UAV-based FSO link, and the performance results shown in this chapter. Finally, fog and rain mitigation with an increasing receiver field of view and corresponding results are seen.

Chapter 5

CODED GROUND-TO-HAP BASED FSO COMMUNICATION SYSTEM USING POLSK MODULATION

5.1 Introduction

Free-Space Optical (FSO) communication, a future emerging technology for next-generation communication systems, was aided by High Altitude Platforms (HAPs). HAP aided FSO communication systems, making a significant contribution to data hunger applications. There are some constraints to establishing an efficient link, such as weather conditions, Angle of Arrival (AoA) fluctuations, and pointing error loss due to the HAP's hovering state. In this chapter, we proposed Ground-to-HAP FSO communication system using Polarization Shift Keying (POLSK) modulation technique. We derived the closed-form expression for the proposed system's Average Bit Error Rate (BER) and plotted the results for various link parameters such as transmitted power, field-of-view, and receiver UAV orientation deviation under different weather conditions rain (light and strong) and fog (light and moderate). Coding techniques (repetition and BCH) are used to improve the ABER performance of the proposed system. The obtained results are compared to both Un-coded and Coded cases. The coding gain achieved is 28.5 dB.

5.2 Main Contributions

The major contributions in the Chapter 5 are as follows,

- Proposed Ground-to-HAP FSO communication system using Polarization Shift Keying (POLSK) modulation technique.
- We improved the performance of Ground-to-HAP link under different weather conditions.
- Coding techniques (repetition and BCH) are used to improve the ABER performance of the proposed system.

The rest of the chapter is organized as follows: Section 5.3 describes the systems and received signal model under consideration. Section 2.4 the channel state modeled under path loss under different weather conditions, atmospheric turbulence fading, pointing loss, AOA fluctuations, and beam wandering effect, is also described. New probability density function (PDF) incorporated the combined effect between the ground-to-HAP link obtained in closed form. Coded Ground-to-HAP FSO Link was introduced in Section 5.5. A derived analytical expression is presented in Section 5.6. POLSK modulation under different weather conditions Results and discussion are presented in Section 5.7. Finally some conclusions, and its remarks are presented in Section 5.8.

5.3 System Model

This chapter focuses on the HAP-based FSO system, as presented in Fig.5.1, that offer fronthaul/backhaul for next-generation wireless communications systems and other applications(remote sensing, broadcasting or telecommunication, navigation, and localization systems, surveillance missions, etc.). Typical distance from the Ground-to-HAP as 17km to 25km for HAP applications above the clouds. In Fig.5.2, we assume the Ground station is fixed. Optical signal transmission is transmitted through the receiver's optical channel; the received signal is a composite effect of path loss, atmospheric turbulence fading, pointing error, AOA fluctuations, and beam wandering effect. The distance between ground to HAP is L . The mean position of the receiver are $R_r = (0, 0, 0)$. Due to random deviations the instantaneous position fluctuation of HAP is $R_i = (r_x, r_y, r_z)$. Here r_x, r_y , and r_z are independent random variables and fluctuation of HAP. The position fluctuation of z-axis are negligible. Orientation deviation of HAP are denoted by θ_{rx} and θ_{ry} along x-z, y-z axis. The position

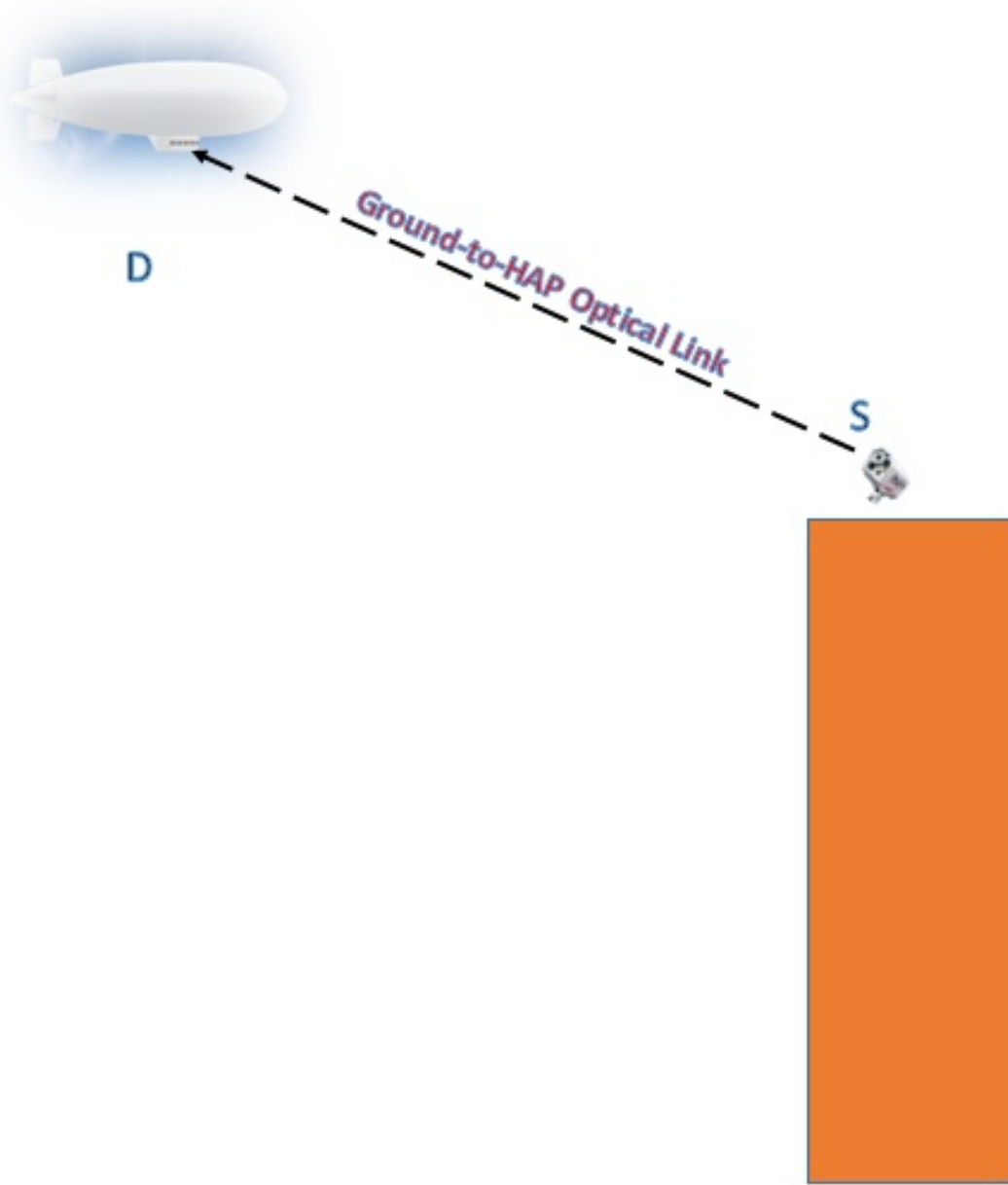


Figure 5.1: Graphical illustration of Ground-to-HAP optical communication link.

and orientation deviations of HAP with a Gaussian distribution, its variance are σ_p^2 , σ_0^2 , respectively. Another parameter that affects the HAP link is the beam wandering effect, mostly caused by large scale turbulence. It is defined as the angular deviation of the beam from the line-of-sight path at the receiver and its variance is defined as

$$\sigma_r = 2.07 \int_{h_0}^H C_n^2(k) (L - k)^2 W_k^{-\frac{1}{3}} \quad (5.1)$$

Where C_n^2 is the turbulence strength as a function of altitude k , h_0 is the height of the transmitter above the ground, H is the height of the HAP, W_k is the beam width, L is the distance from the ground to HAP is given by $(H - h_0) \sec(\zeta)$, where ζ is the HAP zenith angle. C_n^2 value calculated using Hufnagel-Valley (H-V) model. $C_n^2(k)$ is function of k , which can be calculated as

$$C_n^2(k) = 0.00594(V_m/27)^2(10^{-5}k)^{10}e^{-k/1000} + 2.7 * 10^{-16}e^{-k/1500} + S_t e^{-k/100} \quad (5.2)$$

where, V_m is the root-mean-square (rms) wind speed in meter per second (m/s) and S_t is the nominal value of $C_n^2(0)$ at the ground in $m^{-2/3}$

Fig.5.1. shows the optical link between ground-to-HAP using the POLSK modulation at the transmitter. The laser beam propagated through the slant path through a Gamma-Gamma (GG) turbulence channel with additive white gaussian noise (AWGN) with the effect of pointing error, AOA fluctuations, the resultant received beam collected at the photodetector (PD) is mathematically modeled as

$$r = Rhs + n \quad (5.3)$$

h is the normalized channel fading coefficient between Ground to HAP vertical link, which is constant over the period and overall channel loss. R is Responsivity. Here s is the number of symbols transmitted between Ground-HAP FSO link with transmitted power P_t . n is photo noise and which is signal independent zero mean Gaussian noise with variance $\sigma_n^2 = 2eB_eRP_b$ e is electron charge B_e is the photo detector bandwidth P_b back ground power which is defined as $P_b = A_a B_o N_b(\lambda) \Omega_{FOV}$, where $N_b(\lambda)$ is the spectral radiance of the background radiations at wavelength λ , B_o is the bandwidth of the optical filter at the Rx and A_a is the lens area. Moreover, Ω_{FOV} denotes the Rx FOV that can be represented as $\Omega_{FOV} = \pi \theta_{FOV}^2 / 4$, here, $\theta_{FOV} = 2r_p / d_f$ denote the FOV angle, where d_f and r_p are the focal length radius and radius of circular photo detector

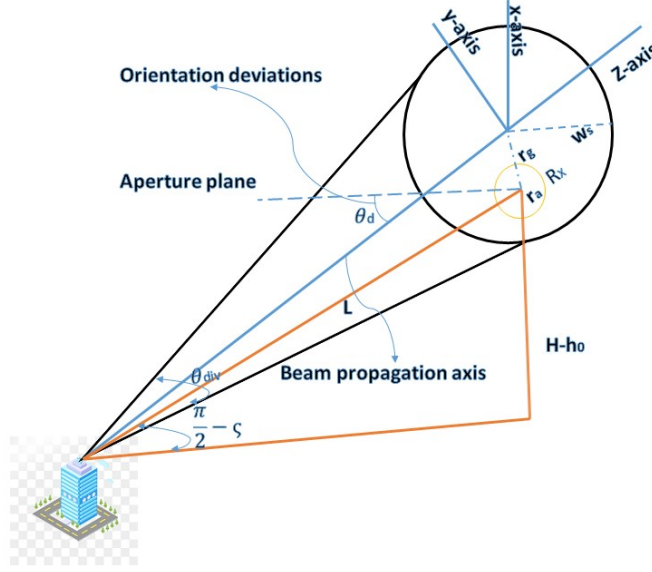


Figure 5.2: The schematic of Ground-to-HAP optical communication link with length L with HAP hovering state parameter values are given in table II [Safi *et al.* (2020), Fig.(2)]

5.4 Channel Model

We derived the Ground-to-HAP channel model with Meijer's G Functions by considering HAP node hovering fluctuations, pointing error, turbulence fading, pathloss and AOA fluctuations. Detailed channel model was derived in chapter 2.4

$$f_h(h) \approx d_2 \delta(h) + f_h(h > 0), \quad (5.4)$$

where

$$d_2 = \exp\left(\frac{-\theta_{FOV}^2}{2\sigma_{rd}^2}\right),$$

$$f_h(h > 0) = \left[1 - \exp\left(\frac{-\theta_{FOV}^2}{2\sigma_{rd}^2}\right)\right] * b_2 * G_{1,3}^{3,0}\left(\begin{matrix} \gamma^2 \\ \gamma^2 - 1, \alpha - 1, \beta - 1 \end{matrix} \middle| \frac{\alpha\beta h}{h_l}\right),$$

$$b_2 = \frac{\left[2\left(\frac{r_a}{W_z}\right)^2\right]^{-\gamma^2} \alpha\beta\gamma^2}{h_l \Gamma(\alpha)\Gamma(\beta)}.$$

5.5 Coded Ground-to-HAP FSO Link

In Ground-to-HAP links, the performance is mainly degraded by its hovering fluctuations of HAP and atmospheric turbulence effect. In this chapter, we evaluated the BER performance of the Ground-to-HAP link with BCH Code and Repetition Code to mitigate the effects mentioned above. To improve the performance of Ground-to-HAP Link, we introduced two Coding techniques in this chapter. The performance of Coded Link is compared with Un-Coded Ground-to-HAP link over G-G turbulence channel. BCH Codes are effectively correct the multiple random error patterns. BCH Codes parameters t , and (n,k) are described with block length $n = 2^m - 1$, Here m is positive integer($m \geq 3$). The number of check bits $n-k \leq mt$ and minimum distance $d_{min} \geq 2t+1$. t is the number of error-correcting BCH Code. Generator polynomial generated from Galois Field $GF(2^k)$ of its roots. $g(x)$ has $\alpha, \alpha^2, \dots, \alpha^{2t}$ and its conjugates as its roots. The $g(x)$ from $X^n + 1$ polynomial by taking X^{n-k} . The generator polynomial obtained as follows [Gupta et al. \(2019\)](#), [Hanna and El Rouayheb \(2018\)](#), [Al-Barrak et al. \(2017\)](#)

$$g(x) = 1 + x^2 + x^4 + x^6 + x^7 + x^9 + x^{10} + x^{13} + x^{17} + x^{18} + x^{20} \quad (5.5)$$

This generator polynomial is used to find the Generator matrix. we adapted this Eq. (5.5) from [\[Ramavath et al. \(2020\), Eq.\(3\)\]](#) The Encoded data is generated with input optical signal and Generator matrix. This encoded BCH Coded data is modulated with POLSK modulation and propagated through the G-G turbulence channel. This optical signal is received at the receiver with PD. Due to hovering fluctuations, the received optical signal is received with errors. This received optical signal is detected and corrected with the Berlekamp-Massey decoding algorithm.

More frequently used error-correcting Code in FSO systems is Repetition Code. Here we repeat the optical input information several times to retrieve the original optical signal corrupted by the optical channel. For an (n, k) repetition codes generator polynomial is given as follows [Gupta et al. \(2019\)](#), [Hanna and El Rouayheb \(2018\)](#), [Al-Barrak et al. \(2017\)](#)

$$g(x) = 1 + x + x^2 \quad (5.6)$$

Here $n = 3$, $k=1$, and its generator matrix is $G = [1 \ 1 \ 1]$. Code rate is k/n . Majority decoding is used for decoding the received Ground-to-HAP optical link at PD

5.6 Average BER

The average BER for the considered ground-to-HAP-based FSO communication link with POLSK modulation closed-form expression was derived. In this Ground-to-HAP communication link, performance is analyzed over the moderate to strong turbulence condition with Meijer's G is derived as [Tsiftsis \(2008\)](#), [Prabu and Kumar \(2015\)](#), [Prabu et al. \(2018\)](#),

$$P_e = \frac{1}{2} \int_0^\infty \operatorname{erfc}\left(\sqrt{\frac{R\xi_{Lo}h}{2\sigma_R^2}}\right) f_h(h) dh \quad (5.7)$$

Eq. (5.7) can be simplified with the help of [[Weisstein et al. \(2004\)](#), Eq.(07.34.03.0619.01)], and substituting $\operatorname{erfc}(\sqrt{x})$ into Eq. (5.7) the simplified form is as

$$\operatorname{erfc}(\sqrt{x}) = \frac{1}{\sqrt{\pi}} G_{1,2}^{2,0} \left(\begin{matrix} 1 \\ 0, 0.5 \end{matrix} \middle| x \right)$$

$$P_e = \frac{a1}{2} + \frac{(1-a1)b2}{2\sqrt{\pi}} \int_0^\infty G_{1,2}^{2,0} \left(\begin{matrix} 1 \\ 0, 0.5 \end{matrix} \middle| \frac{R\xi_{Lo}h}{2\sigma_R^2} \right) * G_{1,3}^{3,0} \left(\begin{matrix} \gamma^2 \\ \gamma^2 - 1, \alpha - 1, \beta - 1 \end{matrix} \middle| \frac{\alpha\beta h}{h_l} \right) dh \quad (5.8)$$

Similarly, by utilizing [[Weisstein et al. \(2004\)](#), Eq.(07.34.21.0013.01)], and after some mathematical manipulations, the expression for BER between Ground-to-HAP communication link performance is derived as

$$P_e = \frac{a1}{2} + \frac{\left[2\left(\frac{r_a}{W_z^2}\right)^2\right]^{-\gamma^2} (1-a1)\gamma^2}{2\sqrt{\pi}\Gamma(\alpha)\Gamma(\beta)} G_{4,3}^{2,3} \left(\begin{matrix} 1, 1 - \gamma^2, 1 - \beta, 1 - \alpha \\ 0, 0.5, -\gamma^2 \end{matrix} \middle| \frac{R\xi_{Lo}h_l}{2\sigma_R^2\alpha\beta} \right) \quad (5.9)$$

5.6.1 BCH Code

BCH Codes are multiple-error-correcting capable binary cyclic Codes. These Codes add the redundant information to the input optical signal. Here k information bits are converted into n bit Code word with $n-k$ bit's as redundant bit's. Here n/k represents Code rate(R). Detailed description of BCH Coded encoding and decoding

for FSO channels was discussed in [Tsiftsis \(2008\)](#), [Prabu and Kumar \(2015\)](#), [Prabu et al. \(2018\)](#). BCH Coded Ground-to-HAP link BER formulation is given below as

$$P_{e,BCH} \approx \frac{1}{n} \sum_{i=t+1}^n i \binom{n}{i} P_e^i (1 - P_e)^{n-i} \quad (5.10)$$

where t is error patterns, n is block length and P_e is the average BER for Coded Ground-to-HAP optical Link under hovering fluctuations.

5.6.2 Repetition Code

Repetition Code is one of the simplest Coding techniques in Coding theory. Its encoding involves repeating the optical information bits N times resulting in $(N, 1)$ block Code, and decoding is done by majority rule is employed. Repetition Code encoding and decoding with FSO channel was analyzed in [Tsiftsis \(2008\)](#), [Prabu and Kumar \(2015\)](#), [Prabu et al. \(2018\)](#). Here $1/N$ is the Code rate. The BER for Ground-to-HAP links under hovering fluctuations for repetition Code is given as follows

$$P_{e,R} \approx \sum_{j=N/2}^N \binom{n}{j} P_e^j (1 - P_e)^{n-j} \quad (5.11)$$

where P_e is the POLSK modulated BER

5.7 Results and Discussions

In this section, we considered the Ground-to-HAP communication optical link with POLSK under different weather conditions. We have mitigated the turbulence effect and weather effect by improving the receiver FOV with POLSK. Derived the analytical results and showed them in previous sections. Derived analytical results are compared with simulation results. We evaluated optical link performance in terms of average BER. Study the impacts of different parameters such as receiver FOV, Orientation deviations, the transmitted beam spot size. Understanding of Ground-to-HAP optical link analyzed with GG model for moderate to strong turbulence conditions. This chapter analysis showed the optimal value selection under different weather conditions for Ground-to-HAP optical link.

In Fig. [Fig.5.3](#), average BER versus transmitted power by varying the different values of Receiver FOV with POLSK modulation was shown. As receiver FOV increases, the optical link's performance with POLSK modulation improves the Ground-to-HAP

Table 5.1: Analytical and Simulation Parameters

Parameters Used for The Numerical Results	
Parameter	Value
Wavelength λ	1550 nm
Responsivity η	0.5
Optical bandwidth B_o	10 nm
Receiver electrical bandwidth B_e	1GHz
Spectral radiance $N_b(\lambda)$	$10^{-3}W/cm^2 - m - srad$
HAP zenith angle ς	45°
Link length L	20km
wind speed V_m	21 m/s
Refractive index structure at the ground $C_n^2(0)$	$1.7 * 10^{-13} m^{-2/3}$

link for the order of mrad's. In Fig. 5.4, plotted the average BER versus FOV for different values of σ_{rd} as orientation deviation fluctuations increase the performance of POLSK optical link considerable performance deviation shown in Fig. 5.4. In Fig. 5.5, different values σ_{rd} with transmitted power results are shown and Fig. 5.6, optimal selection of W_z was evaluated.

Fog is the main attenuation factor between ground-to-HAP optical links. This chapter evaluated the optimal values for Ground-to-HAP optical link under different fog conditions. Selecting the receiver FOV fog effect is mitigated, which shown in Fig. 5.7. results plotted in Fig. 5.7, between medium to light fog condition. For light fog conditions, considerable performance improvement is observed with increasing receiver FOV. In Fig. 5.8, fog affected link performance was shown for different values of orientation deviation (σ_{rd}). Selecting the optimal values of HAP orientation deviations and receiver FOV, we can improve the Ground-to-HAP optical link performance. Rain is another critical factor that affects the optical link. This chapter evaluated the performance under rain strong and light rain conditions. Improved the link performance under POLSK modulation by selecting the results of the optimal values are shown in Fig. 5.9, and Fig. 5.10. In this chapter, we evaluated the

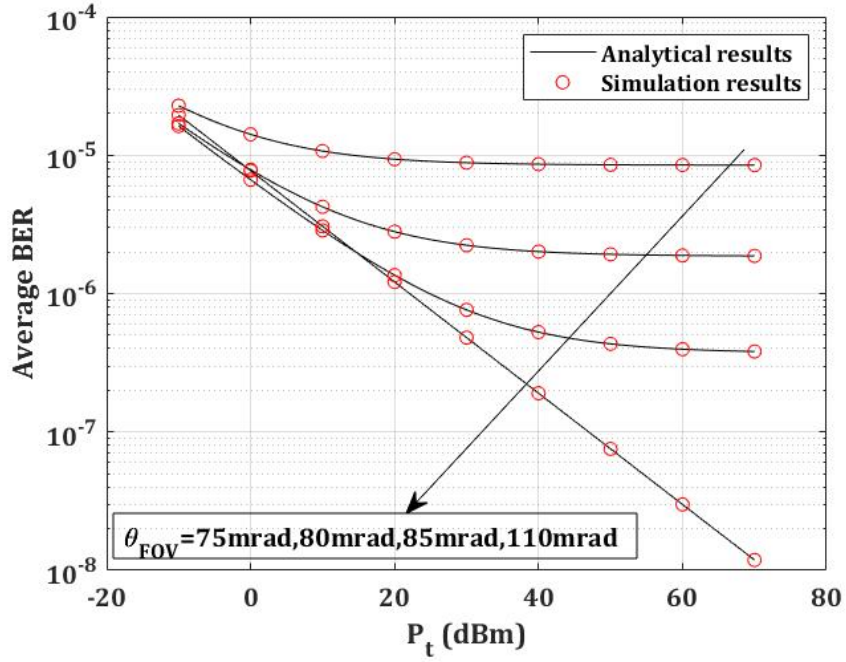


Figure 5.3: Average BER versus transmitted power $P_t(dBm)$ over very clear sky condition for $W_z=2$, $\sigma_{ro} = 0.4$, $\sigma_{rd} = 16mrad$, different values of θ_{FOV} with POLSK modulation

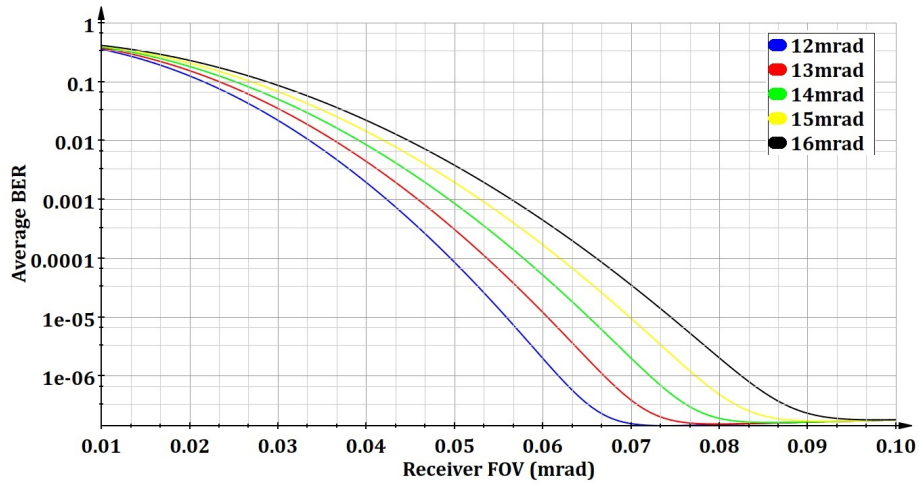


Figure 5.4: Analytical Average BER versus receiver FOV (θ_{FOV}) over very clear sky condition for $W_z=2$, $\sigma_{ro} = 0.4$, different values of σ_{rd} with POLSK modulation

BER performance of Coded Ground-to-HAP link in Fig. 5.11, by considering high values of orientation deviation of HAP with optimal FOV. Here the coding gain for Ground-to-HAP channel evaluated as

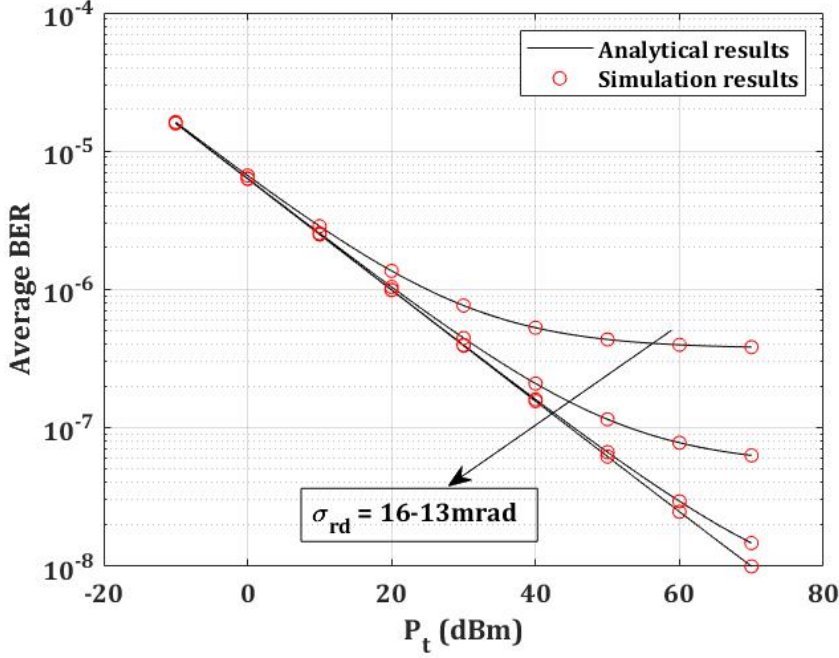


Figure 5.5: Average BER versus transmitted power $P_t(\text{dBm})$ over very clear sky condition for $W_z=2$, $\sigma_{ro} = 0.4$, $\theta_{FOV} = 75\text{mrad}$, different values of σ_{rd} with POLSK modulation.

$$\text{Coding gain (dB)} = 10 \log_{10} \left(\frac{P_t(\text{uncoded system})}{P_t(\text{coded system})} \right) \quad (5.12)$$

The coding gain for Un-Coded to the Coded system between Ground-to-HAP link was 28.5 dB was achieved, which is shown in Fig. 5.11. The coding gain increases remarkably with POLSK modulation as the code size increases with the fixed code rate under the Ground-to-HAP link. The coding gain for the BCH-Coded system over the Repetition Code is 8.5 dB. BCH Code provides a higher coding gain when compared to repetition Code. In Fig. 5.11, We considered two coded techniques performance with un-Coded Ground-to-HAP link. We have reached the theoretical results with analytical results plotted in Fig. 5.11. We concluded that the BCH Coded system provided much better performance compared to the Repetition Code and overall performance improvement possible with BCH Code.

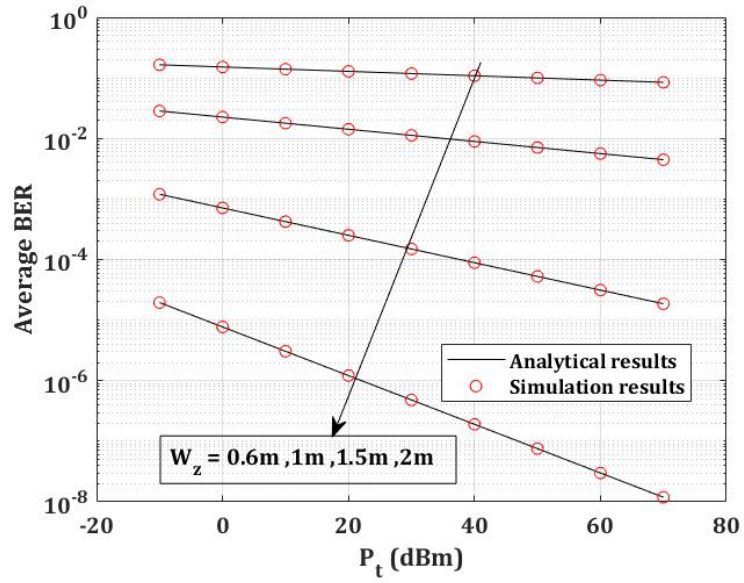


Figure 5.6: Average BER versus transmitted power P_t (dBm) over very clear sky condition for $\sigma_{rd}=13\text{mrad}$, $\sigma_{ro} = 0.4$, $\theta_{FOV} = 75\text{mrad}$, different values of W_z with POLSK modulation.

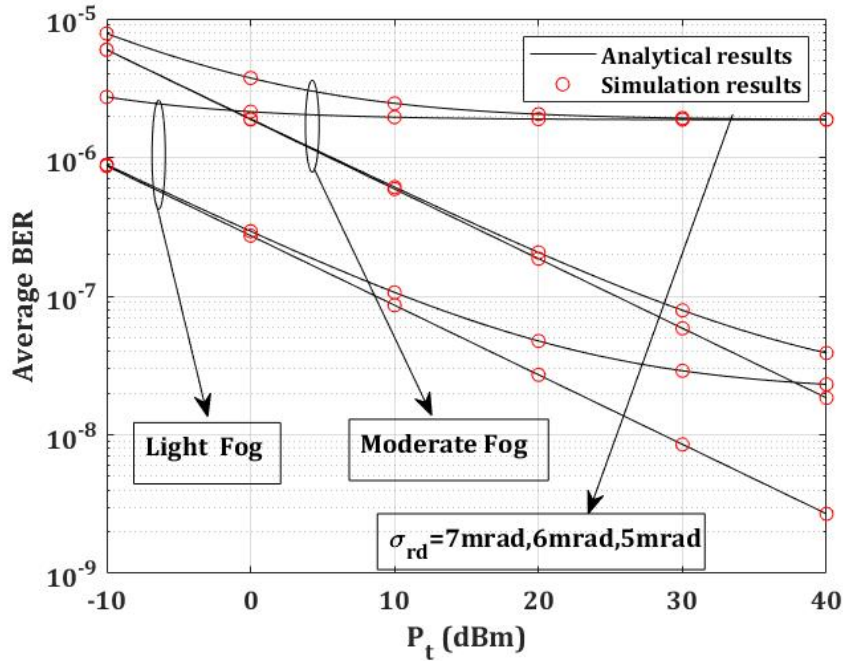


Figure 5.7: Average BER versus Average SNR under different Fog conditions for $W_z=2$, $\sigma_{ro} = 0.4$, $\theta_{FOV} = 15\text{mrad}$, different values of σ_{rd} with POLSK modulation.

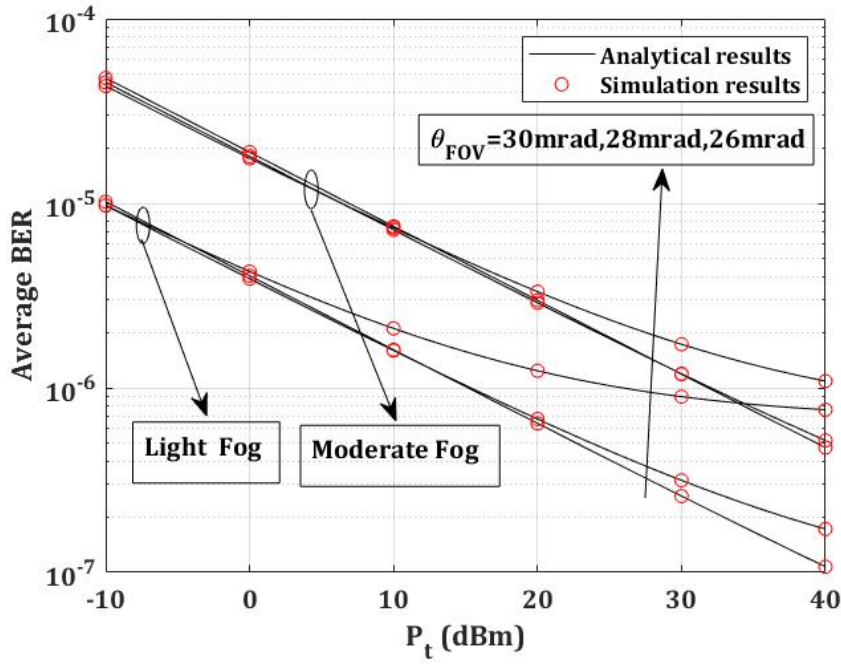


Figure 5.8: Average BER versus average SNR under different fog conditions for $W_z = 2$, $\sigma_{r_o} = 0.4$, $\sigma_{r_d} = 5\text{mrad}$, different values of θ_{FOV} with POLSK modulation.

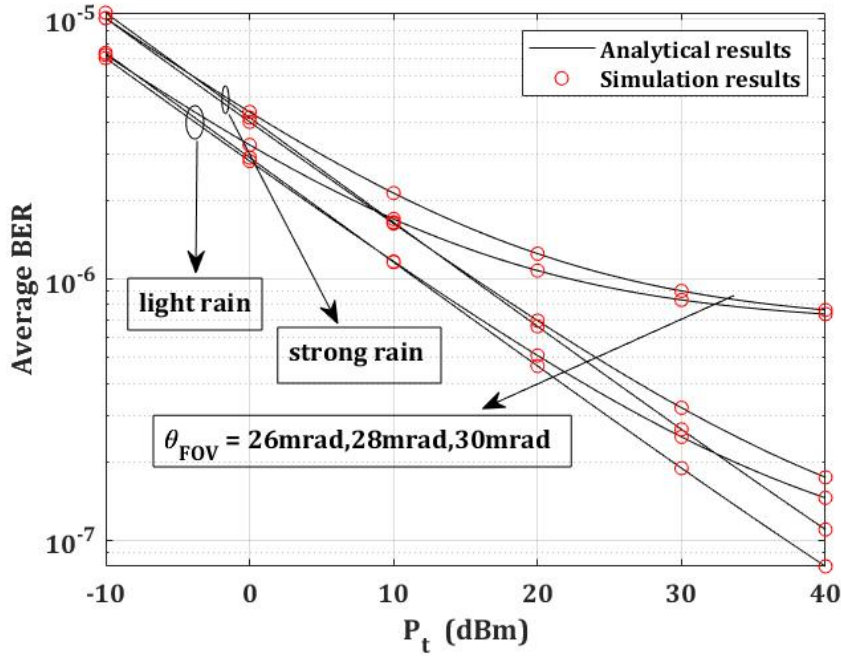


Figure 5.9: Average BER versus average SNR under different rain conditions for $W_z = 2$, $\sigma_{r_o} = 0.4$, $\sigma_{r_d} = 3\text{mrad}$, different values of θ_{FOV} with POLSK modulation.

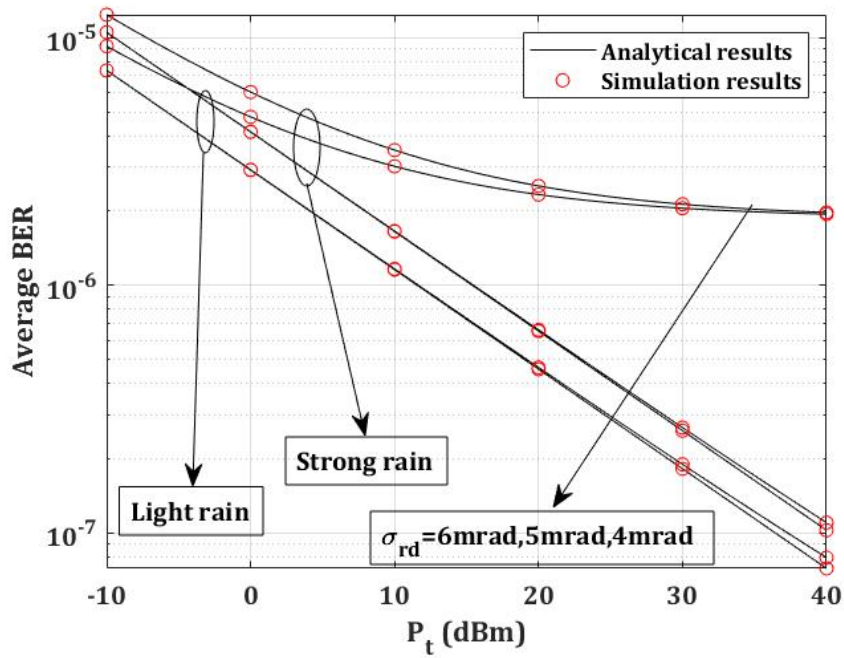


Figure 5.10: Average BER versus average SNR under different rain conditions for $W_z = 2$, $\sigma_{r_o} = 0.4$, $\theta_{FOV} = 30\text{mrad}$, different values of σ_{rd} with POLSK modulation.

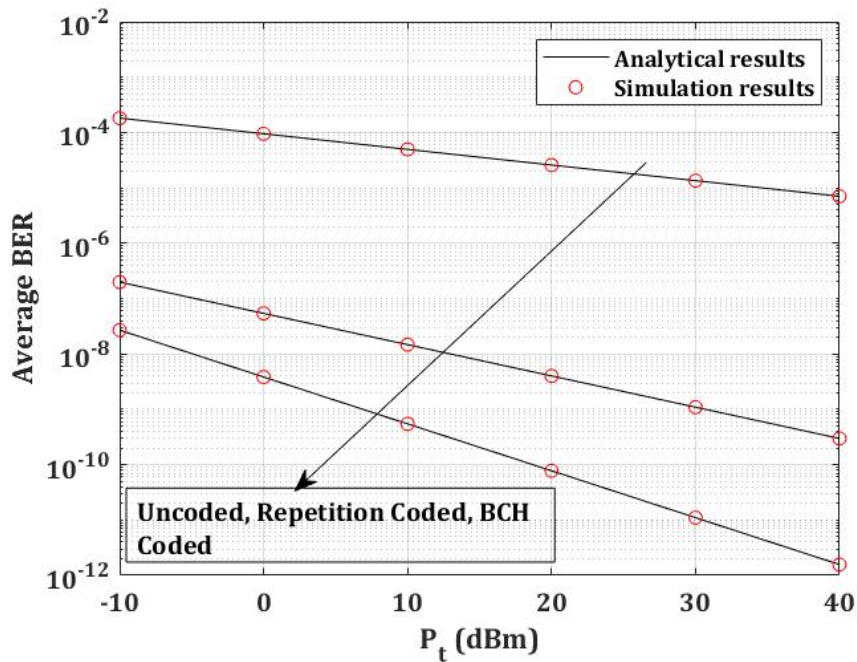


Figure 5.11: Analytical and simulation results for coded Ground-to-HAP Optical Link with POLSK modulation.

5.8 Summary

We evaluated the performance of the Ground-to-HAP optical link under the different weather conditions with POLSK modulation. Optimal values demonstrated in the results section mitigated the weather effect by increasing the Receiver FOV. Closed-form expression is derived between Ground-to-HAP optical link with POLSK by utilizing Meijer's G Functions. Performance improvement under the Fog, rain, and cloud was evaluated under random HAP fluctuations. Finally the performance of Ground-to-HAP Link is evaluated with coding techniques.

Chapter 6

CONVERGENT FSO BASED HAP COMMUNICATION SYSTEM WITH UWOC COMMUNICATION SYSTEM

6.1 Introduction

We analyze the performance of High altitude platforms-underwater wireless optical communication (HAP-UWOC) Communication systems under the Decode-and-forward (DF) relaying protocol. The HAP and UWOC links experience generalized Gamma-Gamma distributed fading, respectively. The transmitter node (S) is placed above the earth at 20Km, where the relay is placed at the ocean. The HAP-to-Ground hovering state channel model, the clear ocean, coastal ocean, Turbid harbor, effect of HAP hovering fluctuations are considered. We derive the closed-form expressions for outage probability and average bit error rate (BER) with the DF relay technique. Derived the End-to-End closed-form expression with Meijer's G functions and derived mathematical expression compared with simulation results. Explores how the clear ocean, coastal water, Turbid harbor, and HAP hovering state fluctuation such as orientation deviation, receiver field-of-view(FOV), performance analysis of dual-hop HAP-UWOC system are evaluated.

Here source S is located 20km above the ocean under a hovering state communicating with the underwater link with the help of decode-and-forward (DF) relay.

Dual-hop HAP-UWOC system link is evaluated by considering HAP and UWOC as GG distributions channel models under hovering state. The closed-form expression for outage and BER is derived. Derived end-to-end analytical expression with Meijer's G functions. Derived analytical expressions compared with system simulations. results show that End-to-End performance is mainly dominated by the UWOC link. HAP-to-Ground link GG distributed with weak turbulence fading under hovering fluctuation, so the performance mainly deviated by UWOC link wherein shown in the results section. We showed the performance analysis of the HAP-to-Ground channel model under hovering fluctuations and compared it with the UWOC link.

6.2 Main Contributions

The major contributions in the Chapter 6 are as follows,

- For the first time proposed the High altitude platforms-underwater wireless optical communication (HAP-UWOC) Communication system.
- End-to-End performance is evaluated with DF relaying.
- In this study performance is evaluated by considering HAP-to-Ground hovering state channel model, the clear ocean, coastal ocean, Turbid harbor, and effect of HAP hovering fluctuations.

The rest of the chapter is structured as follows: In Section 6.3, the framework subtleties have been discussed, and Section 2.5, 2.6, depicts the HAP-UWOC Link channel model. In Section 6.5, the performance of the HAP-UWOC link has been inferred in the closed-form numerical expressions. In Section 6.6, numerical outcomes are introduced with pointing error for Different turbulence Conditions, θ_{FOV} , σ_{ro} , σ_{to} , σ_{tp} , σ_{rp} , distance. Toward the end of Section 6.7, the conclusion of this work has been summed up.

6.3 System Model

Fig.6.1, This shows that a typical HAP-UWOC communication system is considered. Here the optical information such as a collection of sensor data or act as a data relay was transmitted by the source (S) node to the destination node (D) through DF relay (R). Source node (S) HAP in hovering state. Here S node-R node HAP is GG distributed optical turbulence medium. This HAP is placed 20Km above the ocean. This channel is typically limited by clouds, rain, and different weather conditions.

R-D node UWOC link is a strong turbulence medium highly affected by path loss. UWOC link performance is typically limited by distance and type of oceanic water. Here we assumed the R node in a fixed position and UWOC link is GG distributed.

The optical signal transmitted at the HAP with hovering state fluctuations received at the Relay can be modeled as .

$$r_{s,r} = R_{s,r}h_{s,r}X + \eta_{s,r} \quad (6.1)$$

$h_{s,r}$ is the GG distributed channel gain of the S node to R node link, S transmitted optical input signal beam is represented as X , $R_{s,r}$ is Photo detector responsivity of Relay, and $\eta_{s,r}$ is the Gaussian noise with Variance of S-R link. $\sigma_n^2 = 2eB_eRP_b$ e is electron charge B_e is the photo detector band width P_b back ground power which is defined as $P_b=A_aB_oN_b(\lambda)\Omega_{FOV}$, where $N_b(\lambda)$ is the spectral radiance of the background radiations at wavelength λ , B_o is the bandwidth of the optical filter at the R and A_a is the lens area. Moreover, Ω_{FOV} denotes the R FOV that can be obtained as.

$$\Omega_{FOV} = \frac{\pi\theta_{FOV}^2}{4}.$$

Here, $\theta_{FOV}=\frac{2r_p}{d_f}$ denote the FOV angle, where d_f and r_p are the focal length radius of circular PD, respectively.

The optical signal received at the D through relay can be modeled as

$$r_{r,d} = R_{r,d}h_{r,d}\hat{X} + \eta_{r,d} \quad (6.2)$$

Where $R_{r,d}$ is the D responsivity, $h_{r,d}$ is the UWOC strong turbulence induced fading between R to D. \hat{X} is estimated signal at the R and $\eta_{r,d}$ is the AWGN noise with variance $\sigma_{r,d}$.

6.4 Channel Model

In this section, we derived the analytical channel models for HAP-to-Ground, and UWOC systems. Detailed derivation is done in [Chapter. 2, Section 2.5]

6.4.1 HAP-to-Ground Channel Model

The PDF between HAP-to-Ground link can be derived with Meijer's G functions as

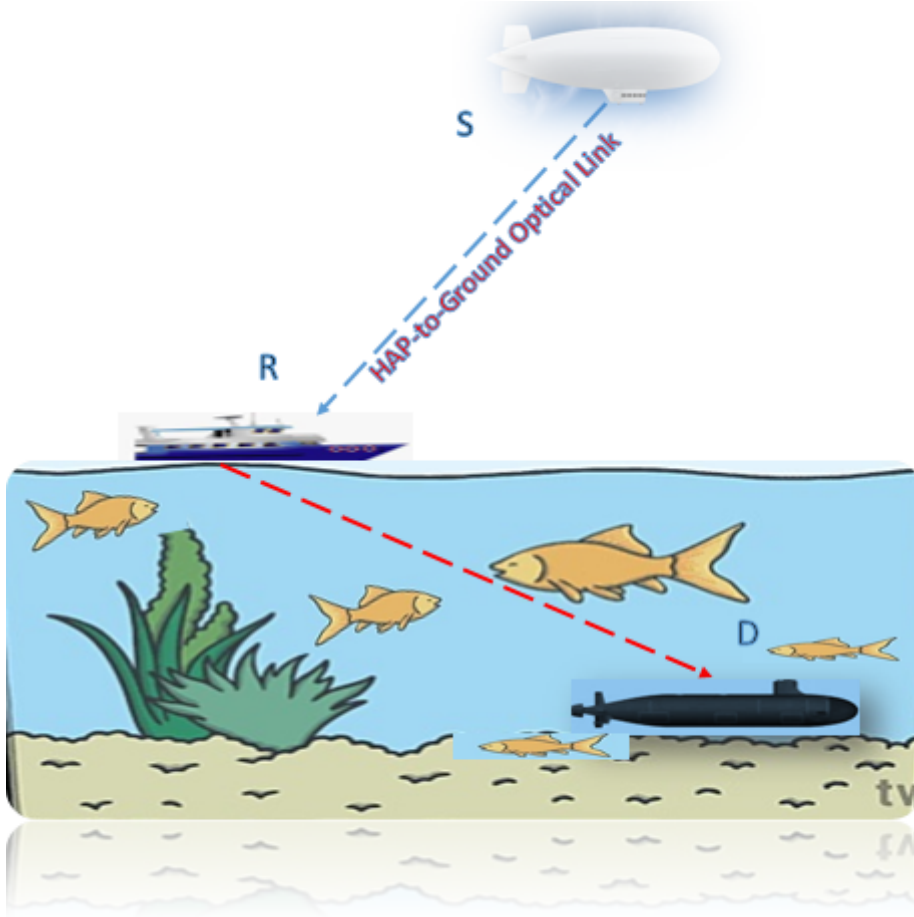


Figure 6.1: schematic diagram of Dual-hop HAP-UWOC System that consist of source (S) in hovering state, relay (R), and a destination (D).

$$f_{h1}(h) \approx \int \frac{1}{h'} f_{h_f}(h/h') f_{h'}(h') dh', \quad (6.3)$$

$$f_{h1}(h) \approx d_2 \delta(h) + f_h(h > 0), \quad (6.4)$$

where

$$d_2 = \exp\left(\frac{-\theta_{FOV}^2}{2\sigma_{rd}^2}\right),$$

$$f_h(h > 0) = [1 - d_2] * b_2 * G_{1,3}^{3,0}\left(\gamma_1^2 \gamma_1^2 - 1, \alpha_1 - 1, \beta_1 - 1 \left| \frac{\alpha_1 \beta_1 h_{s,r}}{h_l} \right.\right),$$

$$b_2 = \frac{\left[2\left(\frac{r_a}{W_z^2}\right)^2\right]^{-\gamma_1^2} \alpha_1 \beta_1 \gamma_1^2}{h_l \Gamma(\alpha_1) \Gamma(\beta_1)}.$$

After simplifying The cumulative distribution function (CDF) of Eq. (6.4) is expressed as

$$F_{h1}(h) \approx d_3 + f_h(h > 0), \quad (6.5)$$

$$d_3 = \exp\left(\frac{-\theta_{FOV}^2}{2\sigma_{rd}^2}\right),$$

$$F_h(h > 0) = [1 - d_3] * b_3 * G_{2,4}^{3,1} \left(\frac{\alpha_1 \beta_1 h_{th}}{h_l} \left| \begin{matrix} \gamma_1^2 + 1, 1 \\ \gamma_1^2, \alpha_1, \beta_1, 0 \end{matrix} \right. \right)$$

$$b_3 = \frac{\left[2\left(\frac{r_a}{W_z^2}\right)^2\right]^{-\gamma_1^2} \gamma_1^2}{\Gamma(\alpha_1) \Gamma(\beta_1)}.$$

6.4.2 UWOC Channel Model

Here we derived the UWOC link channel model for HAP-UWOC link under hovering fluctuations. detailed derivation is derived in [Chapter 2, Section 2.6]

$$f_{h_2}(h) = \frac{\alpha_2 \beta_2 \gamma_2^2}{A_0 h_{pu} \Gamma(\alpha_2) \Gamma(\beta_2)} G_{1,3}^{3,0} \left(\frac{\alpha_2 \beta_2 h}{A_0 h_{pu}} \left| \begin{matrix} \gamma_2^2 \\ \gamma_2^2 - 1, \alpha_2 - 1, \beta_2 - 1 \end{matrix} \right. \right) \quad (6.6)$$

The CDF of Eq. (6.6) is expressed as

$$F_{h_2}(h) = \frac{\gamma_2^2}{\Gamma(\alpha_2) \Gamma(\beta_2)} G_{2,4}^{3,1} \left(\frac{\alpha_2 \beta_2 h_{th}}{A_0 h_{pu}} \left| \begin{matrix} \gamma_2^2 + 1, 1 \\ \gamma_2^2, \alpha_2, \beta_2, 0 \end{matrix} \right. \right) \quad (6.7)$$

6.5 Performance Analysis

Here, we analyzed the performance of HAP-UWOC link under hovering state. The performance evaluated by considering Outage probability and Average BER.

6.5.1 Outage Performance Analysis

The outage probability for end-to-end communication systems under different ocean water conditions and HAP fluctuations can be found by utilizing $f_h(h)$. Cumulative distribution function (CDF) of HAP-UWOC communication system is evaluated at h_{th} . The quality of the HAP-UWOC communication link depends on the instantaneous signal-to-noise ratio (SNR) that falls below specified threshold values [Sandalidis *et al.* (2009b)], [Farid and Hranilovic (2007)].

$$p_{out}(h_{th}) = pr(h \leq h_{th}) = \int_0^{h_{th}} f_h(h)d(h) \quad (6.8)$$

The PDF of the HAP-UWOC system can be expressed in terms of the equivalent Threshold SNR, h_{th} as [Farid and Hranilovic (2007)]

$$\begin{aligned} f_h(h_{th}) &= f_{h_{s,r}}(h_{th}) + f_{h_{r,d}}(h_{th}) \\ &\quad - f_{h_{s,r}}(h_{th})F_{h_{r,d}}(h_{th}) - F_{h_{s,r}}(h_{th})f_{h_{r,d}}(h_{th}) \end{aligned} \quad (6.9)$$

The end-to-end CDF of Eq. (6.9) is

$$F_{h_{s,d}}(h_{th}) = F_{h_{s,r}}(h_{th}) + F_{h_{r,d}}(h_{th}) - F_{h_{s,r}}(h_{th})F_{h_{r,d}}(h_{th}) \quad (6.10)$$

after substituting Eq. (6.5) and Eq. (6.7) in Eq. (6.10), the CDF of the end-to-end system can be expressed as

$$\begin{aligned} F_{h_{s,d}}(h_{th}) \approx d_3 + f_h(h > 0) + \frac{\gamma_2^2}{\Gamma(\alpha_2)\Gamma(\beta_2)} G_{2,4}^{3,1} \left(\frac{\alpha_2\beta_2 h_{th}}{A_0 h_{pu}} \middle| \begin{matrix} \gamma_2^2 + 1, 1 \\ \gamma_2^2, \alpha_2, \beta_2, 0 \end{matrix} \right) - d_3 + f_h(h > 0) \\ \frac{\gamma_2^2}{\Gamma(\alpha_2)\Gamma(\beta_2)} G_{2,4}^{3,1} \left(\frac{\alpha_2\beta_2 h_{th}}{A_0 h_{pu}} \middle| \begin{matrix} \gamma_2^2 + 1, 1 \\ \gamma_2^2, \alpha_2, \beta_2, 0 \end{matrix} \right) \end{aligned} \quad (6.11)$$

6.5.2 Average BER

In this section, a HAP-UWOC communication system based on DF relay for the BER of *IM/DD* modulation analytical expressions is derived. The End-to-End Average BER can be expressed as

$$P_e = P_{e,hap}(1 - P_{e,UWOC}) + P_{e,UWOC}(1 - P_{e,hap}) \quad (6.12)$$

6.5.3 HAP-to-Ground BER

The average BER for the considered HAP-to-Ground-based FSO communication link with OOK modulation closed-form expression was derived. In this HAP-to-Ground communication link, performance is analyzed over the moderate to strong turbulence condition with Meijers G is derived as

$$P_{e,hap} = \frac{1}{2} \int_0^\infty \operatorname{erfc}\left(\frac{RP_t h_1}{\sqrt{2}\sigma_R}\right) f_{h_1}(h) dh \quad (6.13)$$

Eq. (6.13) can be modified with the help of $\operatorname{erfc}(\sqrt{x})$, which is given below and is as

$$\operatorname{erfc}(\sqrt{x}) = \frac{1}{\sqrt{\pi}} G_{1,2}^{2,0} \left(\begin{matrix} 1 \\ 0, 0.5 \end{matrix} \middle| x \right)$$

$$P_e = \frac{a1}{2} + \frac{(1-a1)D3}{2\sqrt{\pi}} \int_0^\infty G_{1,2}^{2,0} \left(\begin{matrix} 1 \\ 0, 0.5 \end{matrix} \middle| \frac{R^2 P_t^2 h_1^2}{2\sigma_R^2} \right) * G_{1,3}^{3,0} \left(\begin{matrix} \gamma_1^2 \\ \gamma_1^2 - 1, \alpha_1 - 1, \beta_1 - 1 \end{matrix} \middle| \frac{\alpha_1 \beta_1 h_1}{h_l} \right) dh_1 \quad (6.14)$$

$$\text{where, } D3 = \frac{\alpha_1 \beta_1 \gamma_1^2 \left[2 \left(\frac{r_a}{W_z^2} \right)^2 \right]^{-\gamma_1^2}}{\Gamma(\alpha_1) \Gamma(\beta_1) h_l}$$

Using [Adamchik and Marichev (1990), Eq.(07.34.21.0013.01)], and after simplifying, the expression for BER between HAP-to-Ground communication link performance is derived as

$$P_e = \frac{a1}{2} + \frac{\left[2 \left(\frac{r_a}{W_z^2} \right)^2 \right]^{-\gamma_1^2} \gamma_1^2 (1-a1) 2^{\alpha_1 + \beta_1 - 2}}{4\pi^{3/2} \Gamma(\alpha_1) \Gamma(\beta_1)} G_{7,4}^{2,6} \left(\begin{matrix} X1 \\ X2 \end{matrix} \middle| \frac{8R^2 P_t^2 h_l^2}{\sigma_R^2 (\alpha_1 \beta_1)^2} \right) \quad (6.15)$$

Where, $X1 = 1, (1 - \gamma_1^2)/2, (2 - \gamma_1^2)/2, (1 - \beta_1)/2, (2 - \beta_1)/2, (1 - \alpha_1)/2, (2 - \alpha_1)/2$
 $X2 = 0, 0.5, -\gamma_1^2/2, (1 - \gamma_1^2)/2$

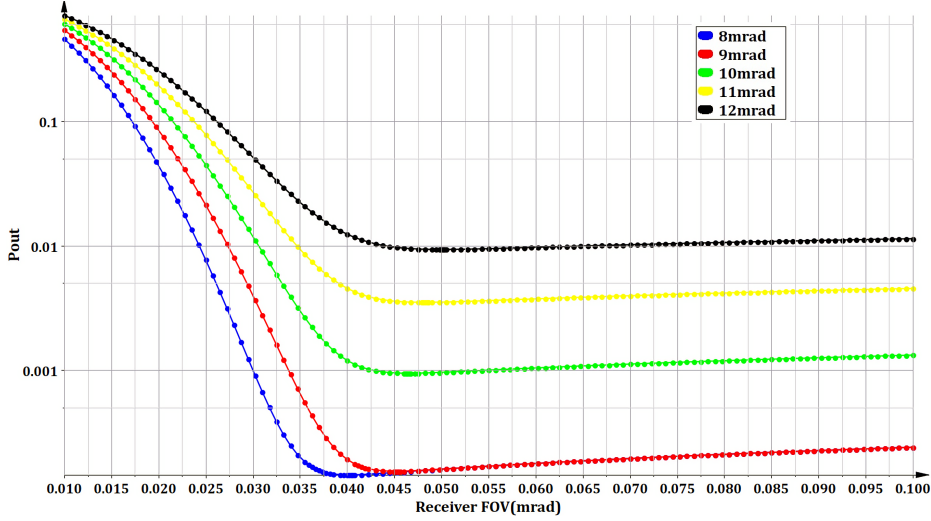


Figure 6.2: Outage Probability of HAP LINK versus Reveiver FOV over Gamma-Gamma turbulence model for different values of σ_{rd}

6.5.4 UWOC BER

The average BER for the considered UWOC based FSO communication link with OOK modulation closed-form expression was derived as

$$P_{e,uwoc} = \frac{\gamma_2^2 2^{\alpha_2 + \beta_2 - 2}}{4\pi^{3/2} \Gamma(\alpha_2) \Gamma(\beta_2)} G_{7,4}^{2,6} \left(\begin{matrix} X_{11} \\ X_{21} \end{matrix} \middle| \frac{8R^2 P_t^2 A_0^2 h_t^2}{\sigma_R^2 (\alpha_2 \beta_2)^2} \right) \quad (6.16)$$

Where, $X_{11} = 1, (1 - \gamma_2^2)/2, (2 - \gamma_2^2)/2, (1 - \beta_2)/2, (2 - \beta_2)/2, (1 - \alpha_2)/2, (2 - \alpha_2)/2$
 $X_{21} = 0, 0.5, -\gamma_2^2/2, (1 - \gamma_2^2)/2.$

6.6 Results and Discussions

This chapter, First evaluates the performance analysis of the HAP-to-Ground channel model under hovering fluctuations with different parameter variations are shown in Figs. 6.1, 6.2, 6.3 and derived the analytical expressions in Eq. (6.5), Eq. (6.7), and Eq. (6.15), respectively. In Fig.??, HAP-to-Ground channel under different receiver FOV values plotted by varying the σ_{rd} . In Fig.6.3 we varied different σ_{rd} values by considering transmitted power versus outage probability. These results are verified with already evaluated Ground-to-HAP channel model results [Safi et al. \(2020\)](#), [Khalighi and Uysal \(2014\)](#), [Kanas and Panagopoulos \(2017\)](#). HAP-to-Ground channel model results are true for lower values of 'h,' Simulation parameter in this chapter is

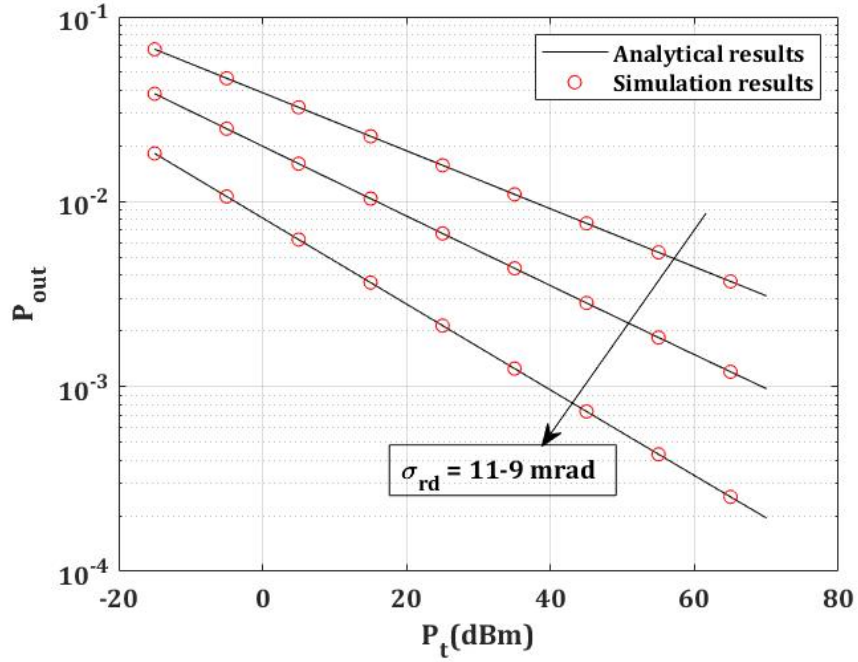


Figure 6.3: Outage Probability of HAP LINK versus Transmitted power over Gamma-Gamma turbulence model for $\sigma_{rd} = 11, 10, 9$ mrad.

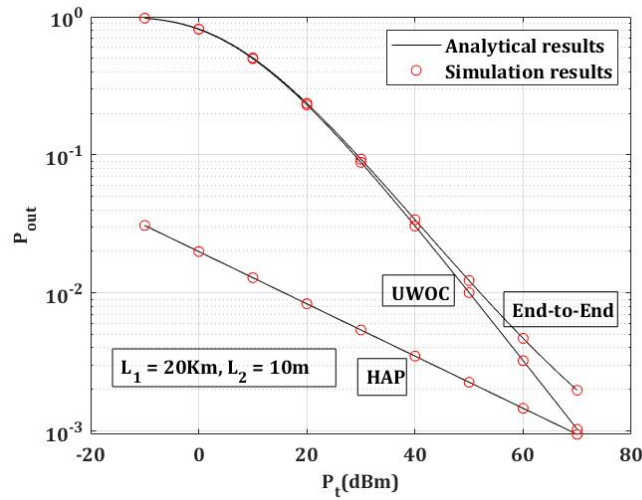


Figure 6.4: Outage Probability of HAP-UWOC LINK versus Transmitted power over Coastal ocean under hovering fluctuations

$r_a=5\text{cm}$, $L_l=20\text{K}$, $W_z=2$ and analytical parameter are given in Table. 15;

Outage Performance analysis of HAP, UWOC, and HAP-UWOC was shown in Fig .6.4 by considering HAP link distance 20Km, UWOC link distance 10m. End-to-End

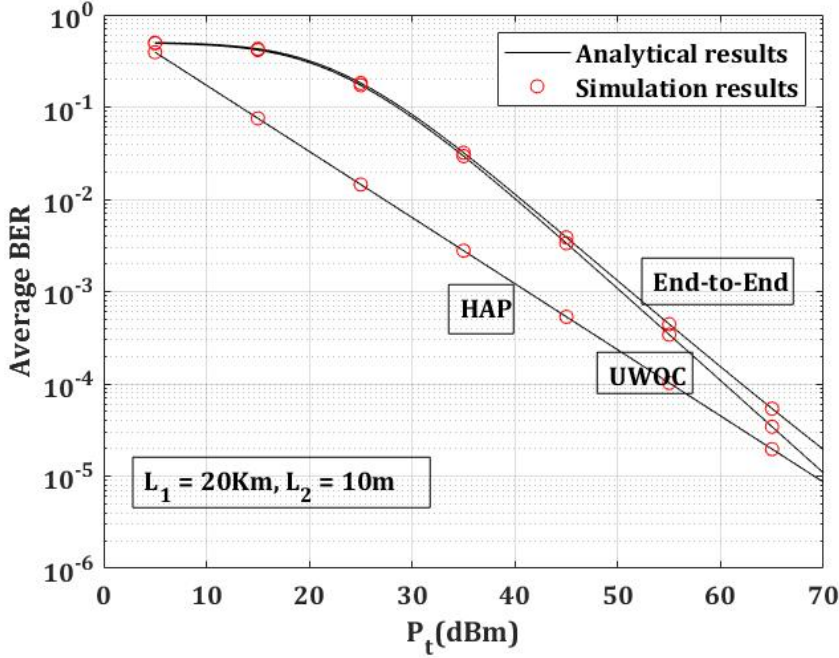


Figure 6.5: Average BER of HAP-UWOC LINK versus Transmitted power over Coastal ocean under hovering fluctuations.

performance is evaluated with DF relay plotted in Fig. 6.4 by considering coastal ocean scenery under hovering fluctuations. Its detailed derivations for End-to-End with DF relay derived in Eqs. 74, 78, 85.

Average BER performance is evaluated in Fig. 6.5 for HAP, UWOC, and HAP-UWOC. In Fig. 6.5 we plotted the Average BER verse P_t for coastal ocean conditions and lower values of orientation deviation fluctuations. we derived the analytical expression for Average BER of HAP, UWOC, HAP-UWOC with DF relay communication link was shown in Eqs. 86, 84, and 82 respectively.

Compared to HAP, the UWOC link has more path loss, so the UWOC link mainly degrades the End-to-End performance. In this chapter we varied the parameter related to UWOC link with DF relay and HAP parameter such receiver FOV, σ_{rd} , σ_{to} , σ_{ro} , σ_{tp} , and σ_{rp} are negligible. Considering Table 6.1 and 6.2, we evaluated the End-to-End performance for different values of turbulence conditions which are given in Table 6.1 and different pointing error ($\gamma_2 = 1, 2, 6$) values of UWOC link.

In Figs. 6.6, 6.7, 6.8, End-to-End Average BER performance is evaluated. Fig. 6.6. we considered Coastal ocean by varying ST, MT, and WT conditions and its

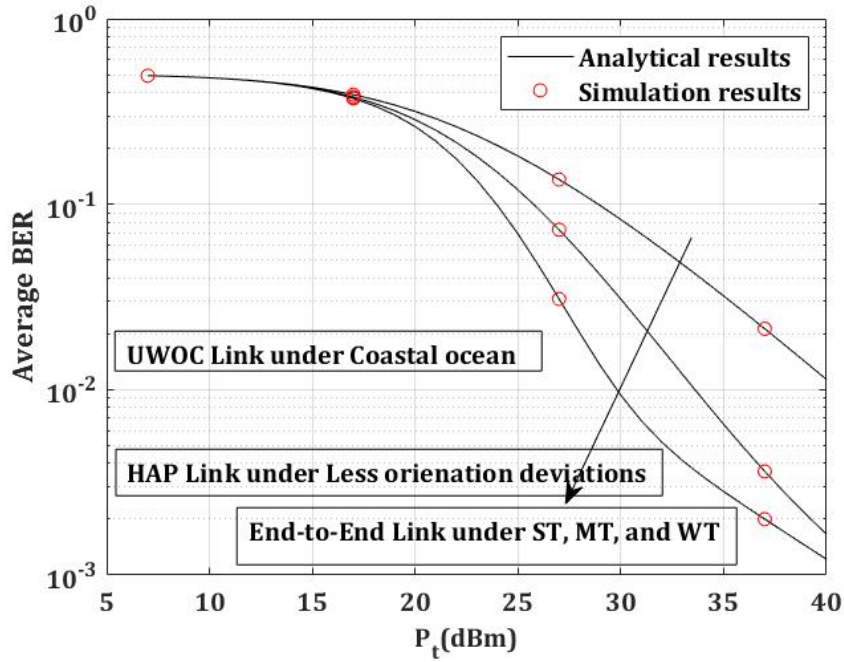


Figure 6.6: Average BER of HAP-UWOC LINK versus Transmitted power over Coastal ocean for strong-to-weak turbulence conditions under hovering fluctuations.

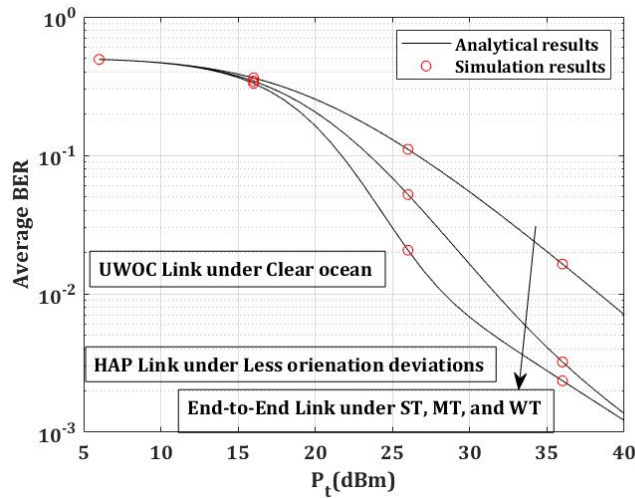


Figure 6.7: Average BER of HAP-UWOC LINK versus Transmitted power over Clear ocean for strong-to-weak turbulence conditions under hovering fluctuations.

End-to-End performance deviations are shown in Fig. 6.6. Fig. 6.7 and Fig. 6.8 are clear ocean, turbid harbor was shown respectively. Fig. 6.9 we plotted between Average BER verse $P_t(dBm)$.The pointing error deviation was varying from 1, 2, 6.

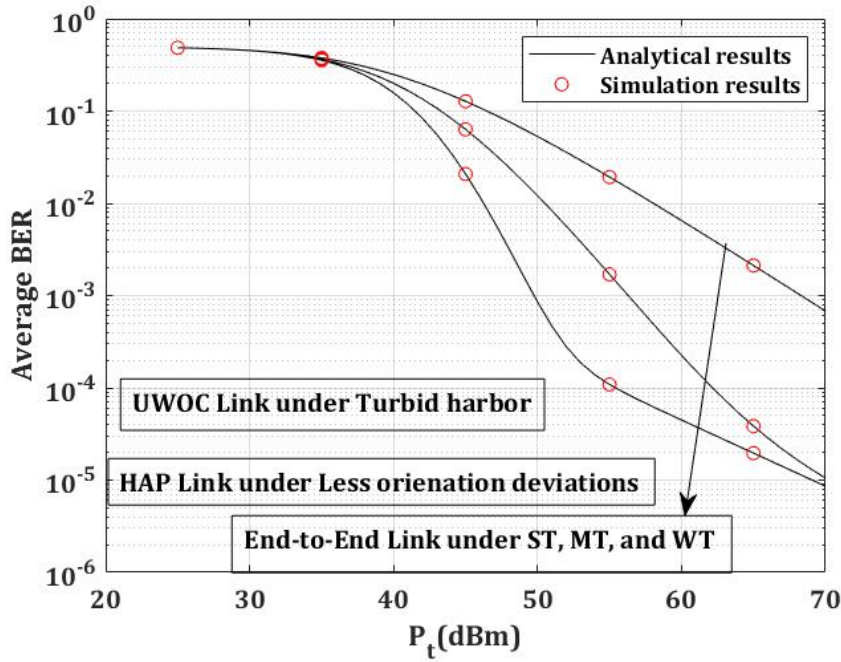


Figure 6.8: Average BER of HAP-UWOC LINK versus Transmitted power over Turbid harbor ocean for strong-to-weak turbulence conditions under hovering fluctuations.

For strong pointing error 1, moderate 2, and for weak pointing error 6 considered in this chapter. The performance of end-to-end relay link mainly depends on the pointing error. This is due to HAP position and orientation fluctuations. For higher values of pointing error, the performance is worst which is shown in the Fig. 6.9. we varied the pointing error from lower values to higher values and resultant performance deviation was shown in the Fig. 6.9. when compared to the fixed position links HAP link has more pointing error loss due its position an orientation deviation.

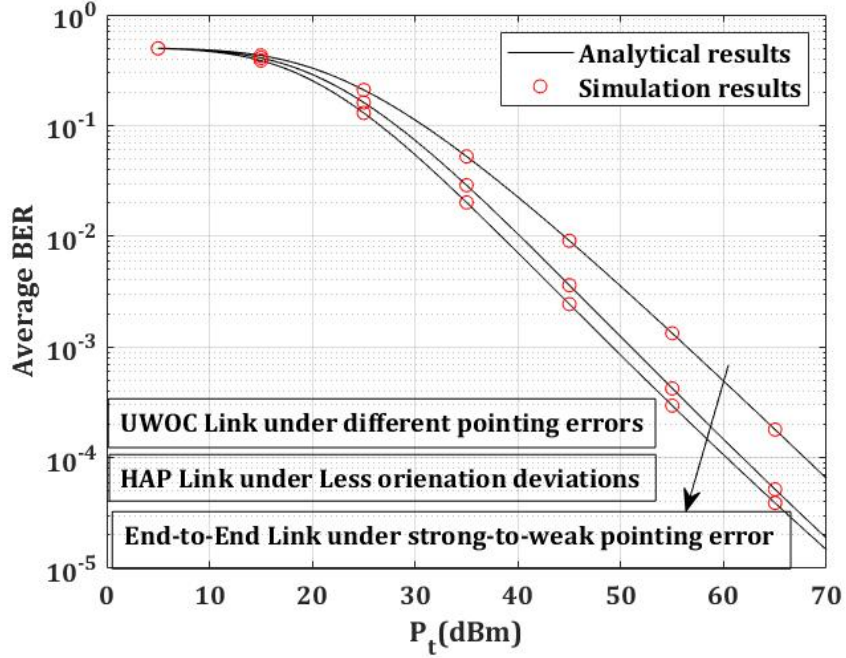


Figure 6.9: Average BER of HAP-UWOC LINK versus Transmitted power over Turbid harbor ocean for strong-to-weak pointing($\gamma_2 = 1, 2, 6$) error under hovering fluctuations.

6.7 Summary

In this chapter, the outage probability and Average BER of the HAP-UWOC system over turbulence channel using IM/DD at the receiver with the DF relay studied. The results of the HAP-UWOC system with DF relay demonstrated. We Compared the HAP, UWOC, and HAP-UWOC link performance. End-to-End performance is evaluated with different oceanic and pointing error conditions. We evaluated the HAP-to-Ground channel performance under OOK modulation with different parameters such as θ_{FOV} , σ_{rd} , σ_{to} , and σ_{ro} . Derived analytical results are compared with Monte-Carlo simulation results which are shown in the results section.

Table 6.1: Turbulence conditions for UWOC link [Zeng *et al.* (2016)].

Turbulence conditions	Parameters
Weak Turbulence(WT)	$\alpha_2=10, \beta_2 =5$
Moderate Turbulence(MT)	$\alpha_2 = 4.1, \beta_2 = 2$
Strong Turbulence(ST)	$\alpha_2 =2 \beta_1 = 1$

Table 6.2: Parameters for HAP and UWOC link.

Parameters Used for The Numerical Results	
Parameter	Value
Wavelength λ_1 for HAP	1550 nm
Wavelength λ_2 for UWOC	530 nm
Link distance(L_1) for HAP	20Km
Link distance(L_2) for UWOC	10m
Responsivity η	0.9
Optical bandwidth B_o	10 nm
Receiver electrical bandwidth B_e	1GHz
Spectral radiance $N_b(\lambda)$	$10^{-3}W/cm^2 - m - srad$
HAP zenith angle ς	40°
Link length L	20km
wind speed V_m	21 m/s
Refractive index structure at the ground $C_n^2(0)$	$1.7 * 10^{-13} m^{-2/3}$

Chapter 7

CONCLUSIONS AND FUTURE DIRECTIONS

7.1 Conclusions

This research mainly focuses on the performance analysis of inter-UAV-based FSO communication systems. We considered the main limitations and challenges of equipped FSO communication systems. We derived the simple analytical channels models under hovering fluctuations of UAV-based FSO communication systems and HAP-UWOC equipped with FSO communication systems. Derived analytical channel models results are verified with simulation results. Both the FSO based communication system's performance was evaluated under different weather conditions. We mitigated the weather condition's effects by increasing receiver FOV. Plotted results are evidence for mitigating rain, snow, Drizzle, clouds. Fog is the main limiting factor as we are expanding the receiver FOV, the performance remains the same. We verified the results with optimal values of receiver FOV and position, orientation deviation of UAV. The derived analytical results are for weak to strong turbulence channel cases. Performance analysis metrics such as outage and BER were analyzed for various channel parameters such as W_Z , Average SNR, θ_{FOV} , σ_{to} , σ_{ro} and other channel parameters. For Inter UAV-based FSO communication systems, we first compared the HD with IM/DD detection. HD detection performance is better by compensating the turbulence and UAVs position, orientation fluctuations.

We introduced POLSK modulation in UAV-based FSO communication systems, which is used to reduce the turbulence effect and improve the link distance. This

POLSK modulation is used for long-range air-to-air applications. In literature, we studied UAV-based FSO system link range is about 0.5k beyond this the performance is worst. By using this POLSK modulation, we improve up to 3km. Optimal values are also provided for the FOV to achieve the minimum BER for different SNR values. In terms of long-distance applications such as air-to-air, ground-to-air, and air-to-ground links, POLSK modulation is the best solution for next-generation fronthaul/backhaul wireless communications applications, and the corresponding results are shown. Distance evaluation was proposed through POLSK modulation for the UAV-based FSO link and the performance results shown in this thesis.

Channel model and evaluating the performance of Ground-to-HAP communication systems under hovering fluctuation is another research area. We derived the analytical expressions for Ground-to-HAP communication systems. We evaluated the performance of the Ground-to-HAP link with POLSK under different weather conditions. Optimal values demonstrated in the results section mitigated the weather effect by increasing the Receiver FOV. Performance improvement under the rain and the cloud was evaluated for the Ground-to-HAP channel. Finally, the performance of the Ground-to-HAP Link is evaluated with coding techniques. The outage probability and Average BER of the HAP-UWOC system over turbulence channel using IM/DD at the receiver with the DF relay studied. The results of the HAP-UWOC system with DF relay demonstrated. We Compared the HAP, UWOC, and HAP-UWOC link performance. End-to-End performance is evaluated with different oceanic and pointing error conditions. We evaluated the HAP-to-Ground channel performance under OOK modulation with different parameters such as θ_{FOV} , σ_{rd} , σ_{to} , and σ_{ro} . Derived analytical results are compared with Monte-Carlo simulation results which are shown in the results section.

7.2 Future Directions

This thesis mainly highlighted the horizontal link of FSO communication under different weather conditions. Considering Vertical link performance under different weather conditions for UAV-based FSO communication is an essential research direction. When compared to the horizontal link, the vertical link is highly attenuated by different weather conditions. Theoretical and experimental performance analysis under different weather conditions is required. Based on weather conditions, alternative communication systems are proposed for specific weather conditions such as millimeter-wave FSO and Hybrid FSO/RF communication systems.

Detailed study of UAV's assisted FSO communication by considering UAV as the relay is not highlighted complete for optical communications. Another important research direction is the placement of the UAVs for higher capacity and link availability. The proper placement of UAVs is not studied thoroughly for future wireless/optical communications. Even we designed the efficient link, the performance mainly depends on the correct placement of UAV's is another growing research of interest.

Appendix I

DERIVATION OF INTER UAV-BASED FSO COMMUNICATION SYSTEMS

A-1 Derivation Of UAV-UAV-FSO Over Gamma-Gamma Channel

From (3) h' is defined and it's PDF is

$$f_{h'}(h') \approx \int \frac{1}{h_{pl}h_{al}} f_{h_{pp}}\left(\frac{h'}{h_{pl}h_{al}}\right) f_{h_{al}}(h_{al}) dh_{al} \quad (\text{A.1})$$

from [12] it is defined as

$$f_{h'}(h') = \frac{2\tau(\alpha\beta)^{\frac{\alpha+\beta}{2}} h'^{\tau-1}}{A_0^\tau h_{pl}^\tau \Gamma(\alpha)\Gamma(\beta)} \int_{\frac{h'}{h_{pl}A_0}}^{\infty} h_{al}^{\frac{\alpha+\beta}{2}-\tau-1} k_{\alpha-\beta}(2\sqrt{\alpha\beta h_{al}}) dh_{al} \quad (\text{A.2})$$

By considering the Eq.(22) and from [18,Eq.(14)] we simplify as follows

$$K_v(x) = \frac{1}{2} G_{2,0}^{0,2} \left(\begin{matrix} -, - \\ \frac{v}{2}, -\frac{v}{2} \end{matrix} \middle| \frac{x^2}{4} \right) \quad (\text{A.3})$$

$$f_{h'}(h') = \frac{2\tau(\alpha\beta)^{\frac{\alpha+\beta}{2}} h'^{\tau-1}}{A_0^\tau h_{pl}^\tau \Gamma(\alpha)\Gamma(\beta)} \int_{\frac{h'}{h_{pl}A_0}}^{\infty} h_{al}^{\frac{\alpha+\beta}{2}-\tau-1} * \frac{1}{2} G_{0,2}^{2,0} \left(\begin{matrix} -, - \\ \frac{\alpha-\beta}{2}, -\frac{\beta-\alpha}{2} \end{matrix} \middle| \alpha\beta h_a \right) dh_{al} \quad (\text{A.4})$$

From [24, eq.(07.34.21.0085.01)] and after simplifications

$$f_{h'}(h') = \frac{\tau\alpha\beta}{A_0 h_{pl} \Gamma(\alpha)\Gamma(\beta)} \left(\frac{\alpha\beta h'}{A_0 h_{pl}} \right)^{\frac{\alpha+\beta}{2}-1} G_{1,3}^{3,0} \left(\begin{matrix} 1 + \tau - \frac{\alpha+\beta}{2} \\ \tau - \frac{\alpha+\beta}{2}, \frac{\alpha-\beta}{2}, \frac{\beta-\alpha}{2} \end{matrix} \middle| \frac{\alpha\beta h'}{A_0 h_{pl}} \right). \quad (\text{A.5})$$

This can be further simplified by considering [24, eq.(07.34.16.0001.01)] along with some mathematical simplifications the PDF of h' derived in Eq.(6)

Appendix II

DERIVATION OF HD DETECTION

A-2 Derivation Of HD Detection Over Log-normal Channel

UAV-UAV-FSO link outage probability can be expressed as

$$p_{out}(h_{th}) = \int_0^{h_{th}} f_h(h) d(h)$$

outage probability for Log-normal channel under HD can be expressed in integral form as

$$= a1\delta(h) + (1 - a1) * d1 * \frac{A_0^\tau \tau^\tau}{(1 + \tau)^\tau \mu_{HD}^\tau} \int_0^{h_{th}} \gamma^{\tau-1} * erfc\left(\frac{\ln\left(\frac{\gamma^\tau}{h_i \mu_{HD} (1+\tau)} + \mu\right)}{\sqrt{8}\sigma_R}\right) d\gamma \quad (A.6)$$

by assuming $\alpha=\tau$, $a=\frac{\mu}{\sqrt{8}\sigma_R}$, $b=\frac{1}{\sqrt{8}\sigma_R}$, $c=\frac{\tau}{h_i(1+\tau)\mu_{HD}}$, the integral term in above equation can be written as.

$$= \int_0^{h_{th}} \gamma^{\alpha-1} * erfc\left(a + b\ln(c\gamma)\right) d\gamma \quad (A.7)$$

In the simplified expression, let $a + b\ln(c\gamma)=y, \gamma=\frac{1}{c} e^{\frac{y-a}{b}}, d\gamma=\frac{1}{cb} e^{\frac{y-a}{b}} dy$, and intergral

region y the above equation can be rewritten as.

$$= \frac{1}{bc^\alpha} e^{\frac{-a\alpha}{b}} \int_{-\infty}^{a+bln(c\gamma)} e^{\frac{y\alpha}{b}} * erfc(y) dy \quad (A.8)$$

Then, by utilizing [24, Eq.(06.27.21.0011.01)],after simplifications we can obtain the closed-form expression of above equation is derived in Eq.(16) .

Bibliography

Abaza, M., R. Mesleh, A. Mansour, et al. (2015). Performance analysis of miso multi-hop fso links over log-normal channels with fog and beam divergence attenuations. *Optics Communications*, **334**, 247–252.

Adamchik, V. and O. Marichev (1990). The algorithm for calculating integrals of hypergeometric type functions and its realization in reduce system. *Proceedings of the international symposium on Symbolic and algebraic computation*, 212–224.

Al-Barrak, A., A. Al-Sherbaz, T. Kanakis, and R. Crockett (2017). Enhancing ber performance limit of bch and rs codes using multipath diversity. *Computers*, **6**(2), 21.

Al-Habash, A., L. C. Andrews, and R. L. Phillips (2001). Mathematical model for the irradiance probability density function of a laser beam propagating through turbulent media. *Optical engineering*, **40**(8), 1554–1563.

Alzenad, M., M. Z. Shakir, H. Yanikomeroğlu, and M.-S. Alouini (2018a). Fso-based vertical backhaul/fronthaul framework for 5g+ wireless networks. *IEEE Communications Magazine*, **56**(1), 218–224.

Alzenad, M., M. Z. Shakir, H. Yanikomeroğlu, and M.-S. Alouini (2018b). Fso-based vertical backhaul/fronthaul framework for 5g+ wireless networks. **56**(1), 218–224. ISSN 1558-1896.

Amphawan, A., S. Chaudhary, Z. Ghassemlooy, and T.-K. Neo (2020). 2×2 -channel mode-wavelength division multiplexing in ro-fso system with pcf mode group demultiplexers and equalizers. *Optics Communications*, **467**, 125539.

- Anandkumar, D.** and **R. Sangeetha** (2021). A survey on performance enhancement in free space optical communication system through channel models and modulation techniques. *Optical and Quantum Electronics*, **53**(1), 1–39.
- Andrews, L. C.** and **R. L. Phillips** (2005). Laser beam propagation through random media.
- Awan, M. S., E. Leitgeb, B. Hillbrand, F. Nadeem, M. Khan, et al.**, Cloud attenuations for free-space optical links. In *2009 International Workshop on Satellite and Space Communications*. IEEE, 2009.
- Bhowal, A.** and **R. S. Kshetrimayum**, *Advanced Spatial Modulation Systems*. Springer, 2021.
- Chlestil, C., E. Leitgeb, N. P. Schmitt, S. S. Muhammad, K. Zettl, and W. Rehm**, Reliable optical wireless links within uav swarms. In *2006 international conference on transparent optical networks*, volume 4. IEEE, 2006.
- Dabiri, M. T., S. Khankalantary, M. J. Piran, I. S. Ansari, M. Uysal, W. Saad, and C. S. Hong** (2021). Uav-assisted free space optical communication system with amplify-and-forward relaying. *IEEE Transactions on Vehicular Technology*.
- Dabiri, M. T., M. Rezaee, I. S. Ansari, and V. Yazdaniyan** (2020). Channel modeling for uav-based optical wireless links with nonzero boresight pointing errors. *IEEE Transactions on Vehicular Technology*.
- Dabiri, M. T.** and **S. M. S. Sadough** (2019a). Optimal placement of uav-assisted free-space optical communication systems with df relaying. *IEEE Communications Letters*, **24**(1), 155–158.
- Dabiri, M. T.** and **S. M. S. Sadough** (2019b). Optimal placement of uav-assisted free-space optical communication systems with df relaying. **24**(1), 155–158. ISSN 1558-2558.
- Dabiri, M. T.** and **S. M. S. Sadough**, Outage analysis of uav-based fso systems over log-normal turbulence channels. In *2019 2nd West Asian Colloquium on Optical Wireless Communications (WACOWC)*. IEEE, 2019c.

- Dabiri, M. T., S. M. S. Sadough, and I. S. Ansari** (2019a). Tractable optical channel modeling between uavs. *IEEE Transactions on Vehicular Technology*, **68**(12), 11543–11550.
- Dabiri, M. T., S. M. S. Sadough, and I. S. Ansari** (2019b). Tractable optical channel modeling between uavs. **68**(12), 11543–11550. ISSN 1939-9359.
- Dabiri, M. T., S. M. S. Sadough, and M. A. Khalighi** (2018a). Channel modeling and parameter optimization for hovering uav-based free-space optical links. *IEEE Journal on Selected Areas in Communications*, **36**(9), 2104–2113.
- Dabiri, M. T., S. M. S. Sadough, and M. A. Khalighi** (2018b). Channel modeling and parameter optimization for hovering uav-based free-space optical links. **36**(9), 2104–2113. ISSN 1558-0008.
- Dabiri, M. T., H. Savojbolaghchi, and S. M. S. Sadough**, On the ergodic capacity of ground-to-uav free-space optical communications. *In 2019 2nd West Asian Colloquium on Optical Wireless Communications (WACOWC)*. IEEE, 2019c.
- Djordjevic, I. B.**, *Advanced optical and wireless communications systems*. Springer, 2018.
- Elsayed, E. E. and B. B. Yousif** (2020). Performance evaluation and enhancement of the modified ook based im/dd techniques for hybrid fiber/fso communication over wdm-pon systems. *Optical and Quantum Electronics*, **52**(9), 1–27.
- Farid, A. A. and S. Hranilovic** (2007). Outage capacity optimization for free-space optical links with pointing errors. **25**(7), 1702–1710. ISSN 1558-2213.
- Fawaz, W., C. Abou-Rjeily, and C. Assi** (2018). Uav-aided cooperation for fso communication systems. *IEEE Communications Magazine*, **56**(1), 70–75.
- Gagliardi, R. M. and S. Karp** (1976). Optical communications. *wi*.
- Ghassemlooy, Z., W. Popoola, and S. Rajbhandari**, *Optical wireless communications: system and channel modelling with Matlab®*. CRC press, 2019.
- Grabner, M. and V. Kvicera**, Fog attenuation dependence on atmospheric visibility at two wavelengths for fso link planning. *In 2010 Loughborough Antennas & Propagation Conference*. IEEE, 2010.

- Gupta, L., R. Jain,** and **G. Vaszkun** (2015). Survey of important issues in uav communication networks. *IEEE Communications Surveys & Tutorials*, **18**(2), 1123–1152.
- Gupta, N., A. Dixit, V. K. Jain,** *et al.*, Performance analysis of bch and repetition codes in gamma-gamma faded fso link. *In 2019 National Conference on Communications (NCC)*. IEEE, 2019.
- Hanna, S. K.** and **S. El Rouayheb** (2018). Guess & check codes for deletions, insertions, and synchronization. *IEEE Transactions on Information Theory*, **65**(1), 3–15.
- Harris, A., J. J. Sluss, H. H. Refai,** and **P. G. LoPresti**, Alignment and tracking of a free-space optical communications link to a uav. *In 24th Digital Avionics Systems Conference*, volume 1. IEEE, 2005.
- Harris, A., J. J. Sluss Jr, H. H. Refai,** and **P. G. LoPresti**, Atmospheric turbulence effects on a wavelength diversified ground-to-uav fso link. *In Free-Space Laser Communication Technologies XVIII*, volume 6105. International Society for Optics and Photonics, 2006.
- Jeffrey, A.** and **D. Zwillinger**, *Table of integrals, series, and products*. Elsevier, 2007.
- Jha, P. K., N. Kachare, K. Kalyani,** and **D. S. Kumar**, Performance analysis of fso using relays and spatial diversity under log-normal fading channel. *In 2018 4th International Conference on Electrical Energy Systems (ICEES)*. IEEE, 2018.
- Johnson, L. J., R. J. Green,** and **M. S. Leeson**, The impact of link orientation in underwater optical wireless communication systems. *In 2014 Oceans-St. John's*. IEEE, 2014.
- Jung, K.-J., S. S. Nam, M.-S. Alouini,** and **Y.-C. Ko** (2020). Unified finite series approximation of fso performance over strong turbulence combined with various pointing error conditions. *IEEE Transactions on Communications*, **68**(10), 6413–6425.

- Kaadan, A., H. Refai, and P. Lopresti** (2016). Spherical fso receivers for uav communication: geometric coverage models. *IEEE Transactions on Aerospace and Electronic Systems*, **52**(5), 2157–2167.
- Kaadan, A., H. H. Refai, and P. G. LoPresti** (2014). Multielement fso transceivers alignment for inter-uav communications. *Journal of Lightwave Technology*, **32**(24), 4785–4795.
- Kaadan, A., D. Zhou, H. H. Refai, and P. G. LoPresti**, Modeling of aerial-to-aerial short-distance free-space optical links. In *2013 Integrated Communications, Navigation and Surveillance Conference (ICNS)*. IEEE, 2013.
- Kanatas, A. G. and A. D. Panagopoulos**, *Radio wave propagation and channel modeling for earth-space systems*. CRC Press, 2017.
- Kaushal, H., V. Jain, and S. Kar**, *Free space optical communication*. Springer, 2017.
- Kaushal, H. and G. Kaddoum** (2016). Optical communication in space: Challenges and mitigation techniques. *IEEE communications surveys & tutorials*, **19**(1), 57–96.
- Kaymak, Y., R. Rojas-Cessa, J. Feng, N. Ansari, M. Zhou, and T. Zhang** (2018). A survey on acquisition, tracking, and pointing mechanisms for mobile free-space optical communications. *IEEE Communications Surveys & Tutorials*, **20**(2), 1104–1123.
- Khalighi, M. A. and M. Uysal** (2014). Survey on free space optical communication: A communication theory perspective. *IEEE communications surveys & tutorials*, **16**(4), 2231–2258.
- Khankalantary, S., M. T. Dabiri, and H. Safi** (2020). Ber performance analysis of drone-assisted optical wireless systems with apd receiver. *Optics Communications*, **463**, 125309.
- Kumar, L. B. and P. Krishnan** (2020). Multi-hop convergent fso-uwoc system to establish a reliable communication link between the islands. *Optics Communications*, **474**, 126107.

- Kumbhani, B.** and **R. S. Kshetrimayum**, *MIMO wireless communications over generalized fading channels*. CRC Press, 2017.
- Lei, H., Z. Dai, K.-H. Park, W. Lei, G. Pan,** and **M.-S. Alouini** (2018). Secrecy outage analysis of mixed rf-fso downlink swipt systems. *IEEE Transactions on Communications*, **66**(12), 6384–6395.
- Leitgeb, E., K. Zettl, S. S. Muhammad, N. Schmitt,** and **W. Rehm**, Investigation in free space optical communication links between unmanned aerial vehicles (uavs). In *2007 9th international conference on transparent optical networks*, volume 3. IEEE, 2007.
- Liu, W., Z. Xu,** and **L. Yang** (2015). Simo detection schemes for underwater optical wireless communication under turbulence. *Photonics Research*, **3**(3), 48–53.
- Majumdar, A. K.**, *Advanced free space optics (FSO): a systems approach*, volume 186. Springer, 2014.
- Nallagonda, V. R.** and **P. Krishnan** (2021*a*). Bit error rate analysis of polarization shift keying based free space optical link over different weather conditions for inter unmanned aerial vehicles communications. *Optical and Quantum Electronics*, **53**(9), 1–15.
- Nallagonda, V. R.** and **P. Krishnan** (2021*b*). Performance analysis of fso based inter-uav communication systems. *Optical and Quantum Electronics*, **53**(4), 1–20.
- Pham, H. T., N. T. Dang,** and **A. T. Pham** (2014). Effects of atmospheric turbulence and misalignment fading on performance of serial-relaying m-ary pulse-position modulation free-space optical systems with partially coherent gaussian beam. *IET communications*, **8**(10), 1762–1768.
- Prabu, K., S. Gupta,** and **S. Jaiswal** (2018). Impact of pointing errors and turbulence effects on polsk and coherent owc-based fso system over generalized turbulence channel model. *Photonic Network Communications*, **36**(1), 96–105.
- Prabu, K.** and **D. S. Kumar** (2015). Mimo free-space optical communication employing coherent bpolsk modulation in atmospheric optical turbulence channel with pointing errors. *Optics Communications*, **343**, 188–194.

- Rahman, A., A. Tom, N. Mohtadzar, Y. Buswig, N. Zamhari, D. Zaidel, S. Sahari, and N. Julai**, A new modulation technique to improve received power under turbulence effects for free space optical communication. *In IOP Conference Series: Materials Science and Engineering*, volume 767. IOP Publishing, 2020.
- Ramavath, P. N., S. A. Udupi, and P. Krishnan** (2020). Experimental demonstration and analysis of underwater wireless optical communication link: Design, bch coded receiver diversity over the turbid and turbulent seawater channels. *Microwave and Optical Technology Letters*, **62**(6), 2207–2216.
- Safi, H., A. Dargahi, and J. Cheng** (2019a). Spatial beam tracking and data detection for an fso link to a uav in the presence of hovering fluctuations. *arXiv preprint arXiv:1904.03774*.
- Safi, H., A. Dargahi, and J. Cheng** (2019b). Spatial beam tracking and data detection for an fso link to a uav in the presence of hovering fluctuations.
- Safi, H., A. Dargahi, J. Cheng, and M. Safari** (2020). Analytical channel model and link design optimization for ground-to-hap free-space optical communications. *Journal of Lightwave Technology*.
- Sandalidis, H. G., T. A. Tsiftsis, and G. K. Karagiannidis** (2009a). Optical wireless communications with heterodyne detection over turbulence channels with pointing errors. **27**(20), 4440–4445. ISSN 1558-2213.
- Sandalidis, H. G., T. A. Tsiftsis, and G. K. Karagiannidis** (2009b). Optical wireless communications with heterodyne detection over turbulence channels with pointing errors. *Journal of lightwave technology*, **27**(20), 4440–4445.
- Schulz, D., V. Jungnickel, C. Alexakis, M. Schlosser, J. Hilt, A. Paraskevopoulos, L. Grobe, P. Farkas, and R. Freund** (2016). Robust optical wireless link for the backhaul and fronthaul of small radio cells. *Journal of Lightwave technology*, **34**(6), 1523–1532.
- Simon, M. K. and M.-S. Alouini**, *Digital communication over fading channels*, volume 95. John Wiley & Sons, 2005.

- Singh, M.** and **J. Malhotra** (2019a). Long-reach high-capacity hybrid mdm-ofdm-fso transmission link under the effect of atmospheric turbulence. *Wireless Personal Communications*, **107**(4), 1549–1571.
- Singh, M.** and **J. Malhotra** (2019b). Performance comparison of high-speed long-reach mode division multiplexing-based radio over free space optics transmission system using different modulation formats under the effect of atmospheric turbulence. *Optical Engineering*, **58**(4), 046112.
- Singh, M., M. L. Singh, G. Singh, H. Kaur, S. Kaur, et al.** (2020). Modeling and performance evaluation of underwater wireless optical communication system in the presence of different sized air bubbles. *Optical and Quantum Electronics*, **52**(12), 1–15.
- Taghi Dabiri, M., M. Rezaee, and I. Shafique Ansari** (2020). Channel modeling uav-based optical wireless links with nonzero boresight pointing errors. *arXiv*, arXiv-2004.
- Tsiftsis, T.** (2008). Performance of heterodyne wireless optical communication systems over gamma-gamma atmospheric turbulence channels. *Electronics Letters*, **44**(5), 372–373.
- Uysal, M.** and **H. Nouri**, Optical wireless communications an emerging technology. In *2014 16th international conference on transparent optical networks (ICTON)*. IEEE, 2014.
- Weisstein, E. W.** *et al.* (2004). Mathworld—a wolfram web resource.
- Wolfram, C.** (2001). The wolfram functions.
- Yan, C., L. Fu, J. Zhang, and J. Wang** (2019). A comprehensive survey on uav communication channel modeling. *IEEE Access*, **7**, 107769–107792.
- Yang, F., J. Cheng, and T. A. Tsiftsis** (2014). Free-space optical communication with nonzero boresight pointing errors. *IEEE Transactions on Communications*, **62**(2), 713–725.
- Zeng, Z., S. Fu, H. Zhang, Y. Dong, and J. Cheng** (2016). A survey of underwater optical wireless communications. *IEEE communications surveys & tutorials*, **19**(1), 204–238.

Zhang, Y., H. Wang, M. Cao, and Z. Bao (2020). Performance evaluation of mppm-coded wireless optical mimo system with combined effects over correlated fading channel. *International Journal of Antennas and Propagation*, **2020**.

Publications Based on the Thesis

Journals:

1. **Nallagonda, V.R.**, and Krishnan, P. "Performance analysis of FSO based inter-UAV communication systems.," Opt Quant Electron 53, 192 (2021). <https://doi.org/10.1007/s11082-021-02843-w>
2. **Nallagonda, V.R.**, and Krishnan, P. "Bit error rate analysis of polarization shift keying based free space optical link over different weather conditions for inter unmanned aerial vehicles communications.," Opt Quant Electron 53, 538 (2021). <https://doi.org/10.1007/s11082-021-03188-0>
3. **Nallagonda, V.R.**, and Krishnan, P. "Bit Error Rate Analysis of Ground-to-High Altitude Platform Free-Space Optical Communications Using Coded Polarization Shift Keying in Various Weather Conditions," Optical and Quantum Electronics., OQEL-D-21-00601R1.-**accepted for Publication.**
4. Nallagonda, V.R.,Bhargava, Kumar, L., Krishnan, P. **Performance Analysis of HAP-UWOC Systems with DF Relaying** Journal of Ambient Intelligence and Humanized Computing (AIHC).-**Under review.**

CURRICULUM VITAE

Nallagonda Vijaya Ratnam

Pedana Post, Pedana Mandal, Krishna District,
Andhra Pradesh - 521366.

☎ : +91 6281940490

✉ : vijayaratnam@gmail.com

Work Experience:

1. Assistant Professor in Vishnu Institute of Technology Bhimavaram from Jan. 2015 - June 2018.

Education:

1. Ph.D. (Optical Wireless Communication), National Institute of Technology Karnataka, Surathkal, 2021.
2. M.Tech.(Communication and Networks), National Institute of Technology Rourkela, 2014.
3. B.Tech. (ECE), Gudlavalleru Engineering College, Andhra Pradesh, 2012.

Research Interests:

Unmanned Aerial Vehicle (UAV), Free Space Optical(FSO).

Publications:

Number of Journal publications: 3